2011-04-18

Nanocomposite High Displacement Strain Gauges for use in Human-Machine Interfaces: Applications in Hand Pose Determination

Thomas B. Calkins
Brigham Young University - Provo

Nanocomposite High Displacement Strain Gauges for use in Human-Machine Interfaces: Applications in Hand Pose Determination

Thomas B. Calkins

A thesis submitted to the faculty of
Brigham Young University
in partial fulfillment of the requirements for the degree of

Masters of Science

David T. Fullwood, Chair
Anton E. Bowden
Mark B. Colton

Department of Mechanical Engineering

Brigham Young University

June 2011

ABSTRACT

Nanocomposite High Displacement Strain Gauges for use in Human-Machine Interfaces: Applications in Hand Pose Determination

Thomas B. Calkins
Department of Mechanical Engineering
Masters of Science

Conductive nanocomposites are finding many uses as multi-functional materials. One recent development involves the creation of high displacement strain gauges, which have potential applications in a variety of engineering roles. The piezoresistive nature of the gauges makes possible their strain sensing capability. The intent of this research is to show that specific High Displacement Strain Gauges can successfully be used in one human-machine interface application that will demonstrate their potential for a range of other human-machine interface applications. This will be shown in the development of these sensors to accomplish hand pose determination. The flexible and inexpensive gauges are attached to several locations on a glove. It is then shown that by linking this glove with software, the position of the hand can be interpreted into the letters of the American Sign Language alphabet. This use of this nanocomposite sensor establishes the potential for future applications. Issues such as accuracy of response, cyclability, recalibration and reliability are discussed. A design of experiments is accomplished in order to evaluate the effects of modification of the gauges in order to overcome these issues. This work develops the potential of these sensors for use in human-machine interface applications such as computer games, remote controls, robotics, prosthetics and virtual reality applications.

Keywords: nanocomposite, strain, sensor, application, nanostrand

ACKNOWLEDGMENTS

I would like to acknowledge the support and assistance from the following individuals in the development of this research: My Heavenly Father for His support and blessings, My wife Shawnda Calkins for her endless support and motivation, Dr. David Fullwood for his guidance, support and patience, Kevin Cole for his insights and unending assistance, Daniel Shelley, Tommy Hyatt, Oliver Johnson, Tim Johnson, Matt Converse, and Stephen Cluff for their assistance and insights, Nathan Hansen, George Hansen, and Conductive Composites (LLC) for their insights, assistance and materials provided, Dr. Anton Bowden and Dr. Mark Colton for their guidance, and Dr. Carl Sorensen and Dr. Dennis Eggett for their help with the DOE process.

TABLE OF CONTENTS

LIST OF TABLES ..... **vii**

LIST OF FIGURES ..... **ix**

1 Introduction **1**

1.1 What other Sensors are out There? 2

1.2 Biomechanics 5

1.3 Human-Machine Interface Applications 6

1.4 ASL Application: Interpreting Hand-Pose with Sensors on a Glove 6

2 Gauge Construction and Composition **9**

2.1 Previous Work on HDSGs 9

2.2 Composition and Capability 10

2.3 Manufacturing Process 11

2.4 Conductivity of the HDSGs 17

2.5 The Design of Experiments 18

2.5.1 Purpose 18

2.5.2 Set-up 18

2.5.3 Process 23

3 Development of the ASL Interpretation Method **27**

3.1 Hand Pose Measurement 27

3.1.1 Glove Set-up 28

3.1.2 Interpretation into ASL 30

3.1.3 Calibration and Response 32

4 Results **35**

4.1 Design of Experiments 35

4.2 ASL Letter Interpretation 45
4.2.1 Sum of the Differences 45
4.2.2 Machine Learning 48
5 Conclusions & Future Work 51
5.1 Potential for other Bio-Measurement Applications 53
5.2 Potential for Further Use in Human-Machine Interface Applications 53
REFERENCES 57
Appendix A. Design of Experiments Data 61
Appendix B. ASL Letter Interpretation Analysis 71

LIST OF TABLES

Table 1: Other Polymer Composite Sensors 4

Table 2: Design of Experiments Variations 19

Table 3: Previously Tested Volume % Gauge Tests 22

Table 4: Measurement Data for the 8 Statistically Significant Trials in the DOE 25

Table 5: ASL Letter Knuckle Angle Differentiations 29

Table 6: List of Constants for Scaling of Each Trial 41

Table 7: DOE Statistical Evaluation 42

Table 8: Evaluation of DOE 44

Table 9: SD % Accuracy (Left: Independent Data, Right: Data Used for Mean) 47

Table 10: ML % Accuracy (Left: Independent Data, Right: Non-Independent Data) 48

Table A-1: Changes in Length of HDSGs in DOE 69

Table B-1: List of Resistance Values During Formation of Letters A-E 71

Table B-2: Mean Values of Each Letter for Each Gauge 75

Table B-3: Evaluation of Accuracy Using Sum of the Differences 75

LIST OF FIGURES

Figure 1: SEM Image of NNS 10kX (Courtesy of Tim Johnson) 10

Figure 2: SEM EBSD Image of NCCF within Nanocomposite 3kX.....11

Figure 3: Set-up to Cut NCCF 12

Figure 4: Method of Filtering NNS (40 Mesh Screen) 13

Figure 5: Pre-Filtered and Post-Filtered Nanostrands (respectively) 14

Figure 6: Acrylic Mold Surface with Tape Boundaries.....15

Figure 7: Fiberglass Mold Surface - Acrylic Boundaries 15

Figure 8: Vacuum Chamber (Left) and Vacuum Pump (Right) 16

Figure 9: Cut End of NCCF 12kX (Potential Void Formation Surface) 20

Figure 10: Small part of Failure Surface of Nanocomposite HDSG 1629X 21

Figure 11: NNS Filtered with 40 Mesh Screen (Left) and a 60 Mesh Screen (Right) 23

Figure 12: Locations of HDSGs on Hand.....29

Figure 13: Prototype Glove with HDSGs and Connections 30

Figure 14: Lab-View Program to Interpret Resistances with Sum of Differences Equation.31

Figure 15: Resistance Plot of Channel 5 while performing Letter ‘A’ Several Times.....33

Figure 16: Trial 1, Scaled Resistivity over Displacement, Full Test (L), 50-60sec (R) 36

Figure 17: Trial 2, Scaled Resistivity over Displacement, Full Test (L), 50-60sec (R) 37

Figure 18: Trial 3, Scaled Resistivity over Displacement, Full Test (L), 50-60sec (R) 37

Figure 19: Trial 4, Scaled Resistivity over Displacement, Full Test (L), 50-60sec (R) 38

Figure 20: Trial 5, Scaled Resistivity over Displacement, Full Test (L), 50-60sec (R) 38

Figure 21: Trial 6, Scaled Resistivity over Displacement, Full Test (L), 50-60sec (R) 39

Figure 22: Trial 7, Scaled Resistivity over Displacement, Full Test (L), 50-60sec (R) 39

Figure 23: Trial 8, Scaled Resistivity over Displacement, Full Test (L), 50-60sec (R) 40

Figure 24: Trial 1, Manual Measurement (Displayed in KiloOhms).....40
Figure 25: Plastic Deformation Causing Compression in HDSG Test.....43
Figure 26: 3-Dimensions of 12-D Resistivity Space, Showing 5 Letter Groups.....46
Figure 27: Another View of Same 3-D Space (A=Rd, B=Gr, C=Bl, D=Mg, E=Bk).....46
Figure 28: Machine Learning Plot of Accuracy of Letter 'E' (Larger X = Greater Error).....49
Figure A-1: Resistivity & Displacement Plots of Trial 1 Test of 200 Cycles 61
Figure A-2: Resistivity & Displacement Plots of Trial 2 Test of 200 Cycles 62
Figure A-3: Resistivity & Displacement Plots of Trial 3 Test of 200 Cycles 63
Figure A-4: Resistivity & Displacement Plots of Trial 4 Test of 200 Cycles 64
Figure A-5: Resistivity & Displacement Plots of Trial 5 Test of 200 Cycles 65
Figure A-6: Resistivity & Displacement Plots of Trial 6 Test of 200 Cycles 66
Figure A-7: Resistivity & Displacement Plots of Trial 7 Test of 200 Cycles 67
Figure A-8: Resistivity & Displacement Plots of Trial 8 Test of 200 Cycles 68
Figure A-9: Screen-Shot from Cyclic Load Testing (40% Strain, 10 Cycles) 69
Figure B-1: Machine Learning Evaluation of Letter A (Independent Data Set) 80
Figure B-2: Machine Learning Evaluation of Letter B (Independent Data Set).....81
Figure B-3: Machine Learning Evaluation of Letter C (Independent Data Set).....82
Figure B-4: Machine Learning Evaluation of Letter D (Independent Data Set) 83
Figure B-5: Machine Learning Evaluation of Letter E (Independent Opposite Data Set) 84

1 INTRODUCTION

Each year computer processing capabilities make leaps and bounds, which improves our quality of life in numerous ways. However, the speed of our interaction with computers, in many instances, is limited by the speed of typing. One way of increasing this interaction speed is to enable the computer to interpret our motion by means of sign language. This would also improve accessibility of communication to many people who use sign language (ASL being the 4th most used language in the USA[1]). This thesis intends to introduce a whole new technique in Human-Machine Interface (HMI) by interpreting finger pose using high elongation strain sensors. They offer a superior HMI methodology in many ways to current HMI tools used in this area due to their flexibility, instantaneous response, and accuracy. These high elongation strain sensors (or high displacement strain gauges) are nanocomposite devices which measure displacement based on changes in resistance which occur in the sensors when they are strained. Some of the drawbacks of the current gauges include a limited number of cycles from un-stretched to stretched positions (~100 cycles), as well as the current thickness of the gauges (~1 mm) which limits motion and increases potential for void formation. The design of experiments discussed later in this paper will address these issues.

1.1 What other Sensors are out There?

These nanocomposite high displacement strain gauges (HDSGs) are not the only gauges available to sense large changes in strain, but they do sense a much higher strain than most [2, 3]. Noting this, it is important to also recognize that developments of HMI technologies are growing with the rest of technology [4, 5]. As computers have become less and less expensive, and more people are gaining access to that technology, more methods of communication between humans and machines are appearing.. This is mostly due to the desire of Consumers to have greater functionality with their technology [6]. The nanocomposite strain gauges provide a new method to increase functionality for HMI applications.

The field of HMI applications includes a variety of different devices. These primarily deal with the interaction between humans and machines. Some common devices that fit into this spectrum are the computer keyboard, mouse, joystick, game controller, and remote controller among many others. Some which may not be as familiar are haptic interface devices, virtual reality systems, mechanical linkages, and pressure sensitive controls among many others [7]. More specifically, there are the parts of these devices that actually measure the interaction. Such as the keys on the keyboard that cause different electrical signals to be sent to the computer depending on which key (or combination of keys) which are pressed. Similarly, the HDSGs act as a device that can be used to measure high displacement in a variety of applications. Such as computer games, remote controls, robotics, prosthetics and virtual reality systems. Essentially it acts as a sensor to be used for many different purposes.

There are many HMI sensors currently available. These include pressure sensitive buttons, carbon composite bending sensors, force sensors, carbon/polymer bend sensors, conductive paste sensors and others [2, 8-14]. A great deal of research has been done using these

different sensors in pressure sensitivity and vibration, but very little has been done towards high strain measurements (See Table 1). Carvahlo & Radwin demonstrate the use of conductive polymer sensors to measure force changes in compression based on the changes in resistance of their Interlink Electronics sensor [10]. Ventrelli & Beccai developed a carbon black epoxy sensor for compression and shear strain measurements [2]. Aldraihem analyzed the use of carbon black epoxy as a polymer paint sensor for vibration analysis [14]. Zhang characterized the effects of bending in a carbon black epoxy sensor [11]. Biddiss & Chau, in their study of sensors for use in hand prosthesis, did a comparison of biomimetic sensors which show capabilities in vibration, bending, and even strain (up to 10-20%) [9]. Among all of these there is significant research in conductive nanocomposite sensors, but very few sensors have capability in high strain measurement. One of the biomimetic sensors (polypyrrole) which is capable of strain shows similar capabilities to the HDSGs. They claim that it has a "dynamic range ten times that of conventional strain gauges," which comes out to be around 10-20% strain [9]. So here we have a sensor capable of tracking high strain. Another gauge capable of high strain, that is closer to the HDSGs used in this research, is a carbon black in polyisoprene sensor [13]. Knite characterized the capabilities of these sensors in measuring vibration, compression, and strain (up to 40%) [13]. With limited possibilities available this research supports the fact that the HDSGs are a valid high strain sensor that can be used in HMI applications. The Nickel nanocomposite strain gauges used in this research can reach strains up to 60% with a measurable resistance change, which provides an easy method to measure change in length unique to polymer composite gauges. The HDSGs increase functionality for HMI applications by providing another high strain measurement device along with this increase in strain capability.

Table 1: Other Polymer Composite Sensors

Sensor Type	Function/use	Comments	Author Reference
Conductive Polymer Sensors	Compression	Reacts Similar to HDSGs in Compression	Carvahlo, Radwin
Carbon Black in epoxy	Bending	14-19% CB by mass, put on Transparency films	W. Zhang, et. al.
Carbon Black in epoxy	Vibration & Noise	Thin Film application	O. Aldraihem, et. al.
Carbon Black in Silicone	Pressure & Shear Strain	14% shear strain	Ventrelli, Beccai
Polypyrrole	~10-20% strain	Biomimetic, biocompatible	Biddiss, Chau
Polyvinylidene Flouride	Vibration	Biomimetic, Contact Sensor	Biddiss, Chau
Carbon Black in Polyisoprene	Up to 40% strain	Very similar to HDSGs	M. Knite, et. al.

In recent news in the gaming industry, motion tracking through video-sensing has improved enough for use [6]. Microsoft has developed an infra-red scanning device to allow Xbox 360 users to play games without any controller (Microsoft Kinect). This device uses two infra-red scanners and an RGB camera to map out the individual, the room they are in as well as interpret their motion for game play. Interestingly enough, this technology is not very different from optical marker tracking, which is commonly used in biomechanics research [15-22]. Optical marker tracking is very effective and accurate but it is not the only way of accomplishing biomechanical measurement. The nanocomposite strain gauges supply an inexpensive alternative, and provide accuracy within 10% of optical marker tracking [23]. The major difference between optical marker tracking and Microsoft Kinect is that in optical marker tracking there are markers placed on the subject which two or more video cameras will track. These precise videos are then interpreted by computer software. On the other hand, with Kinect

there are no markers. Microsoft spent a great deal of time and research into tracking a variety of people and interpreting their bone structure, regardless of shape and clothing worn, so that this technology could be used for Microsoft's gaming systems [6]. Although this gaming system is somewhat revolutionary, it will not be as accurate as optical marker tracking due to the proximity of the cameras to the individual, and, more importantly, the limit of 30 frames per second of the Microsoft Kinect cameras. On the other hand with the HDSGs, there are applications in which they would have clear advantages over both optical marker tracking as well as Microsoft Kinect. One example of this is robotic surgery, where a robot would follow the direct motions of the surgeon while the surgeon is miles away. Although it is not quite there yet, a disposable pair of these gloves could be connected to a laptop with a program to interpret the motion of the surgeon's hands, which would then be transferred to the robot in the hospital. The surgeon would see the motion of the robot actually making the precise cuts via cameras mounted on the robot and would be able to perform the surgery in the same mannerisms that they would normally use. The accuracy would be closer than with Kinect and it would not need additional video-cameras, markers or a specific backdrop in order to accurately read the motions. This is just one example of a potential use for this type of HMI technology.

1.2 **Biomechanics**

Before focusing on the specific application of Hand-Pose determination through ASL interpretation, a broader look at the potential of these HDSGs will be overviewed. Previous research has been done which has shown the effective use of these HDSGs as a gauge to measure the displacement in cow ligaments, opening the door for use as a biomechanical sensor [23]. The primary reason for the success of these gauges in biological applications, including biomechanics, is its high strain measurement capability. Many applications in biomechanics

need high displacement measurements in order to cover their full range of motion. This HDSG will measure up to 40% strain displacement with a reasonable degree of accuracy. Although the accuracy may need to be improved for some applications, it is not beyond the scope of others. There is great potential for further use here.

1.3 **Human-Machine Interface Applications**

Just as the ligament strain measurement has opened the opportunity for further exploration in biomechanics, this ASL interpretation will open opportunity for further exploration within HMI applications. Human-machine interface sensors, applied to hand motion tracking, is an application which has been getting more attention [8, 9, 15, 19, 22]. Using the nanocomposite strain gauges will provide a potential inexpensive and accurate alternative. More specifically here, however, it gives a new method to measure hand pose. This should allow more opportunity for growth in the use of these gauges for other HMI applications.

1.4 **ASL Application: Interpreting Hand-Pose with Sensors on a Glove**

Though this sounds wonderful, the HDSGs are still in the early stages of development. There is still enough noise in the signal output that hinders the gauges from giving precision motion, thus limiting its capabilities. For example, a 0.25 cm motion of the end of one's finger which may take only 5 degrees of motion change at the knuckle is very difficult to recognize as a specific resistance. It may be possible to measure the range of the resistance that it will fall within but not the specific resistance value. Further optimization of the gauges will be done in the future. At this point in the development of the HDSGs it will be shown that the resistance range reading from the gauge can be used in order to measure hand pose.

This will be done by attaching gauges to the knuckles of a glove and measuring the resistance change across the gauges. As the hand is put in the position of an ASL alphabetical letter the resistances can be read into a computer and the letter identified by the computer as the correct ASL letter. The process by which this is accomplished will be discussed in further detail in the applications section of this paper.

What is accomplished by this research is the development and application of HDSGs for use in ASL interpretation. Encompassed within this research is the optimization of a manufacturing process of HDSGs for this application, design of the machine interface system to suit ASL, calibration of the prototype in order to compensate for degradation of the gauges and unique user characteristics, mapping of the space within ASL and optimizing the control of that space, and introducing machine learning techniques to this work to show its future potential.

The application of direct translation of ASL to the computer will open the door to numerous new HMI techniques for these HDSGs in the areas of simulation, virtual reality, bio and robotic applications, and will generally accelerate the interface between humans and machines.

2 GAUGE CONSTRUCTION AND COMPOSITION

2.1 Previous Work on HDSGs

There has been significant work accomplished in developing these HDSGs prior to their use in this research. The primary element of the HDSGs is the nickel nanostrands (NNS) which were developed and manufactured by Conductive Composites L.L.C. [24]. Gardner and Johnson analyzed the piezoresistive nature of these NNS mixed in a polymer matrix [25, 26]. The effectiveness and optimization of these nanocomposites for strain measurement was analyzed further by Johnson [27]. The chopped nickel-coated carbon fiber (NCCF) was added to stabilize the resistivity profile output in strain measurement plots. It provided a better conductive path through the nanocomposite. So, with a greater understanding of the HDSGs, a model of their piezoresistive nature, based on percolation theory and quantum tunneling, was developed by Johnson and Fullwood [28-30]. Further characterization in voltage contrast microscopy and exploration in measuring ligament strain using the HDSGs was accomplished by Hyatt [31]. This previous research has opened the window for development of these HDSGs for many other applications and further research. Thus this research develops the HDSGs for applications in hand pose determination, exposing them to the field of human-machine-interfaces.

2.2 **Composition and Capability**

These gauges are currently capable of measuring strains up to 60%, thus showing great promise as HDSGs [23, 26]. The gauges which currently give the best properties are composed of three ingredients: silicone rubber, nickel nanostrands and chopped nickel-coated carbon fibers, (See Figures 1 & 2). The NNS are created by Conductive Composites L.L.C. through a proprietary chemical vapor deposition process. The NCCF are also produced and donated by Conductive Composites L.L.C. The three ingredients are mixed together using a planetary centrifugal mixer within the cure time of the silicone. This silicone rubber (Sylgard 184) is the matrix that holds the nanocomposite conductive reinforcements together, the nickel nanostrands are what carry the electrical current through the composite, and the nickel coated carbon fibers stabilize the resistance curve while the nanocomposite is stretched, as well as supporting the current flow within the gauge [26].

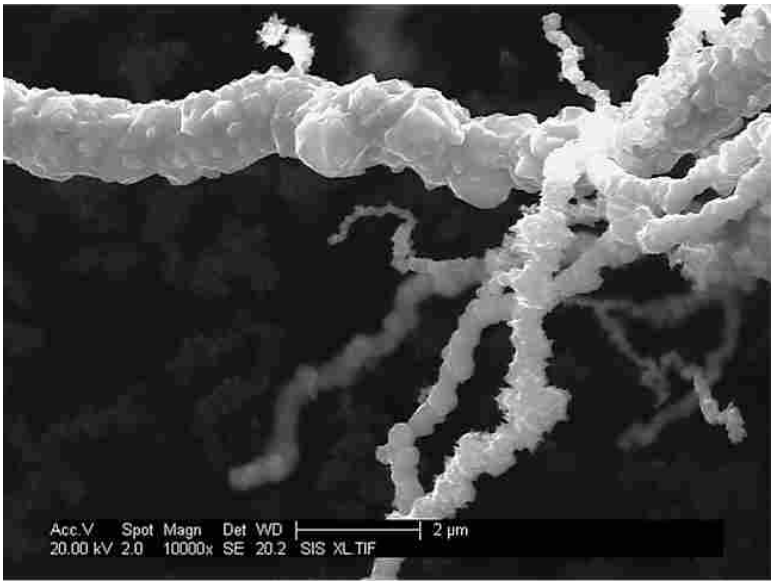

Figure 1: SEM Image of NNS 10kX (Courtesy of Tim Johnson)

The cured nanocomposite material will yield a specific resistance when a voltage passes through it (10–1,000,000 Ω depending on the mix ratios). Then when the material is stretched, the change in resistance will follow a repeatable curve which will measure above 40% strain before failure, sometimes reaching 60% [27]. Hyatt has shown that accurate strains can be measured along this curve with less than 10% error [23].

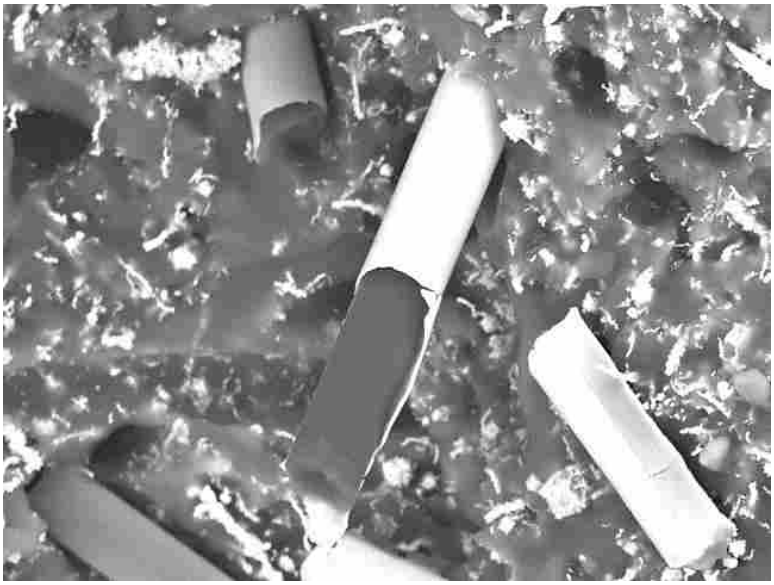

Figure 2: SEM EBSD Image of NCCF within Nanocomposite 3kX

2.3 **Manufacturing Process**

In order to produce these HDSGs there are several steps that need to be accomplished. There is also a great deal of variability that can be experimented with, in the manufacturing process, which will be discussed further in the design of experiments section of this paper. The steps to manufacture the primary gauges used in this research begin with the NCCF. The NCCF that was used in this research has 20 weight percent Nickel coating the carbon fibers. Using these

fibers, they are then cut to 2mm lengths (typically using a rotary cutter, a ruler and wetted with Isopropyl alcohol to keep them contained, See Figure 3).

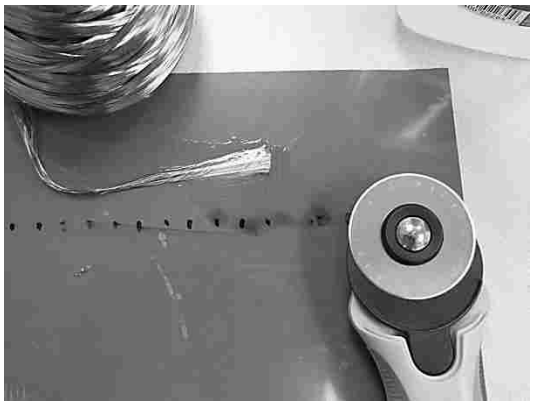

Figure 3: Set-up to Cut NCCF

Once the NCCF is dried the appropriate amounts can be weighed for mixture with the Silicone. These amounts are determined using the desired output volume (V in cubic centimeters) along with the appropriate amounts of NNS, calculated using the following properties and equations (See below).

Density of Ni (ρ_{Ni})= 8.9 g/cc [32]

Density of Carbon Fiber (ρ_{cf}) = 1.78g/cc [32]

Density of Sylgard 184 Silicone Elastomer (ρ_{Si}) = 1.03g/cc [33]

Volume % of NNS = 9%

Volume % of NCCF = 3%

$$\boldsymbol{Volume\ \%\ of\ Ni\ in\ NCCF} = \frac{\mathbf{100} \times \frac{\mathbf{20}}{\boldsymbol{\rho_{Ni}}}}{\frac{\mathbf{20}}{\boldsymbol{\rho_{Ni}}} + \frac{\mathbf{100-20}}{\boldsymbol{\rho_{cf}}}} = \mathbf{4.75}\% \quad \textbf{(1)}$$

NCCF Density: $\boldsymbol{\rho_{NCCF}} = \mathbf{8.9} \times \frac{\mathbf{20}/\boldsymbol{\rho_{Ni}}}{\frac{\mathbf{20}}{\boldsymbol{\rho_{Ni}}} + \frac{\mathbf{100-20}}{\boldsymbol{\rho_{cf}}}} + \mathbf{1.78} \times \frac{(\mathbf{100-20})/\boldsymbol{\rho_{cf}}}{\frac{\mathbf{20}}{\boldsymbol{\rho_{Ni}}} + \frac{\mathbf{100-20}}{\boldsymbol{\rho_{cf}}}} = \mathbf{2.119}\boldsymbol{g/cc}$) **(2)**

$$\boldsymbol{Weight\ of\ NNS = V(cc) * \frac{9}{100} * \rho_{Ni}} \quad \textbf{(3)}$$

$$\boldsymbol{Weight\ of\ NCCF = V(cc) * \frac{3}{100} * \rho_{NCCF}} \quad \textbf{(4)}$$

$$\boldsymbol{Weight\ of\ Silicone = \left[V(cc) - \left(V(cc) * \frac{9}{100}\right) - \left(V(cc) * \frac{3}{100}\right)\right] * \rho_{Si}} \quad \textbf{(5)}$$

Using these equations to determine the appropriate weights, the NNS then need to be screened through a 40 mesh wire screen (typically done using a glass rod). When the NNS are made by Conductive Composites they are in a 'cake' form that needs to be blended into smaller clusters, which they do prior to distribution. However, these smaller clusters are still too large to create a good distribution of NNS within the nanocomposite gauge. By forcing the NNS through the 40 mesh screen it breaks up the NNS further, into strands that will distribute very well in the silicone matrix (See Figure 4 & Figure 5).

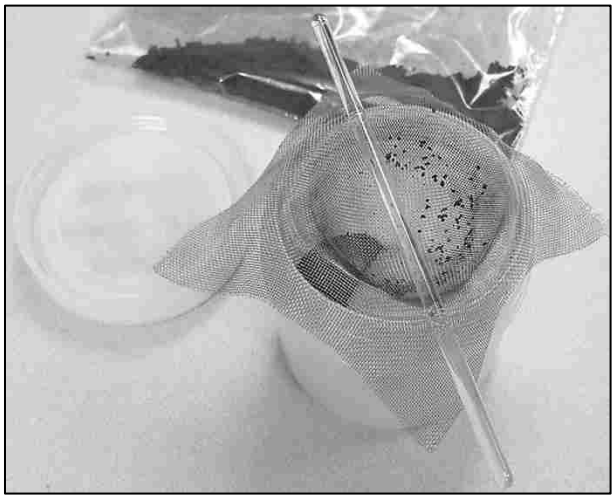

Figure 4: Method of Filtering NNS (40 Mesh Screen)

Once this is done the actual mixture of the elements can be accomplished. The silicone comes as a two-part elastomer using 10 parts base with 1 part catalyst (by weight). So, the weight of the silicone calculated in Equation (2-5) is separated by 1/11 catalyst and 10/11 base.

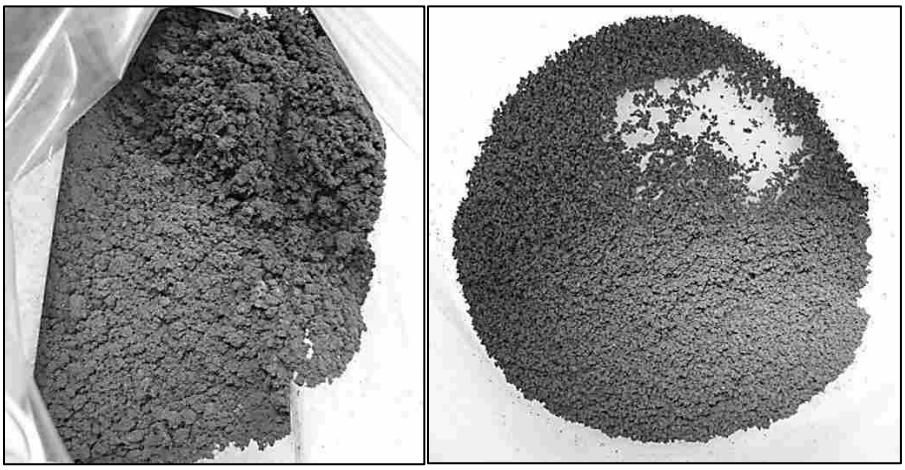

Figure 5: Pre-Filtered and Post-Filtered Nanostrands (respectively)

The measured amounts of silicone base and the chopped NCCF are mixed together using a THINKY ARM-310, THINKY Corporation, Tokyo. centrifugal mixer until the NCCF are fully wetted (which usually only takes 30 seconds in the mixer). Sometimes the chopped NCCF clump together, so if there are still clumps after mixing in the THINKY, it is then mixed by hand with a glass rod to break the clumps up again. This process of mixing is repeated until there are no recognizable clumps of NCCF. Then the measured amounts of filtered NNS and silicone catalyst are added and the mixture is mixed again in the THINKY to distribute and fully wet the NNS. If the NNS are not fully wetted, Methyl-Ethyl-Keytone solvent is added to thin the sample. MEK nearly always needs to be added at this point in order to lower the viscosity of the solution enough to pour it into a mold, even if the NNS are fully wetted. Once the silicone catalyst has been added there is less than 2 hours of working time before the sample will have

begun setting [33]. The next steps need to be done within that timeframe. The mixture is then spread out onto a smooth mold surface (such as an acrylic or fiberglass sheet) with boundaries lining the mold section (such as tape) in order to spread the mixture to the correct thickness (See Figure 6 & Figure 7). This mold surface with boundaries creates the initial volume calculated in cubic centimeters discussed earlier.

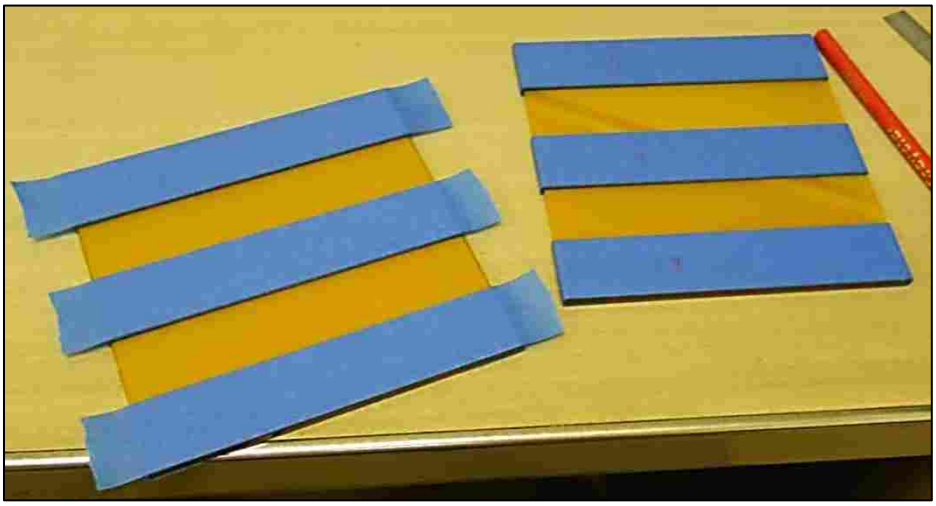

Figure 6: Acrylic Mold Surface with Tape Boundaries

Figure 7: Fiberglass Mold Surface - Acrylic Boundaries

With the composite mixture laid out on the mold it is placed inside a vacuum chamber in order to decrease the amount of porosity of the sample. The vacuum chamber is then pulled down to full vacuum (500mmHg) several times, using a 10CFM vacuum pump, in order work the bubbles out of the samples (See Figure 8). Following this, the samples are allowed to cure for over 48 hours at room temperature, for 45 minutes at 100˚C, for 20 minutes at 125˚C, or for 10 minutes at 150˚C. Following this cure time the gauges are then ready to be cut to the appropriate size using a razorblade. These gauges are then ready for use as a strain measurement device, although there is some minor initial stress relaxation in the gauges over the first few cycles before the length will stretch and return to its initial length (See Design of Experiments in Results Section 4.1). So, the gauges normally need to be stretched a few times to the desired displacement prior to actual use.

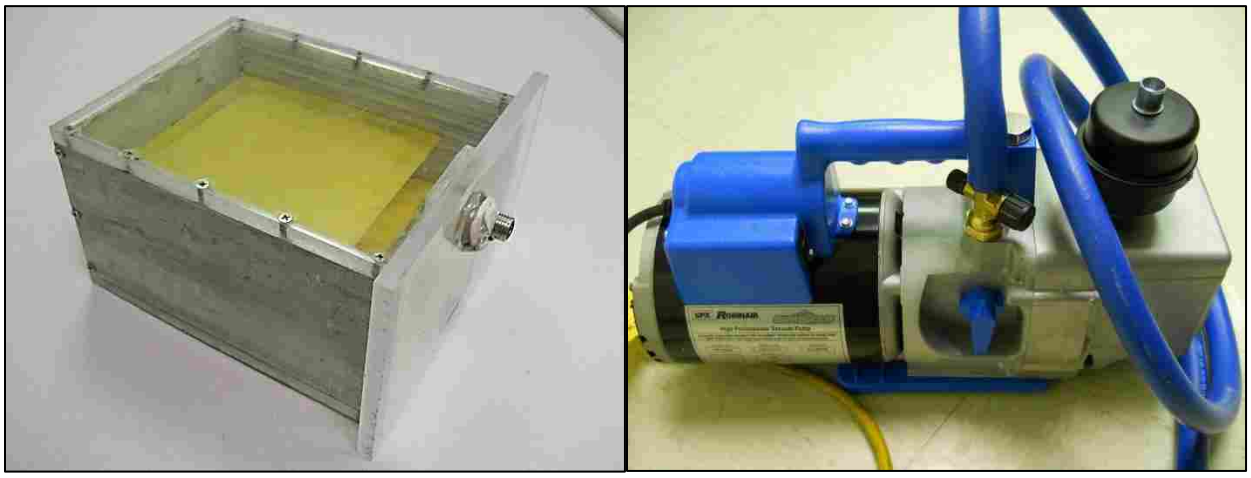

Figure 8: Vacuum Chamber (Left) and Vacuum Pump (Right)

2.4 **Conductivity of the HDSGs**

When a typical metallic strain gauge is stretched, the resistance increases because of the decrease in cross-sectional area of the conductive path. However, the nanocomposite strain gauge, due to its particular piezoresistive nature, has the opposite reaction [26]. When it is strained the resistance decreases. This is due to the method by which the voltage conducts across the HDSG. The nanostrands are separated on all sides by a thin layer of silicone, which would act as an insulating barrier to electrical conductivity, except that in this case voltage does actually pass through these barriers due to an effect called Quantum Tunneling [34-36]. When the nanocomposite gauge is stretched, the silicone which separates some of the nickel nanostrands, undergoes Poisson thinning. As one might expect, the thinner barriers offer less resistance to the transferring of voltage via this Quantum Tunneling phenomenon. This concept is the reason for the decrease in resistance with the increase in strain. This resistivity profile which follows the changes in strain can be modeled using percolation theory [27]. This is very helpful in understanding the micromechanics of these gauges but will not be covered further within this paper.

In order to better understand the potential of these gauges, this chapter will focus more on the material property improvement possibilities in order to improve potential use as a HMI sensor. One aspect of this is taken up in the design of experiments (DOE) which will evaluate the potential improvements of these gauges statistically.

2.5 **The Design of Experiments**

2.5.1 Purpose

This nanocomposite strain gauge appears to be just as versatile (or more versatile) than any of the current high displacement measurement methods currently available. They are capable of real-time measurement, and in many cases are more cost effective than other methods [23]. However, there is need for improvement of the current gauges capabilities. As discussed in the introduction the gauges currently are not capable of much more than 100 cycles from 0% strain to 20% strain. Also mentioned in the introduction was the fact that the gauges are currently fairly thick (1mm). Producing thinner gauges would allow for more versatility in the use of these gauges due to the decreased amount of material used and the increased flexibility of the gauges with thinner cross-sections. To properly evaluate the gauges a DOE was accomplished in order to see which potential changes in the creation process would make the largest improvements to the cyclic loading and allow for thinner samples. Within the DOE there are several dependent variables that will be monitored for changes during the cyclic load tests. These include: resistivity, cycles to failure, change in resistivity during cyclic testing, and changes in gauge factor.

2.5.2 Set-up

The statistical DOE was set up with eight test mixtures using a 2^{6-3} method which was then randomized (See Table 2). The six variables being considered were the percent NNS by volume, the percent NCCF by volume, the length of the NCCFs, the filter screen size used to give more uniform animal size to the NNS, the choice of adding Silicone Primer to the NNS &

NCCF, as well as the end thickness of the sample. Two values were chosen for each of these variables to allow for measurable variation in the gauge material properties (See Table 2).

Table 2: Design of Experiments Variations

Trial	% Nanostrands	% Carbon Fiber	Length of Strands	Filter Size	Silicone Primer (Y/N)	Thickness
1	11% by Volume	3% by Volume	0.5 mm	60 mesh	Yes	1.0 mm
2	9% by Volume	5% by Volume	0.5 mm	60 mesh	No	0.5 mm
3	9% by Volume	5% by Volume	2 mm	40 mesh	Yes	1.0 mm
4	9% by Volume	3% by Volume	2 mm	60 mesh	Yes	0.5 mm
5	11% by Volume	5% by Volume	0.5 mm	40 mesh	Yes	0.5 mm
6	9% by Volume	3% by Volume	0.5 mm	40 mesh	No	1.0 mm
7	11% by Volume	3% by Volume	2 mm	40 mesh	No	0.5 mm
8	11% by Volume	5% by Volume	2 mm	60 mesh	No	1.0 mm

Performing only eight tests tends to limit the statistical outcome of the design of experiments, but it does allow for general trends to be determined based on the 6 different variables. With the primary purpose of this design of experiments to improve usability and durability of the gauges, a few theories were put into the design of experiments in order to improve the HDSGs. These theories directed the choices of what properties to vary. The ranges were determined from manufacturing process experience and the desire for each of the gauges to function.

One of these theories concerned decreasing void formation and eventual failure of the HDSGs. In any short fiber composite material there is potential for void formation at the end of the fibers (See Figure 9). This is primarily due to strain within the composite. When the nanocomposite material is strained there is almost no stretching of the NCCFs relative to the silicone around them. The NCCF is the larger potential proponent of this failure mode due to the increased size and stiffness of the NCCF over the NNS (See Figure 10). The greater the number of cycles, and the further the gauges are stretched, the more voids will form. After these voids

have formed, they will become larger and then connect with other voids. This weakens the electrical contact and, eventually, causes complete failure of the gauge such as the gauge in Figure 10. In an effort to evaluate the effect of this potential void formation, one of the variations used in the DOE was to shorten the lengths of the nickel coated carbon fibers. This will allow for more stretching of the silicone and lower internal stresses created by the fibers.

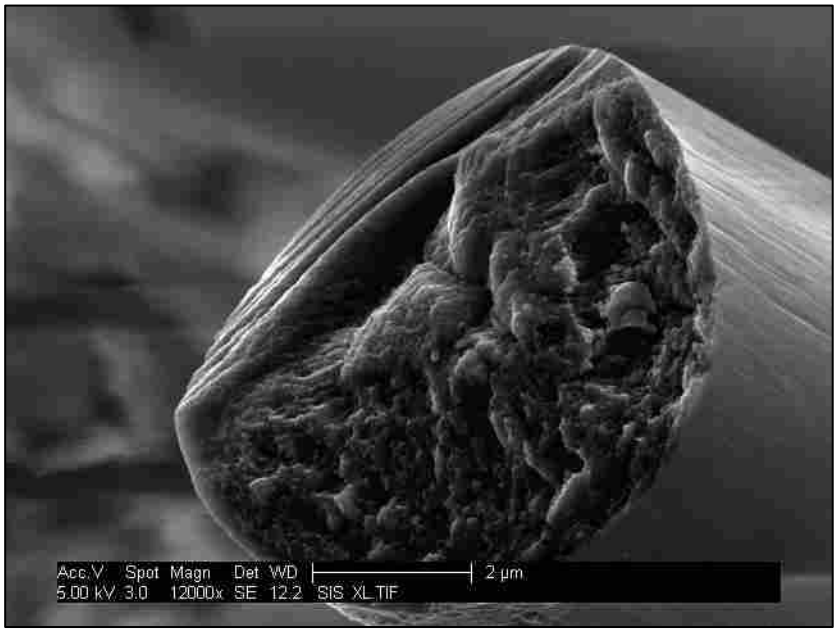

Figure 9: Cut End of NCCF 12kX (Potential Void Formation Surface)

Using 0.5mm long fibers instead of 2mm long fibers will adequately show the difference in endurance of the sample under cyclic loading and will determine if this failure mode is the primary failure mode in the composite. However, along with this decreased internal stress there is also decreased conductivity in the disconnected 0.5mm lengths of fiber versus the 2mm fibers. The 2mm long NCCF allow a more effective voltage connection between NNS groupings. This loss will hopefully be taken up in the increased NCCF in the tests with 5% NCCF instead of 3%.

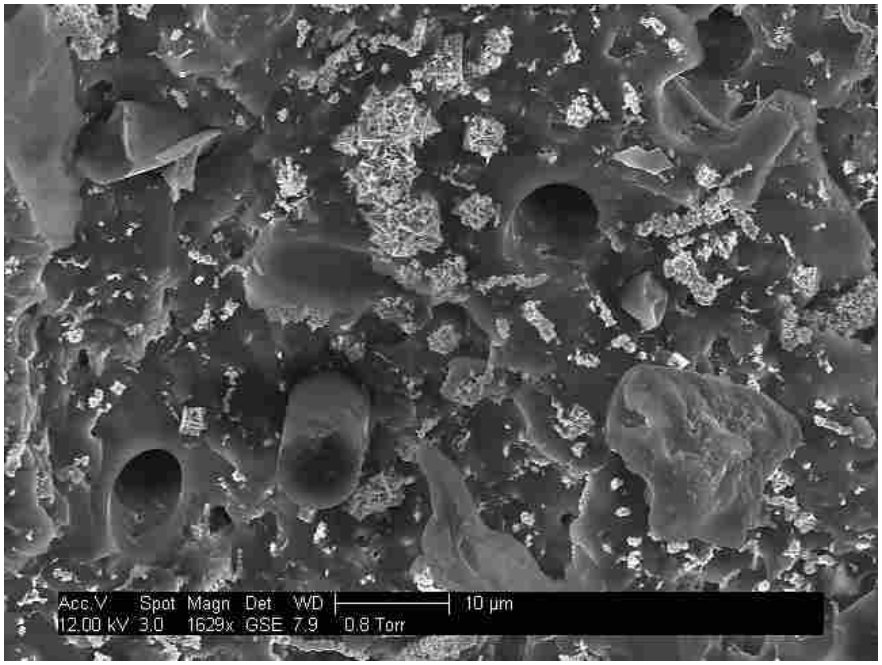

Figure 10: Small part of Failure Surface of Nanocomposite HDSG 1629X

Another important modification to the gauges is the macro-physical shape. The current gauge thickness is approximately 1mm. Using this thick of a gauge when measuring high displacements can create unnecessary inaccuracy in strain measurement for ductile samples. The major source of error caused by using a thick strain gauge comes when the silicone gauge adds stiffness to the sample it is attached to, thus increasing the load capacity of the sample. When this is the case, the reading of the gauge will be measurably lower because of the added support that the gauge is giving to the sample. In order to evaluate the effects of reducing this inaccuracy (as well as reducing the manufacturing cost of the gauges), varying the thickness of the HDSGs was added as another factor in the DOE.

Testing of different volume percentages of the components of the gauge material has already been done (See Table 3) but a true statistical distribution has not been accomplished [27]. These were primarily done in order to find the biggest change in resistivity between the strained

and unstrained positions as well as the clearest resistivity vs. strain path. This testing is what led to the choice of volume percentages of 9% Nickel nanostrands, 3% nickel coated carbon fiber, and 88% silicone rubber. The goal of the DOE, on the other hand, is to determine what manufacturing process parameters and strain gage composition changes will have the greatest effect on the strain gage properties. Using this data we will be able to focus on modifying these properties which have the greatest effect on increasing the cyclic loading capability of the nanocomposite gauge.

Table 3: Previously Tested Volume % Gauge Tests

% NNS	7	7	7	7	9	9	9	11	11
% NCCF	1	2	3	4	1	2	3	1	2
% Silicone	92	91	90	89	90	89	88	88	87

The variation in mesh size will allow better understanding of the role of the NNS in the nanocomposite sensor. The mesh size minimizes Nickel nanostrand cluster size. The holes in the 60 mesh screen are approximately half the size of the holes in the 40 mesh screen (See Figure 11).

The last variability in the DOE is the use of silicone primer (Octamethyltrisiloxane) to assist in adhesion of the curing silicone to the NNS and NCCF. Silicone does not stick to objects very well. In fact your typical silicone bathroom caulk does not stick to the tile, plastic, or porcelain, but flows very well into cracks and hold itself in the elastomeric shape that it is put in prior to curing and doesn't really stick to anything but itself. The benefit is that it fills in the cracks and gaps well enough to keep other moisture from getting into those spaces. The question then, is whether this material property of silicone is a major reason why the HDSGs fail in such a small number of cycles or not.

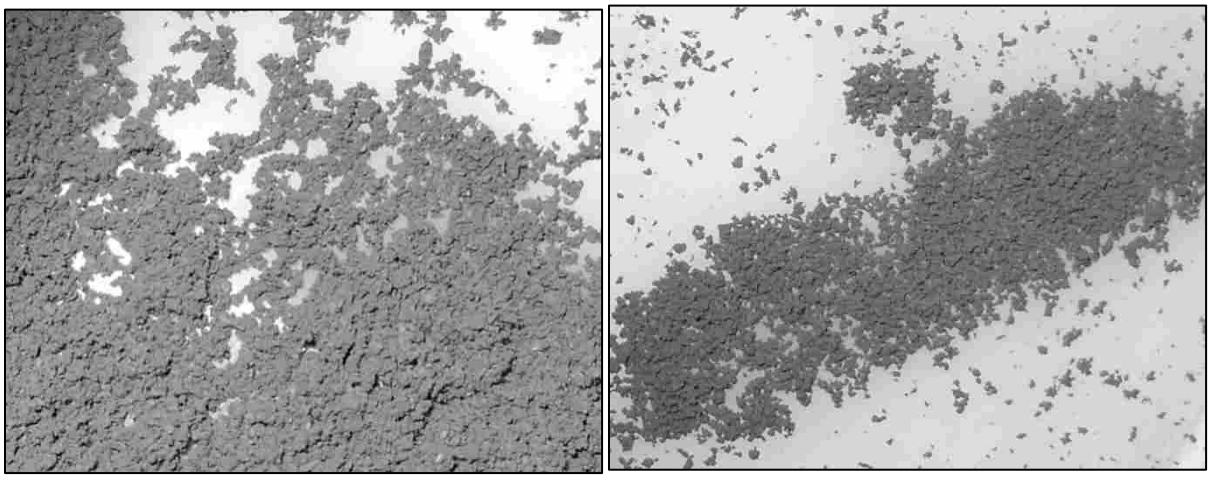

Figure 11: NNS Filtered with 40 Mesh Screen (Left) and a 60 Mesh Screen (Right)

The silicone primer (manufactured by Dow Corning, who also manufactures Sylgard 184 silicone) is applied to the surface that one wishes to adhere the silicone to and allowed to dry. Then this prepared surface is coated with curing silicone which will cure to this prepared surface, rather than just to itself. The effectiveness of the silicone primer on micro and nano-sized particles is yet to be seen, but will be evaluated in the testing done in the DOE as well.

2.5.3 Process

The process followed for the experiment is as follows (for the specific measurements and weights See Table 4):

Step 1: Filter correct amounts of dry NNS using 60 mesh and 40 mesh screens appropriate per test and set aside (See Table 4).

Step 2: Weigh out correct lengths of NCCF (2mm or 0.5mm) into 8 separate 150ml mixing containers.

Step 3: For Silicone Primer Samples: Pour NCCF into individual metal dishes.

Step 4: For Silicone Primer Samples: Weigh out amounts of filtered NNS into individual metal dishes (See Table 4).

Step 5: For Silicone Primer Samples: Soak NCCF in each of the metal dishes & NNS in each of the metal dishes with Silicone Primer underneath a Fume Hood.

Step 6: For Silicone Primer Samples: Let NCCF & NNS dry underneath the Fume Hood.

Step 7: For Silicone Primer Samples: Put NCCF into correct 150ml mixing containers.

Step 8: Add measured amounts of Silicone Base and Catylist to NCCF for each of the 8 samples (See Table 4).

Step 9: Mix each sample in THINKY centrifugal mixer for 30 seconds.

Step 10: Mix each sample by hand with a glass rod, as necessary, in order to break up clusters of NCCF into Silicone.

Step 11: Repeat steps 9 through 10 as many times as necessary in order to obtain full dispersion of the NCCF into the Silicone base.

Step 12: For NON-Silicone Primer Samples: Weigh out amounts of filtered NNS (See Table 4).

Step 13: Add NNS to appropriate containers.

Step 14: Mix each of the 8 samples in THINKY centrifugal mixer for 15 seconds.

Step 15: Mix each sample by hand with a glass rod, as necessary, in order to break up clusters of NNS into Silicone mixture.

Step 16: Add small amounts of Methyl Ethyl Keytone (MEK) solvent, as necessary, in order to thin out sample. (Note: Use Ventilated area when working with MEK solvent.)

Step 17: Repeat Steps 14 through 15 as necessary to get NNS fully distributed and Repeat Step 16 as necessary to obtain a pourable mixture.

Step 18: Pour out onto Acrylic surfaces between taped sections with correct depths.

Step 19: Use Razor-blade to level mixtures on Acrylic plates.

Step 20: Put all plates in Vacuum chamber and pull trials to full vacuum several times in order to work out porosity in test samples.

Table 4: Measurement Data for the 8 Statistically Significant Trials in the DOE

Trial 1		Trial 2		Trial 3		Trial 4	
% nanostrands	11% by Volume 3.17 grams	% nanostrands	9% by Volume 1.29 grams	% nanostrands	9% by Volume 2.59 grams	% nanostrands	9% by Volume 1.29 grams
% carbon fiber	3% by Volume 0.2 grams	% carbon fiber	5% by Volume 0.17 grams	% carbon fiber	5% by Volume 0.34 grams	% carbon fiber	3% by Volume 0.1 grams
Length of strands	0.5 mm	Length of strands	0.5 mm	Length of strands	2 mm	Length of strands	2 mm
filters	60 Gauge	filters	60 Gauge	filters	40 Gauge	filters	60 Gauge
Silicone Primer Coating NiNS & Fiber?	Yes	Silicone Primer Coating NiNS & Fiber?	No	Silicone Primer Coating NiNS & Fiber?	Yes	Silicone Primer Coating NiNS & Fiber?	Yes
Thickness	1.00 mm	Thickness	0.50 mm	Thickness	1.00 mm	Thickness	0.50 mm
Silicone	2.86 grams	Silicone	1.43 grams	Silicone	2.86 grams	Silicone	1.46 grams
- Base	2.60 grams	- Base	1.30 grams	- Base	2.60 grams	- Base	1.33 grams
- Catylist	0.26 grams	- Catylist	0.13 grams	- Catylist	0.26 grams	- Catylist	0.13 grams
Expected Surface Area:	25.4 mm Wide 127 mm Long	Expected Surface Area:	25.4 mm Wide 127 mm Long	Expected Surface Area:	25.4 mm Wide 127 mm Long	Expected Surface Area:	25.4 mm Wide 127 mm Long
Trial 5		**Trial 6**		**Trial 7**		**Trial 8**	
% nanostrands	11% by Volume 1.58 grams	% nanostrands	9% by Volume 2.59 grams	% nanostrands	11% by Volume 1.58 grams	% nanostrands	11% by Volume 3.17 grams
% carbon fiber	5% by Volume 0.17 grams	% carbon fiber	3% by Volume 0.2 grams	% carbon fiber	3% by Volume 0.1 grams	% carbon fiber	5% by Volume 0.34 grams
Length of strands	0.5 mm	Length of strands	0.5 mm	Length of strands	2 mm	Length of strands	2 mm
filters	40 Gauge	filters	40 Gauge	filters	40 Gauge	filters	60 Gauge
Silicone Primer Coating NiNS & Fiber?	Yes	Silicone Primer Coating NiNS & Fiber?	No	Silicone Primer Coating NiNS & Fiber?	No	Silicone Primer Coating NiNS & Fiber?	No
Thickness	0.50 mm	Thickness	1.00 mm	Thickness	0.50 mm	Thickness	1.00 mm
Silicone	1.4 grams	Silicone	2.93 grams	Silicone	1.43 grams	Silicone	2.79 grams
- Base	1.27 grams	- Base	2.66 grams	- Base	1.30 grams	- Base	2.54 grams
- Catylist	0.13 grams	- Catylist	0.27 grams	- Catylist	0.13 grams	- Catylist	0.25 grams
Expected Surface Area:	25.4 mm Wide 127 mm Long	Expected Surface Area:	25.4 mm Wide 127 mm Long	Expected Surface Area:	25.4 mm Wide 127 mm Long	Expected Surface Area:	25.4 mm Wide 127 mm Long

These 8 different samples were then cut into 25.4mm by 12.7mm strips in order to do tensile testing on. Samples were strained from 0% to 20% strain in a cyclic load at a one Hertz period with amplitude of 10% strain. The gauge length of each sample at the start of each test was 12.7mm. They were then cycled 200 times each in order to analyze the degradation, endurance and resistivity accuracy of each sample (See Appendix A: Figures A-1 through A-9). The results are shown in Section 4.1.

The purpose of this DOE is to seek potential ways to improve these gauges for use in Hand Pose Determination applications. This application will adequately show what these gauges are capable of, and open opportunity for further exploration and use in the future. This will be discussed in greater detail in the next section.

3 DEVELOPMENT OF THE ASL INTERPRETATION METHOD

The scope of this work is very limited as far as interpreting all of ASL. There is a great deal of the ASL forms that are not possible to track with a single glove, primarily because of the arm motion and double-hand gestures. The scope of this work only includes the ASL alphabet, and the analysis is based off of only 5 letters of the alphabet to demonstrate usability and potential. A full analysis of the ASL alphabet has not been completed for this work, but with some further analysis and future work the glove designed in this paper would be capable of the entire alphabet. This will all be discussed further in this chapter.

3.1 **Hand Pose Measurement**

To measure the pose of one's hand using HDSGs a few details needed to be taken care of. In order for these displacement sensors to measure hand pose they need a displacement measurement. The gauges needed to be placed across each knuckle to accomplish this. A method of interpreting the resistance readings into the letters of the American Sign Language (ASL) alphabet also needed to be reached. However, in an effort to minimize the number of gauges needed to measure each ASL letter, the differences between hand pose for the various letters needed to be determined as well.

In order to evaluate the differences of each letter a spreadsheet was formed (See Table 5). Each letter of the alphabet was performed by myself (a Novice - using online figures along with

previous experience as a guide) and the angle of each knuckle for each letter was tabulated as a reference to use while later writing the computer program.

3.1.1 Glove Set-up

By comparing each of the letters of the alphabet using this spreadsheet, it was determined that all of the letters of the ASL alphabet could be expressed using only 12 gauges. This was done by comparing the angles determined for each letter, with the angles for each of the other letters, to see if leaving out some of them would still keep each letter unique by at least one knuckle angle (See Table 5). The 12 gauge locations determined are shown, in order, in Figure 12. Having eliminated the unnecessary gauge positions the prototype glove could then be developed. However, this brought in some challenges of its own. Two in particular needed to be addressed. The first of these concerned the attachment of the ends of the gauges to a surface so that they could be stretched. This difficulty comes from the matrix material being composed of silicone rubber. The second challenge is the method by which the wires are connected to ends of the gauges in order to read resistances from the 12 gauges. Having a wire embedded in the sample causes a stress concentration because of the relative size of the wire, so there is difficulty with this as well.

These were both solved using small clamps (small electrical fuse connectors) to solder the wires to and clamp onto the gauges with (See Figure 13). The inside surfaces of the clamps provided a sufficient conductive path to measure the resistance of the gauges. A multi-purpose quick-set epoxy was used to adhesively bond these clamps to the glove following the soldering of the wires to each clamp. This was done with two clamps facing each other at measured distances apart across the knuckles of the glove, in order to accommodate the lengths of the gauges used.

Table 5: ASL Letter Knuckle Angle Differentiations.

A	Joint 1	2	3
Finger 1	90	90	90
Finger 2	90		90
Finger 3	90		90
Finger 4	90		90
Thumb	0		
Wrist (side)	0		

B	Joint 1	2	3
Finger 1	0	0	0
Finger 2	0		0
Finger 3	0		0
Finger 4	0		0
Thumb	90		
Wrist (side)	0		

C	Joint 1	2	3
Finger 1	0	90	45
Finger 2	0		45
Finger 3	0		45
Finger 4	0		45
Thumb	45		
Wrist (side)	0		

D	Joint 1	2	3
Finger 1	0	0	0
Finger 2	45		90
Finger 3	45		90
Finger 4	45		90
Thumb	45		
Wrist (side)	0		

E	Joint 1	2	3
Finger 1	90	90	90
Finger 2	90		90
Finger 3	90		90
Finger 4	90		90
Thumb	90		
Wrist (side)	0		

F	Joint 1	2	3
Finger 1	90	90	45
Finger 2	0		0
Finger 3	0		0
Finger 4	0		0
Thumb	90		
Wrist (side)	0		

G	Joint 1	2	3
Finger 1	0	0	0
Finger 2	90		90
Finger 3	90		90
Finger 4	90		90
Thumb	0		
Wrist (side)	45		

H	Joint 1	2	3
Finger 1	0	0	0
Finger 2	0		0
Finger 3	90		90
Finger 4	90		90
Thumb	45		
Wrist (side)	45		

I	Joint 1	2	3
Finger 1	0	0	0
Finger 2	90		90
Finger 3	90		90
Finger 4	90		90
Thumb	45		
Wrist (side)	0		

J	Joint 1	2	3
Finger 1	0	0	0
Finger 2	90		90
Finger 3	90		90
Finger 4	90		90
Thumb	45		
Wrist (side)	45		

K	Joint 1	2	3
Finger 1	0	0	0
Finger 2	0		0
Finger 3	90		90
Finger 4	90		90
Thumb	0		
Wrist (side)	0		

L	Joint 1	2	3
Finger 1	0	0	0
Finger 2	90		90
Finger 3	90		90
Finger 4	90		90
Thumb	0		
Wrist (side)	0		

M	Joint 1	2	3
Finger 1	90	90	0
Finger 2	90		0
Finger 3	90		0
Finger 4	90		90
Thumb	90		
Wrist (side)	0		

N	Joint 1	2	3
Finger 1	90	90	0
Finger 2	90		0
Finger 3	90		90
Finger 4	90		90
Thumb	90		
Wrist (side)	0		

O	Joint 1	2	3
Finger 1	45	45	45
Finger 2	45		45
Finger 3	45		45
Finger 4	45		45
Thumb	0		
Wrist (side)	0		

P	Joint 1	2	3
Finger 1	0	0	0
Finger 2	90		0
Finger 3	90		0
Finger 4	90		0
Thumb	0		
Wrist (sd/b)	0		

Q	Joint 1	2	3
Finger 1	90	0	0
Finger 2	90		90
Finger 3	90		90
Finger 4	90		90
Thumb	0		
Wrist (side)	0		

R	Joint 1	2	3
Finger 1	45	0	0
Finger 2	0		45
Finger 3	90		45
Finger 4	90		45
Thumb	45		
Wrist (side)	0		

S	Joint 1	2	3
Finger 1	90	90	90
Finger 2	90		90
Finger 3	90		90
Finger 4	90		90
Thumb	45		
Wrist (side)	0		

T	Joint 1	2	3
Finger 1	90	90	0
Finger 2	90		0
Finger 3	90		0
Finger 4	90		0
Thumb	90		
Wrist (side)	0		

U	Joint 1	2	3
Finger 1	0	0	0
Finger 2	0		0
Finger 3	90		90
Finger 4	90		90
Thumb	45		
Wrist (side)	0		
Finger side	45		

V	Joint 1	2	3
Finger 1	0	0	0
Finger 2	0		0
Finger 3	90		90
Finger 4	90		90
Thumb	45		
Wrist (side)	0		
Finger side	0		

W	Joint 1	2	3
Finger 1	0	0	0
Finger 2	0		0
Finger 3	0		0
Finger 4	90		45
Thumb	90		
Wrist (side)	0		

X	Joint 1	2	3
Finger 1	0	90	45
Finger 2	90		90
Finger 3	90		90
Finger 4	90		90
Thumb	45		
Wrist (side)	0		

Y	Joint 1	2	3
Finger 1	90	90	90
Finger 2	90		90
Finger 3	90		90
Finger 4	90		0
Thumb	0		
Wrist (side)	0		

Z	Joint 1	2	3
Finger 1	45	0	0
Finger 2	90		90
Finger 3	90		90
Finger 4	90		90
Thumb	45		
Wrist (side)	45		

Figure 12: Locations of HDSGs on Hand

This allowed the gauges to be replaced, as necessary, in that the clamps can be opened and closed without too much difficulty. Unfortunately the clamps themselves did not have quite enough force to keep the HDSGs from slipping out of them. To help the gauges stay within the clamps, cyanoacrylate glue ("Krazy Glue") was used on the under surface of the ends of each gauge to assist in keeping the gauges from slipping out of the clamps. This successfully kept the gauges from slipping out and provided accurate resistivity readings to the data aquisition system.

Figure 13: Prototype Glove with HDSGs and Connections

3.1.2 Interpretation into ASL

In order for the readings from the gauges to be translated into ASL letters a LabVIEW program was created. While the user performs letters with the glove on, the program can then interpret the letter by comparing it against the letters already calibrated in the system. LabVIEW

is ideal because of its robust signal measurement capabilities. Among other things, it is able to measure 12 simultaneous resistances at the same time.

It is capable of this using the NI cDAQ-9172 (and DAQ Assistant within the program) and with three NI 9219 cartridges plugged into it (which house 4 resistance inputs per port). Each resistance is directly measured by gauges hooked up to the glove in the orientation shown in Figure 12. The signals coming into the program are then passed to a signal splitter which separates each of the twelve individual signals into their corresponding unique channels. A real-time resistance waveform plot is generated for each individual signal as well as a comprehensive resistance waveform plot for all channels simultaneously (See Figure 14).

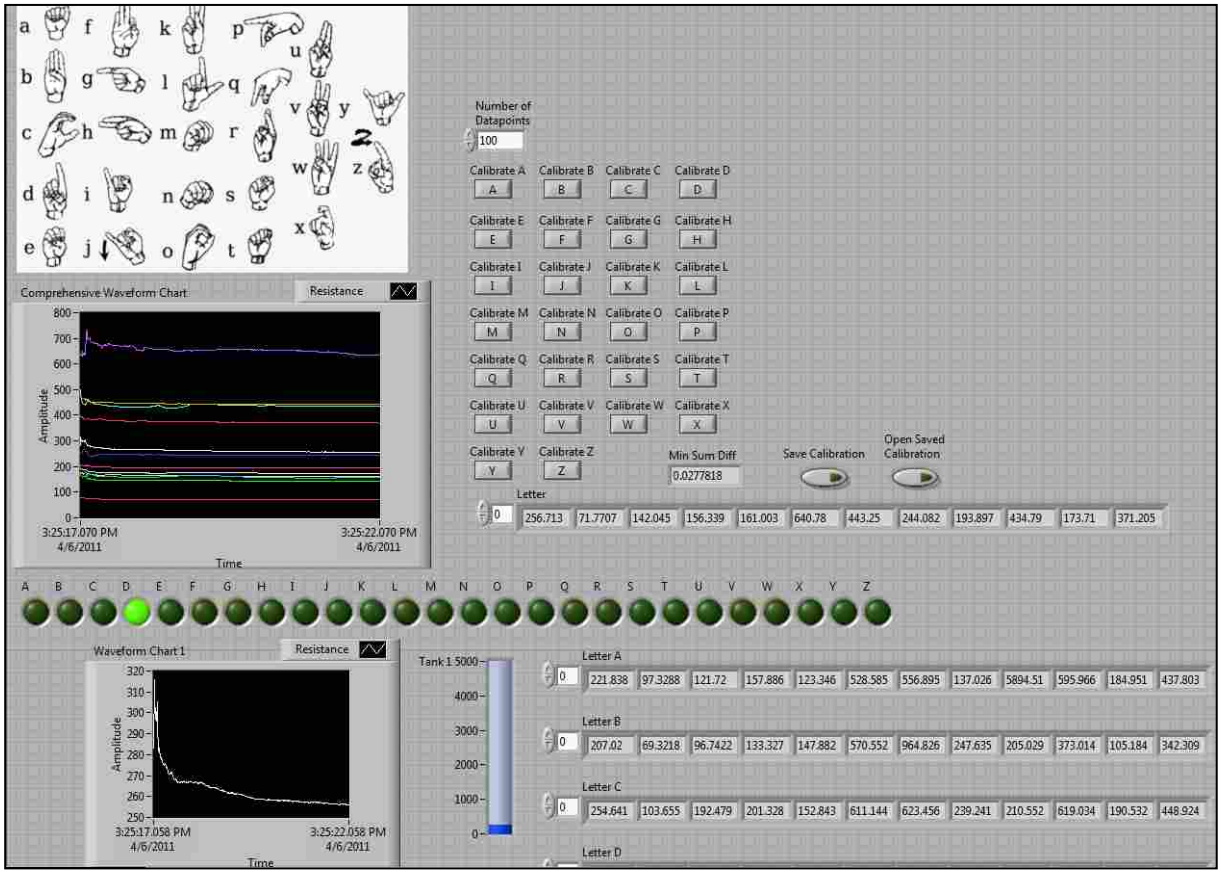

Figure 14: Lab-View Program to Interpret Resistances with Sum of Differences Equation

The program is capable of quickly recording data from each of the 12 resistance measurements to a specified file location for review.

3.1.3 Calibration and Response

From each channel the resistance measured is what the program uses to interpret the hand pose into an ASL letter. In Figure 14 it shows the letter 'D' being recognized by the program and lighting up the letter (which was the hand pose formed). The potential for the program is to be able to measure the correct letter 100% of the time. The current program is capable of about 62% accuracy (See Section 4.2.1).

In order for the program to recognize that a letter has been formed, a change in resistance must occur. A slope change downward means a flexure of the specific gauge (the finger is bending at that knuckle). Holding that letter for at least one second will allow a relatively constant resistance measurement (As shown in the troughs of Figure 15). When the letter is then released and returns back there is a steeper slope upward which often spikes and the resistivity is not near as consistent as before. With these two major slope changes the program could enter a letter on the one's computer screen (as if typing using the sign of the glove). This could be recognized very quickly by the computer because of how fast the gauges measure the response. The program is not currently capable of recognizing the changes in letters yet, but it is very possible using labVIEW. In the Figure 15 below (a resistivity plot taken from the program created in LabVIEW), it is shown that this type of profile could be easily recognized by the program. We see that the periods where the letter "A" is formed are the lower resistance measurements (staying close to 50 Ohms), and the upper resistance measurements are where the letter is released (varying around 150-200 Ohms).

The calibration for each letter is done somewhat differently. First, the number of data points to be used to calculate a collection of 12 mean resistances is entered in the "Number of Datapoints" box (See Figure 14). A letter is then formed by the user. Each of the 26 letters of the alphabet has their own calibration button. The button corresponding to the letter formed by the user is then depressed. The user continues to hold the letter for a short period of time.

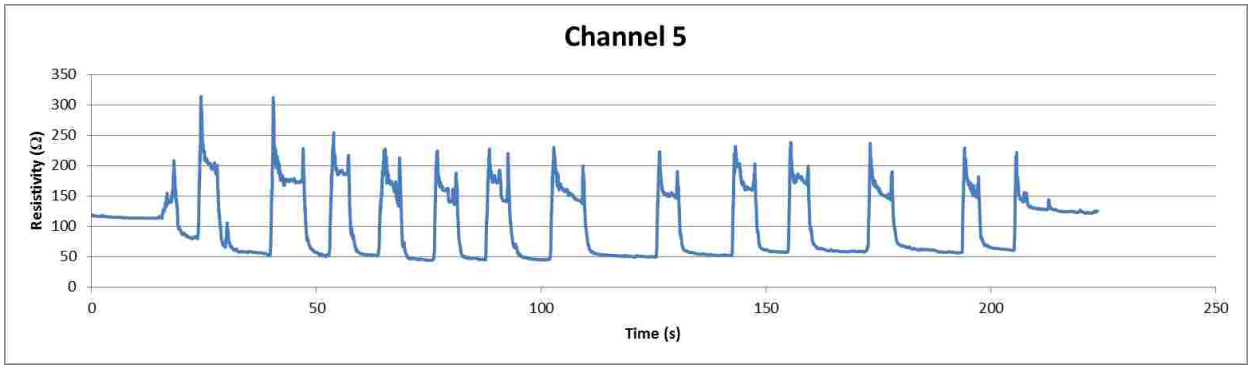

Figure 15: Resistance Plot of Channel 5 while performing Letter 'A' Several Times

The calibration will collect the resistance data points at a rate of 100 data points per second for all 12 gauges. This means that the "short period of time" that is required for the user to hold the letter is determined by the number of data points chosen to create the mean resistances. This process can be somewhat time-consuming for all 26 letters. So, for convenience, once a calibration has been done it can be saved and then loaded later. It is recommended that at least 20 data points be used for the calibration so that a reasonable mean can be established for each letter (See 4.2). It is possible for the same user to be able to come back and use a previous calibration, but it is not currently as accurate as when it has been calibrated just prior to use. Also, if one user completes a calibration and another user attempts to use the glove, the calibration will most likely not function correctly. So, there are some current

limitations in the calibration of the glove. This is somewhat disappointing but could potentially be fixed using machine learning software in place of the sum of the differences method. This will be discussed further in Section 4.2.

As mentioned earlier, the current program will not recognize the separation between two letters formed. It simply compares hand pose formed, to the set of calibrated letters, and lights up the letter closest to that letter. For actual implementation this would need to be improved, but for the purposes of this research, the fact that we can actually measure hand pose is the point. The purpose of this research is to demonstrate the potential of theses HDSGs for use in this application and show that it can be extremely successful as a HMI device.

4 RESULTS

4.1 Design of Experiments

In previous testing several of the gauges have begun to deteriorate at about 100 cycles. In order to evaluate how well the modifications in the DOE improved the cyclic loading 200 cycles were performed for each of the 8 trials, so that it could be determined if the region of deterioration had been increased. Each of the eight different gauges in the DOE was therefore cycled 200 times at 1 Hz and recorded at 100 Hz data acquisition speed. This means that over the 200 cycles at least 20,000 data points were collected (See Figures 16-23). In order to compare the resistivity measurements to the displacement the resistivity was normalized to the same scale as the displacement. This is shown in Figures 16-23, but in order to better visualize the fit of the resistivity profile to the displacement a stable region (from 50-60 seconds) of each trial is shown as well. This section of time was chosen in order to see a relatively stable section from each of the 8 trials.

When looking at these figures the drastic differences between some of them are quickly noticed. Trial 1 gave no significant resistivity measurements over the entire course of the test, thus the flat line (See Figure 16). This occurs because of the limitation of the data acquisition system (DAQ). The NI 9219 cartridges are only capable of measuring from 0 to 10.5 kΩ of resistance. Using a multimeter and the same gauge length, it was determined that the lower limit of resistivity for trial 1 is about 40 kΩ at 20% strain (See Figure 24). This upper limit of 10.5 kΩ

of resistance (which is shown as a lower boundary because of the inverse resistivity of the plots) appears in trials 3-6 as well (See Figures 18-21). In trials 3, 4 & 6 this cut-off simply lowers the upper limit measured by the DAQ (See Figure 18, Figure 19, & Figure 21). However, in trial 5 this is not the case. Trial 5 is hovering just above the 10.5 kΩ range and so while a few of the displacement profiles are measured, not very many are caught by this gauge (See Figure 20). Looking back at trial 3 we notice that there is actually a complete cycle missing in its measurement as well, which means that it is hovering a little closer to 10.5 kΩ than trials 4 & 6. Another interesting phenomenon is shown in trials 2, 3, 5, 6, 7, & 8 (See Figures 17-18 & 20-23). A gradual decrease is noticed (which is an increase in resistivity). The reason for this is primarily a plastic deformation of the gauges which will be discussed further at the end of this section.

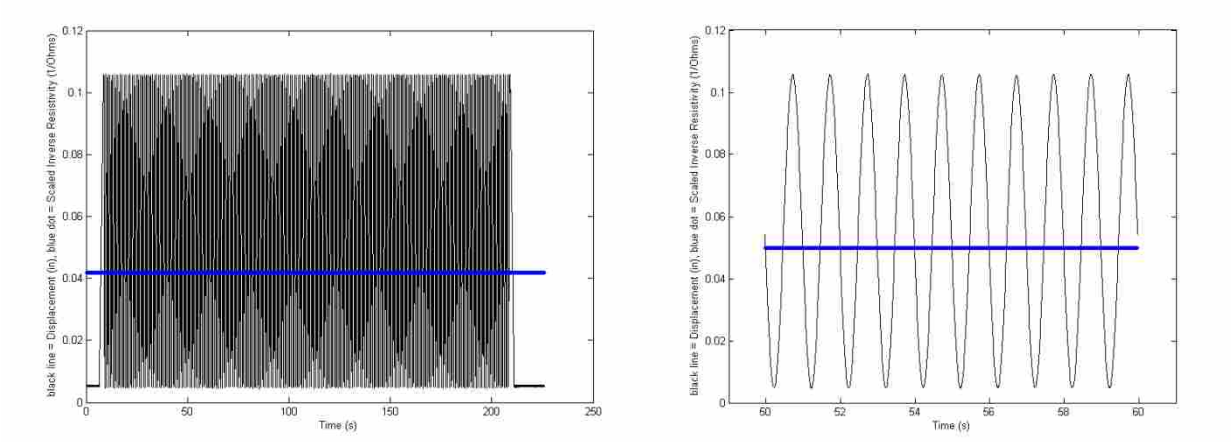

Figure 16: Trial 1, Scaled Resistivity over Displacement, Full Test (L), 50-60sec (R)

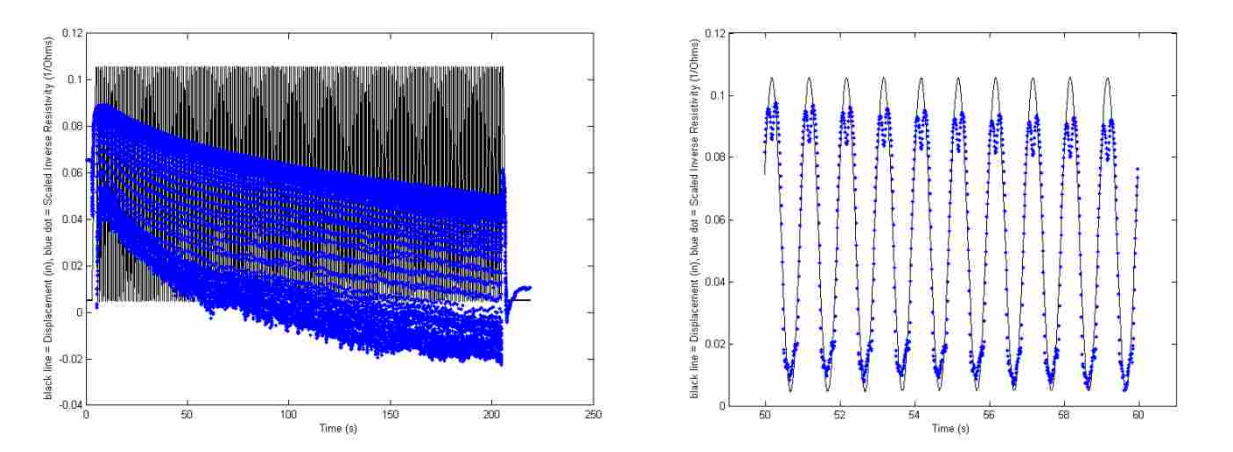

Figure 17: Trial 2, Scaled Resistivity over Displacement, Full Test (L), 50-60sec (R)

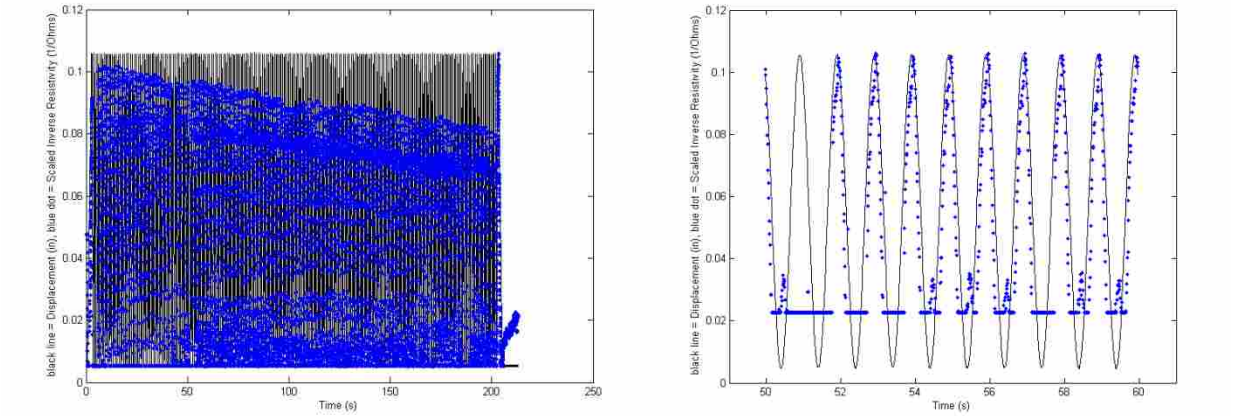

Figure 18: Trial 3, Scaled Resistivity over Displacement, Full Test (L), 50-60sec (R)

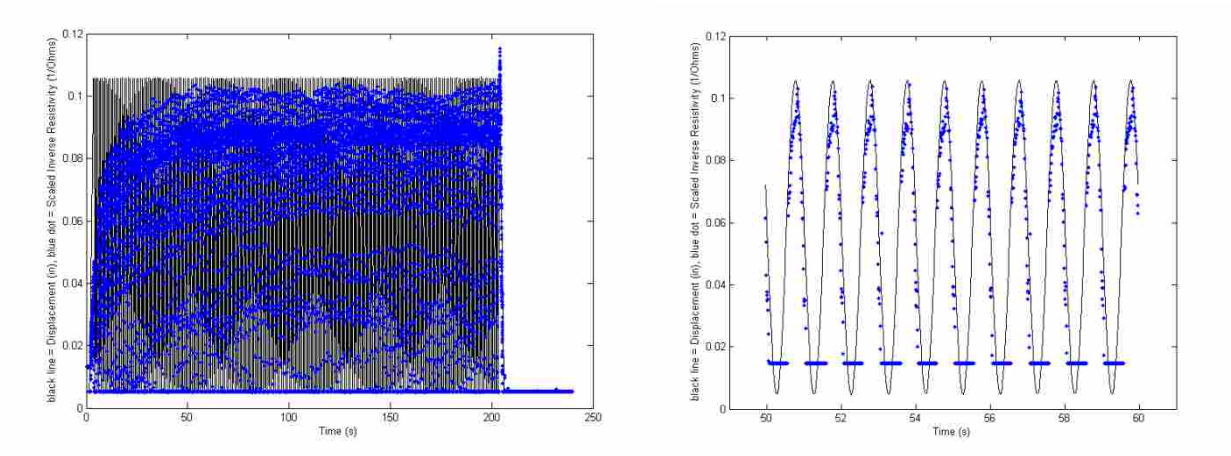

Figure 19: Trial 4, Scaled Resistivity over Displacement, Full Test (L), 50-60sec (R)

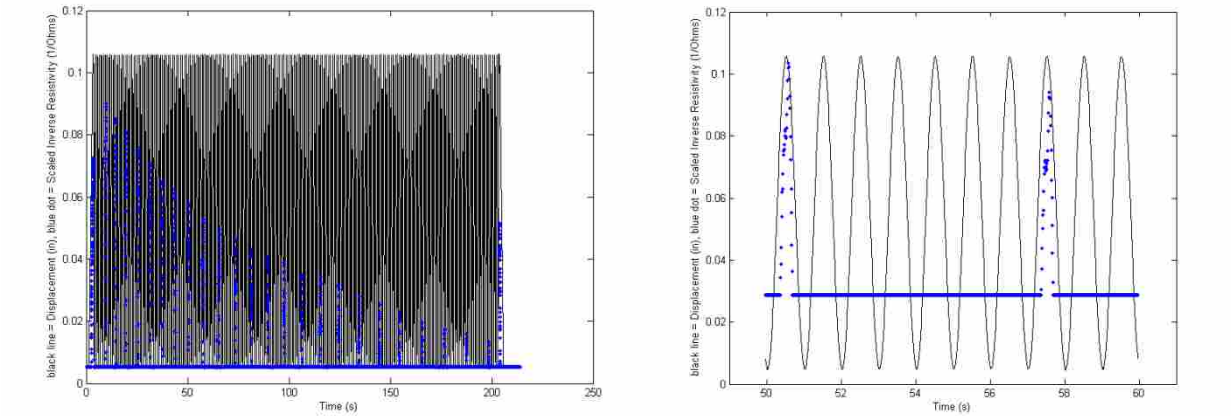

Figure 20: Trial 5, Scaled Resistivity over Displacement, Full Test (L), 50-60sec (R)

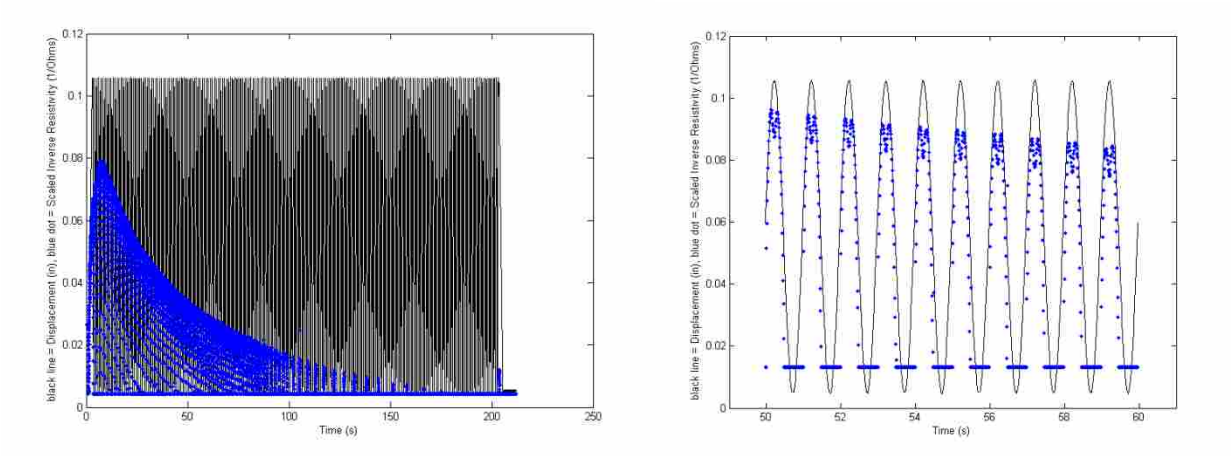

Figure 21: Trial 6, Scaled Resistivity over Displacement, Full Test (L), 50-60sec (R)

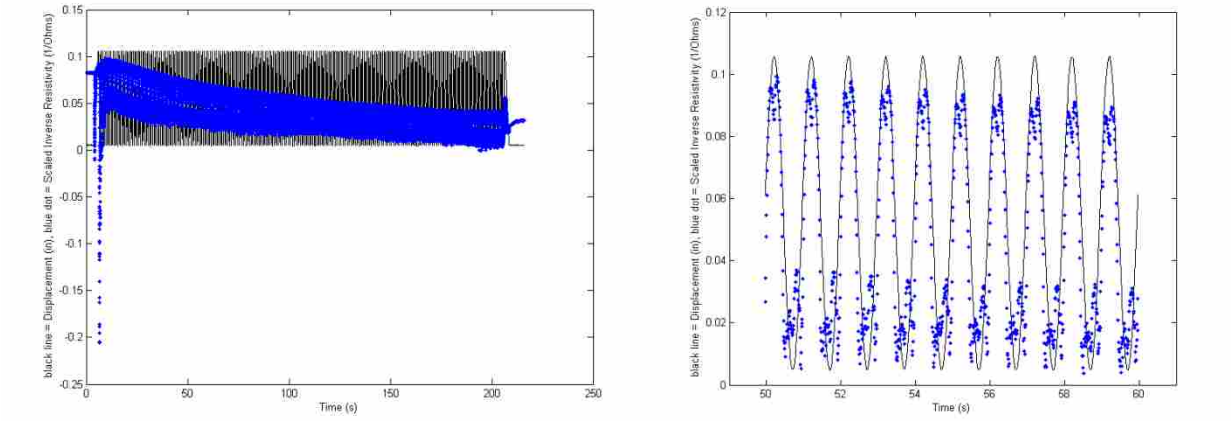

Figure 22: Trial 7, Scaled Resistivity over Displacement, Full Test (L), 50-60sec (R)

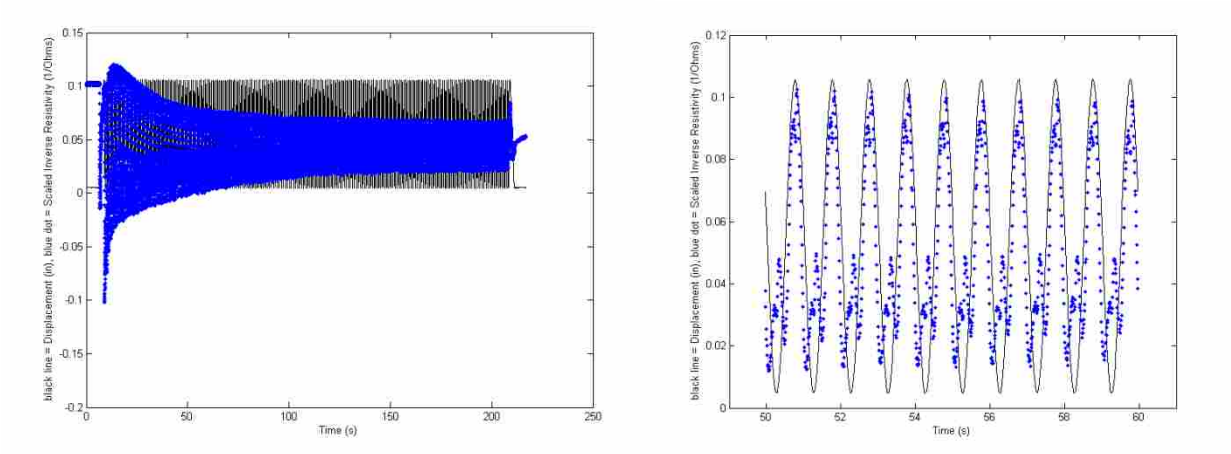

Figure 23: Trial 8, Scaled Resistivity over Displacement, Full Test (L), 50-60sec (R)

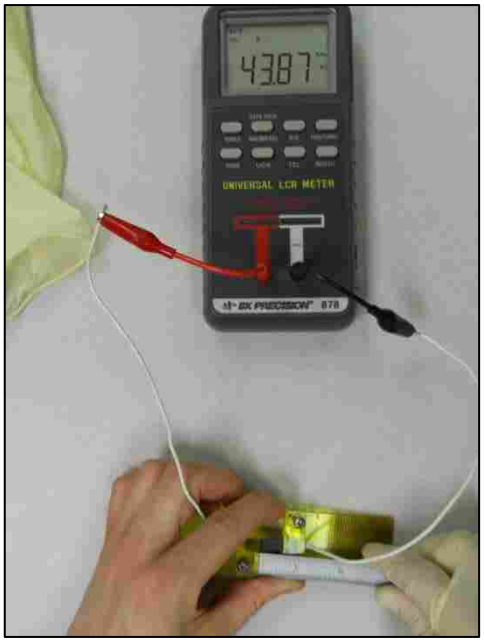

Figure 24: Trial 1, Manual Measurement (Displayed in KiloOhms)

The material properties of the HDSGs have a great effect on their strain measurement capability. Each HDSG made has a slightly different resistivity which changes with the manufacturing process, material quantities and cross-sectional area. Even when all of these three are constant between two separately manufactured gauges, the initial resistivity can be (and often

is) slightly different. In this case (when these three are constant) the way that the gauges react to strain displacements is the same. In the DOE on the other hand, all of these three were varied in each gauge, but while we did vary the parameters of the gauges the test conditions were kept the same for all trials. In order to evaluate the quality of the various gauges with this variability, we calibrated the resistivity readings to the known strain value by using a function of the form of Equation (6).

$$\boldsymbol{f(\rho) = a_1(\rho - a_4)^{a_2} - a_3} \quad \textbf{(6)}$$

Where ρ is the resistivity, and $a_1 - a_4$ are the four scaling constants which vary with each trial (See Table 6). The quality of each gauge was then judged based on the overall error between the calibrated strain and the actual strain displacement as defined by the constants in Table 6. Unfortunately the resistivity for Trial 1 was above the resistance limit of the resistivity measurement device at 10,500 Ω (using a NI cDAQ-9172 chassis with a NI9219 cartridge to measure resistance). Thus it failed the DOE. However, using Equation (6) the Trial 1 points were brought down to the same scale as the displacement profile in order to allow comparison of this failed resistivity measurement with the rest of the data measurements (See Table 6).

Table 6: List of Constants for Scaling of Each Trial

	Trial 1	Trial 2	Trial 3	Trial 4	Trial 5	Trial 6	Trial 7	Trial 8
a_1	1.0715	1.079	0.5595	0.5401	0.9376	0.2029	32.0756	39.0798
a_2	-0.344	-0.1112	-0.0736	-0.0889	-0.0378	-0.0988	-0.2978	-1.5599
a_3	0.0024	0.5428	0.277	0.2306	0.6563	0.07366	4.4453	0.1515
a_4	1.6134	-99.0328	72.1061	90.633	76.6134	5.2496	-708.255	-20.8035

Once the 8 trials were scaled, as shown above, they could then be compared with the actual displacement curve. This was done over the entire 200 cycles in order to truly evaluate the effect of long term cyclic loading of the samples (See Appendix A: Figures A-1 through A-8 for Data Comparison). From this comparison the average percent error was calculated over the entire range of the data for each trial (See Table 7). This was used to evaluate which factors have the greatest effect on improving the HDSGs.

Table 7: DOE Statistical Evaluation

	% NNS	% NCCF	Length of NCCF (mm)	Filter Size (mesh)	Si Primer (y/n)	Thickness (mm)	Average % Error
Trial 1	11	3	0.5	60	yes	1.0	190
Trial 2	9	5	0.5	60	no	0.5	88
Trial 3	9	5	2.0	40	yes	1.0	61
Trial 4	9	3	2.0	60	yes	0.5	41
Trial 5	11	5	0.5	40	yes	0.5	71
Trial 6	9	3	0.5	40	no	1.0	68
Trial 7	11	3	2.0	40	no	0.5	101
Trial 8	11	5	2.0	60	no	1.0	132

In previous testing using the standard gauges, accomplished by Hyatt, the error reached was between 5.5% and 8.9% [23]. Interestingly the average percent error in this experiment is significantly higher. There are several reasons for this, most of which come from differences in the material properties of the DOE trials compared with the HDSGs used in previous research, which affects the accuracy. Another reason comes from an initial plastic deformation which occurs in the samples over the first few cycles of strain displacement (See Appendix A: Figures A-1 through A-8). However, because the tabs holding the HDSGs are acrylic and held in simply using clamping force, it is possible that some of this increased error is also due to the gauges

slipping out of the clamps. This plastic deformation (and possible slipping) caused the samples to be in compression at the bottom of each of the displacement cycles (See Figure 25). This phenomenon caused the gauges to decrease in resistivity rather than continue to increase in resistivity at the bottom of each sine wave in the displacement (See Figure 25, Note that the resistivity is inverted in order to align it with the displacement, so increasing resistivity is downward and decreasing is upward). This phenomenon typically only occurs during the first few cycles and the resistivity remains constant afterward (until degradation of the gauge begins). This is typical of this type of HDSG. For some of these trials in the DOE, however, the resistivity gradually increased along the entire 200 cycles (See Figures 17-18 & 20-23 & Appendix A: Figures A-1 through A-8).

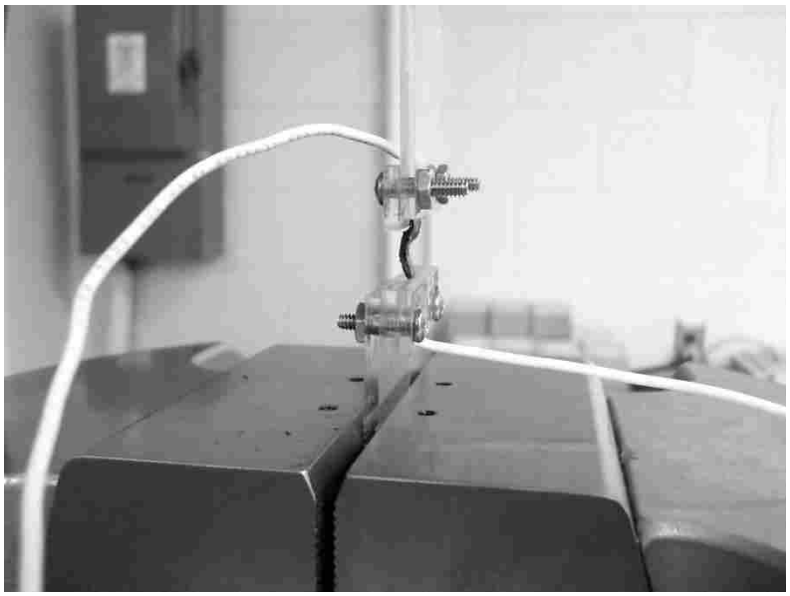

Figure 25: Plastic Deformation Causing Compression in HDSG Test

The amount of measured Plastic Deformation in 240 cycles for each gauge averaged 1.09mm (0.043in) of plastic deformation (See Appendix A: Table A-1). Although this could not be accounted for in the grading of the DOE, the error is analyzed the same for each test. So,

using the percent error as grading criteria is still valid, as it is still captured in the error analysis. A possible solution to overcome this factor for future work would be to pre-strain the gauges a few times in order to reduce this effect. Also, if the gauges are slipping, improving the clamping surface of the tabs would also be recommended. Using this grading criterion, each of the 6 variations in the DOE was evaluated using the following equation [37]:

$$\frac{\left(\frac{\sum R_i}{4}\right) - \left(\frac{\sum R_j}{4}\right)}{2} \quad \textbf{(7)}$$

Where ΣR_i & ΣR_j are the sum of the 4 terms in the Average % Error column which line up with the trials that correspond to the column of interest and i & j correspond to the two variations within that column. So for the % NNS column the four Average % Error responses aligned with 11% NNS in Table 7 are 190, 71, 101, & 132 and the other four responses in the Average % Error column aligned with 9%NNS are 88, 61, 41, & 68. This equation is then calculated for each of the six columns in Table 7 (%NNS, %NCCF, Length of NCCF, Filter Size, Silicone Primer, & Thickness). This provides us with the statistical relative weighting of each of each variable (Shown in Table 8).

Table 8: Evaluation of DOE

	Relative Weight
11% NNS	29.50
5% NCCF	-6.00
0.5mm NCCF	10.25
60 Mesh Filter	18.75
With Primer	-3.25
0.5mm Thick	-18.75

Thus if the evaluation from Equation (7) is high in the Relative Weight column of Table 8, it means that that row of interest has the greatest effect on the variation of the curve fit of the cyclic loaded sample according to the DOE.

The evaluation shows that modifying the volume percent of NNS has the greatest effect followed by the Filter Size and the Thickness. Each seem to have a large effect on the cyclic loading curve fit of the HDSGs. It also shows that the use of the Silicone Primer seems to have very little effect, along with the percentage of NCCF. The length of the Fiber has some effect but likely should not be focused on for any future cyclic loading improvements. These results will be discussed further in Section 5.

4.2 **ASL Letter Interpretation**

Translation of the measured resistance values into letters of the alphabet can be accomplished in various ways. In order to test a few of these methods, a manageable set of 5 letters was chosen. Two calibration techniques were used to relate resistance measurements to the pose of each letter. The first method was a Euclidean distance measure between points within the multidimensional resistivity space. The second method was by means of a machine learning approach. Approximately forty cycles of an open hand (no letter formed) to a closed hand (in the form of a letter) were recorded in resistivity plots (See Appendix B: Table B-1). This provided enough data to select 200 values to divide and compare against each other (40 for each letter).

4.2.1 Sum of the Differences

The Euclidean distance between points in a multidimensional space is determined by means of a sum of the differences equation. It is difficult to understand this multidimensional

space, due to the fact that the resistivity space is defined by 12 dimensions. However, by projecting this space onto 3 dimensions it can be seen that of 100 points, the 5 letters can be clearly separated in groups (See Figure 26 & Figure 27).

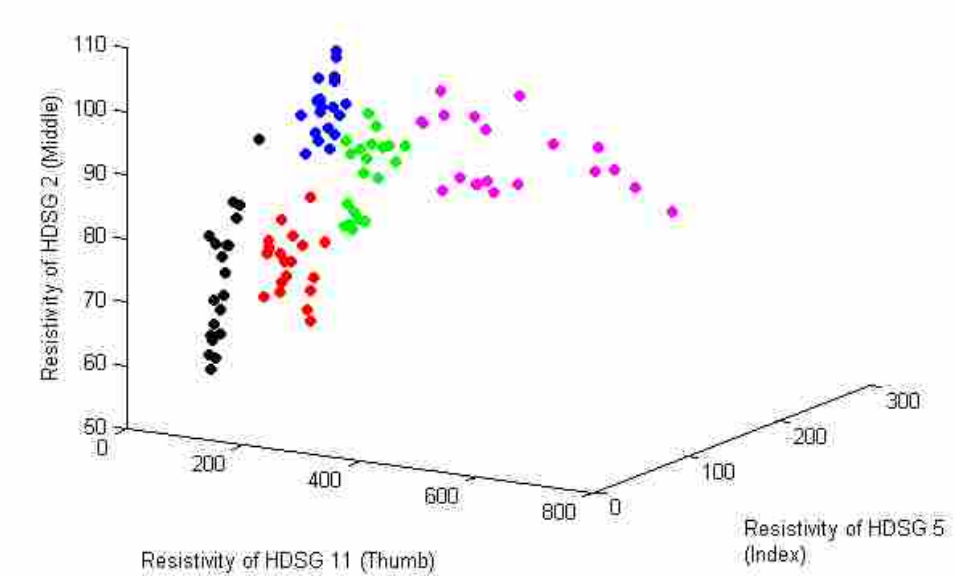

Figure 26: 3-Dimensions of 12-D Resistivity Space, Showing 5 Letter Groups

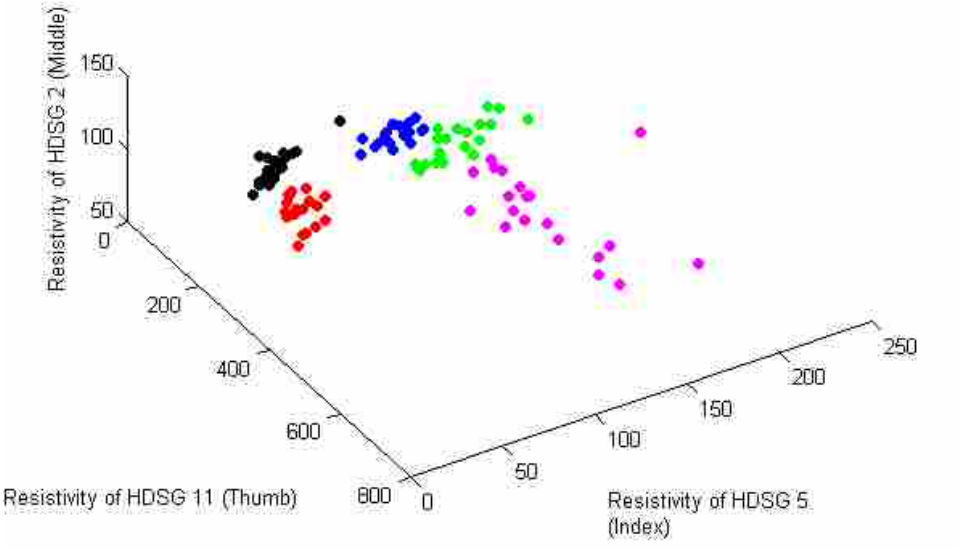

Figure 27: Another View of Same 3-D Space (A=Rd, B=Gr, C=Bl, D=Mg, E=Bk)

The central point of each grouping of each letter can be found by determining the mean of each dimension of each letter. This will give us a point in 12 dimensional space, for each of the 5 letters, that we can then compare a new set of 100 data points to, using the sum of the differences equation. The sum of the differences equation used is shown below:

$$\boldsymbol{Sum\ of\ the\ Differences\ in\ Letter\ A} = \frac{\sum_{i=1}^{12}(r_{Ai}-\mu_{Ai})^2}{\sum_{i=1}^{12}(r_{Ai})^2} \quad \textbf{(8)}$$

Where r is the current resistance value measured from each resistor and μ is the mean resistance of each resistor of the 20 letters which were input into the system. In order to validate this method half of the 200 data points were used to obtain mean values and the other half were used as an independent data set to test the Euclidean distance. An average of 62% recognition accuracy could be obtained from the 5 letters measured (See Table 9, For Complete Evaluation See Appendix B: Tables B-2 & B-3). Not surprisingly, if the same data used to create the mean was evaluated an increased average is reached.

Table 9: SD % Accuracy (Left: Independent Data, Right: Data Used for Mean)

Percent Correct		Percent Correct	
A	60%	A	100%
B	100%	B	90%
C	55%	C	85%
D	70%	D	95%
E	25%	E	70%
Average:	62%	**Average:**	88%

4.2.2 Machine Learning

In order to improve the accuracy of letter recognition, Weka machine learning software was employed to determine what could be achieved using the same data [38]. A Multi-Layer Perceptron (Neutral Net) classifier was used in order to obtain the most accurate fit. It was found that an average of 97% accuracy could be reached using an independent data set (See Table 10). Again if the original data is used to learn from an increased average is reached.

Table 10: ML % Accuracy (Left: Independent Data, Right: Non-Independent Data)

Percent Correct		Percent Correct	
A	95%	A	100%
B	100%	B	100%
C	90%	C	100%
D	100%	D	100%
E	99%	E	97%
Average:	97%	**Average:**	99%

The accuracy plot of letter 'E' for the Independent data is shown below in Figure 28. Where the orange points on the right are the correct letter and the blue points on the left are the incorrect letters. Thus with the threshold level set at 0.3 on the vertical axis, all but one of the points on the right of the plot will be recognized as the letter 'E' and all of the points on the left will be correctly distinguished from the letter 'E'. The plot is displayed so that the larger the size of the "X" the greater the error is. Images of the plots for the rest of the letters are shown in Appendix B.

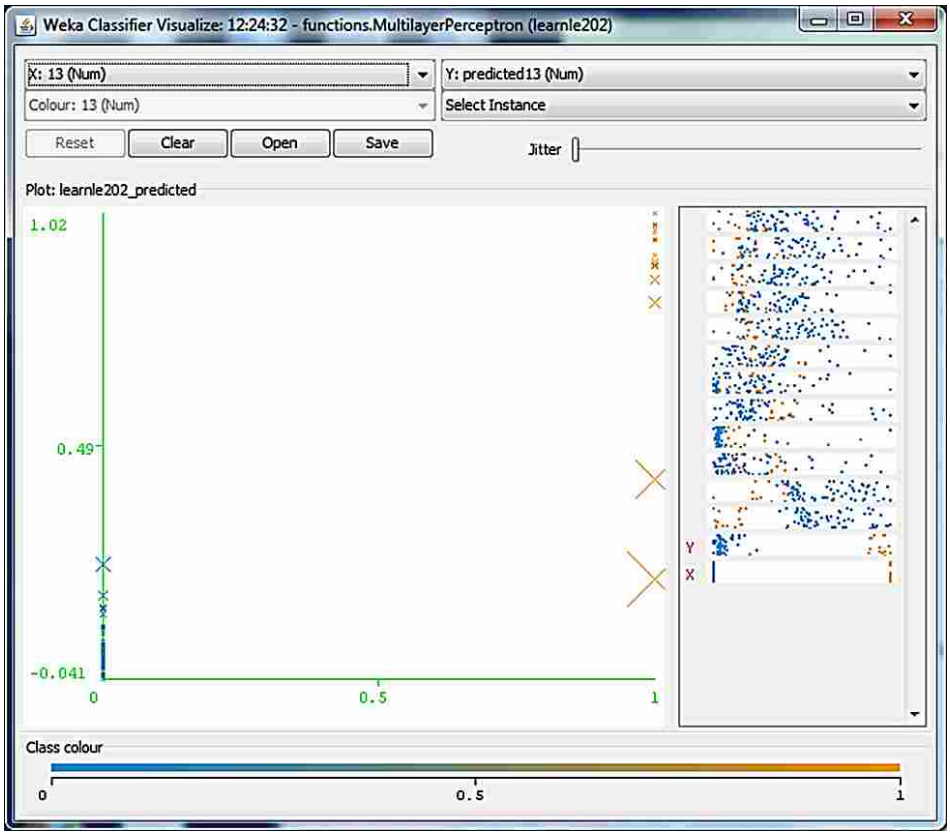

Figure 28: Machine Learning Plot of Accuracy of Letter 'E' (Larger X = Greater Error)

An important thing to recognize with machine learning is that the more data the software has to "learn" from, the more accurate it becomes. So, with more data, 100% accuracy could potentially be achieved. This is primarily because the training set used for this machine learning evaluation is a relatively small training set for machine learning software. With a greater number of values to "learn" from, the program could more easily recognize the differences between this letter and the other 4 letters in this test.

5 CONCLUSIONS & FUTURE WORK

In evaluating the data obtained from the glove and the DOE, it can be seen that, with further development, these gauges could be used for actual motion tracking of the hand rather than just hand pose measurements. By using machine learning one could also more closely evaluate the differences between each gauge at each knuckle. Along with calibration this could allow for such things as the remote surgery operation, discussed earlier in this paper, and other specific uses. Improvements to the material properties of the HDSGs may also be required for these applications, but that is not beyond reach.

From the mean difference (in resistivity space) between each of the 5 letters measured we see that it is 62% effective in determining the correct letter based on a reference of 20 data points. From the machine learning recognition, 97% effectiveness can be achieved with only 20 data points per letter. Both of these could also be improved with more data points and improvements in the gauges themselves.

From the Design of Experiments it was found that the percent of NNS seems to have the largest effect on the cyclic loading of the HDSGs. Although this effect is important to further develop, a great deal of research has already been invested in the development of these NNS [27]. If further work is to be done using cyclic loaded gauges this will be an important area to keep track of, but the better areas to develop further would be the variations in Filter Size and Thickness. The Filter Size will vary not only the particle size of the NNS but also the

distribution. Understanding the effect that this element has will be important for any future work in cyclic loading. According to the results, the variation in the success of the cyclic loading curve fit is equally spread by changing the Thickness of the HDSGs. Understanding this effect is also important, but mainly due to the fact that the gauges are more flexible and less expensive when thinner gauges are made. Interestingly the use of Silicone Primer, the percent NCCF, and length of NCCF did not have much effect on the curve fit capability of the cyclic loaded gauges. It is also interesting that the Silicone Primer had the least effect over the cyclic loaded samples. It had the potential to decrease the void formation within the Silicone which may have lengthened the cyclic loading of the samples (See 2.5.2). However, it also increased the boundary between the conductive fibers which decreases the quantum tunneling and thus the conductivity of the gauge [29]. So, perhaps the use of it within the gauges balanced out. This may be the reason for Trial 1 having such high resistivity readings (above 10,500Ω). From this DOE, the most important effect is probably in the fact that the gauge from the DOE which was closest to our standard manufacturing process lasted 200 cycles without decreasing in resistivity (See Figure 19). This effect encourages the notion that an increase in cyclic loading capacity is possible for these gauges. The DOE also shows that there is room for improvement in these gauges which gives hope for their use in many future applications.

From this research it can be seen that these high displacement strain sensors are capable of the application of ASL interpretation. It can also be seen that many other applications aside from hand pose may be possible as well. This is true, not only in human-machine interface applications, but also bio-measurement, motion tracking, and remote motion sensing applications (such as in outer space, high radiation zones, or near high-explosives).

5.1 **Potential for other Bio-Measurement Applications**

In the areas of biomechanics, biomedical measurement, and other measurements of the body many areas of future work could be researched. One example of this could be using these gauges in something of the form of an adhesive bandage with two wires attached. With these gauges manufactured very thin along with a silicone coating they could easily be used as an adhesive displacement measuring device of various different sizes.

Although these HDSGs are capable of very high strain displacement, which is necessary in biological measurement, the use of nickel causes one to question the validity of using this device on people. This comes from the fact that a common allergy is found in skin contact with nickel [39]. This concern can quickly be abated with the fact that these gauges can easily be coated in the same silicone as the matrix is currently made up of. The silicone matrix, by itself, has a much higher strain displacement capacity than when Silicone is infused with the NNS and NCCF. Thus the gauge inside of the silicone coating will fail before the silicone itself. In this case the device would be useless and would have to be replaced anyway. So it would not be used in a situation where it would be necessary to have skin contact with the nickel.

5.2 **Potential for Further Use in Human-Machine Interface Applications**

This application of ASL interpretation also shows the simplicity of using these devices to connect users with computer-controlled applications. The word “simplicity” is used in the sense that it is simple to interpret resistance readings compared with many of the other complex measurement methods available [6, 8, 9]. Evaluation of resistance readings is fairly simple as well. So that extension to other interface applications could potentially require very little innovation in interpreting the signals from these gauges for their use.

One of the clearest steps of future work following this research is to optimize the gauges for more precise measurement tracking. Though the precision of these gauges is reasonable, even greater accuracy would widen the range of applications for use. Especially within hand motion tracking, because there are so many miniscule movements that one's fingers are capable of that are currently difficult to track with any method. As discussed earlier, the DOE shows what areas to focus on in order to fully understand the limitations of these HDSGs. It seems, however, that extremely high fatigue loading might not be possible with this specific nanocomposite. Thus a temporary use of these gauges may be the only option (though this has not yet been determined). Noting this, these HDSGs are still capable of many different sensor applications. This research has shown that there is great potential for accomplishing this by further development of these HDSGs.

Other future work that could be done, specific to this research, includes work on the program and the glove. Improvements and analysis of the program, such as implementing machine learning and analyzing the entire alphabet could be accomplished. The glove itself is very much an early prototype and several improvements could be accomplished, such as using smaller wires sown into the glove and lower profile gauge contacts applied. The current glove is also somewhat bulky and a different type of glove that formed better to the hand while still providing some stiffness at the contact locations would be a great improvement as well.

This work has shown that the use of HDSGs can be extended beyond simple engineering measurement tasks to something that could potentially be used in one's home as an interface device with a computer to interpret ASL. This is truly the goal of engineering: to benefit mankind. This HMI application is one of many that could benefit from the use of these HDSGs. Others include virtual reality applications which often use hand motion, remote control devices

for measuring deflection, robotics which often mimic human functionality, prosthetics, and even computer games. The potential for the use of these HDSGs is widespread and future research will determine what it will be used for next.

REFERENCES

1. Scott, S., Lee, J.H. (2003) *Serving Clients Who Use Sign Language*. The ASHA Leader.
2. Ventrelli, L., Beccai, L., Mattoli, V., Menciassi, A., Dario, P.,. *Development of a stretchable skin-like tactile sensor based on polymeric composites*. in *IEEE International Conference on Robotics and Biomechanics*. 2009. Guilin, China.
3. Voss, K., Wanser, K.,, *Strain Sensors Having Ultra-High Dynamic Range*, in *US Patent No. 5668324*. 1997: United States.
4. Manaris, B., *Natural Language Processing: A Human-Computer Interaction Perspective*, in *Advances in Computers*, V.Z. Marvin, Editor. 1998, Elsevier. p. 1-66.
5. Carroll, J.M., *Evaluation, Description and Invention: Paradigms for Human-Computer Interaction*, in *Advances in Computers*, C.Y. Marshall, Editor. 1989, Elsevier. p. 47-77.
6. Crawford, S. *How Microsoft Kinect Works*. HowStuffWorks.com 2010 [cited 2011 08 January].
7. Bouzit, M., et al. *The Rutgers Master II-ND force feedback glove*. in *Haptic Interfaces for Virtual Environment and Teleoperator Systems, 2002. HAPTICS 2002. Proceedings. 10th Symposium on*. 2002.
8. Gentner, R., Classen, J., *Development and evaluation of a low-cost sensor glove for assessment of human finger movements in neurophysiological settings.* Journal of Neuroscience Methods, 2009. **178**: p. 138-147.
9. Biddiss, E., Chau, T., *Electroactive polymeric sensors in hand prostheses: Bending response of an ionic polymer metal composite.* Medical Engineering & Physics, 2006. **28**: p. 568-578.
10. Carvalho, A., Radwin, R.,, *A new method for extending the range of conductive polymer sensors for contact force.* International Journal of Industrial Ergonomics, 1996. **17**: p. 285 - 290.
11. Zhang, W., Blackburn, R., Dehghani-Sanij, A.,, *Carbon Black Reinforced Epoxy Resin Nanocomposites as Bending Sensors.* Journal of Composite Materials, 2008. **00**: p. 1 - 10.
12. Kure, K., Kanda, T., Suzumori, K., Wakimoto, S.,, *Flexible displacement sensor using injected conductive paste.* Sensors & Actuators A, 2008. **143**: p. 272 - 278.
13. Knite, M., et al., *Polyisoprene-carbon black nanocomposites as tensile strain and pressure sensor materials.* Sensors and Actuators A: Physical, 2004. **110**(1-3): p. 142-149.
14. Aldraihem, O.J., W.N. Akl, and A.M. Baz, *Nanocomposite functional paint sensor for vibration and noise monitoring.* Sensors and Actuators A: Physical, 2009. **149**(2): p. 233-240.
15. Cook, J., Baker, N., Cham, R., Hale, E., Redfern, E.,, *Measurements of Wrist and Finger Postures: A Comparison of Goniometric and Motion Capture Techniques.* Journal of Applied Biomechanics, 2007. **23**: p. 70 - 78.
16. Lujan, T.J., et al., *Simultaneous measurement of three-dimensional joint kinematics and ligament strains with optical methods.* J Biomech Eng, 2005. **127**(1): p. 193-7.
17. McCulloch, A.D. and J.H. Omens, *Non-homogeneous analysis of three-dimensional transmural finite deformation in canine ventricular myocardium.* J Biomech, 1991. **24**(7): p. 539-48.

18. Nicolella, D.P., et al., *Machine vision photogrammetry: a technique for measurement of microstructural strain in cortical bone.* J Biomech, 2001. **34**(1): p. 135-9.
19. Sasaki, A., Hashimoto, H., Yokota, S., Ohyama, Y.,, *Image-Based Finger Pose Measurement for Hand User Interface*, in *IEEE*. 2010: Rzeszow, Poland.
20. Sato, K., et al., *Measurement of local strain on cell membrane at initiation point of calcium signaling response to applied mechanical stimulus in osteoblastic cells.* J Biomech, 2007. **40**(6): p. 1246-55.
21. Smutz, W.P., Drexler, M., Berland, L.J., Growney, E., An, K.N.,, *Accuracy of a Video Strain Measurement System.* Journal of Biomechanics, 1996. **29**(6): p. 813 - 817.
22. Zhang, X., Lee, S., Braido, P.,, *Determining finger segmental centers of rotation in flexion–extension based on surface marker measurement.* Journal of Biomechanics, 2003. **36**: p. 1097 - 1102.
23. Hyatt, T., et al., *Nanocomposite sensors for wide range measurement of ligament strain*, in *Proceedings of the SEM Annual Conf & Exposition on Experimental and Applied Mechanics*. 2010: Indianapolis, IN.
24. Hansen, G. *The roles of nanostrands and nickel coated fibers in electrically conductive composite design*. in *SAMPE Fall Technical Conference - 37th ISTC, October 31, 2005 - November 3, 2005*. 2005. Seattle, WA, United states: Soc. for the Advancement of Material and Process Engineering.
25. Gardner, C.J., et al. *Piezoresistive Effect in Nickel Nanostrand - Polymer Composites*. in *TMS*. 2009. San Francisco.
26. Johnson, O.K., et al. *Extreme piezoresistivity of silicone/nickel nanocomposite for high resolution large strain measurement*. in *TMS 2010*. 2010. Seattle.
27. Johnson, O., et al., *Optimization of Nickel Nanocomposite for Large Strain Sensing Applications.* Sensors and Actuators A, 2010.
28. Johnson, O.K., et al., *Multi-scale Model for the Extreme Piezoresistivity in Silicone/Nickel "Nanostrand"/Nickel Coated Carbon Fiber Nanocomposite*, in *TMS 2010*. 2010: Seattle.
29. Johnson, O. and D. Fullwood, *A percolation/quantum tunneling model for the unique behavior of multifunctional Silicone/Nickel Nanostrand nanocomposites*, in *SAMPE*. 2010: Salt Lake City.
30. Fullwood, D., O. Johnson, and G. Hansen. *Structure Metrics and Their Evolution in Piezo-resistive Nanocomposites*. in *ICCES*. 2010. Las Vegas.
31. Hyatt, T., *Piezoresistive Nanocomposites: Characterization and Applications*, in *Mechanical Engineering*. 2010, Brigham Young University: Provo.
32. Callister, W.D., *Fundamentals of Materials Science and Engineering: An Integrated Approach*. 2nd ed. 2006, Hoboken, NJ: John Wiley & Sons, Inc. 838.
33. DowCorning.com, *Information about Dow Corning Brand Silicone Encapsulants*, in *Dow Corning*. 2000-2008, www.dowcorning.com. p. 6.
34. *Peratech Limited:* http://www.peratech.com/. [cited 2010 10 June]; Quantum Tunneling Composites]. Available from: http://www.peratech.com/.
35. Bloor, D., et al., *Metal-Polymer Composite with Nanostructured Filler Particles and Amplified Physical Properties.* Appl Phys Lett, 2006. **88**: p. 102-103.
36. Palmer, J. (9 Feb 2010) *Quantum trick for pressure-sensitive mobile devices*. BBC News, http://news.bbc.co.uk/2/hi/science/nature/8504373.stm.

37. Montgomery, D.C., Runger, G.C., Hubele, N.F., *Engineering Statistics*. 2nd ed. 2001, New York: John Wiley & Sons.
38. Mark Hall, E.F., Geoffrey Holmes, Bernhard Pfahringer, Peter Reutemann, Ian H. Witten, *The Waikato Environemnt for Knowledge Analysis (WEKA) Data Mining Software: An Update.* SIGKDD Explorations, 2009. **11**(1).
39. Lu, L.K., E.M. Warshaw, and C.A. Dunnick, *Prevention of Nickel Allergy: The Case for Regulation?* Dermatologic Clinics, 2009. **27**(2): p. 155-+.

APPENDIX A. DESIGN OF EXPERIMENTS DATA

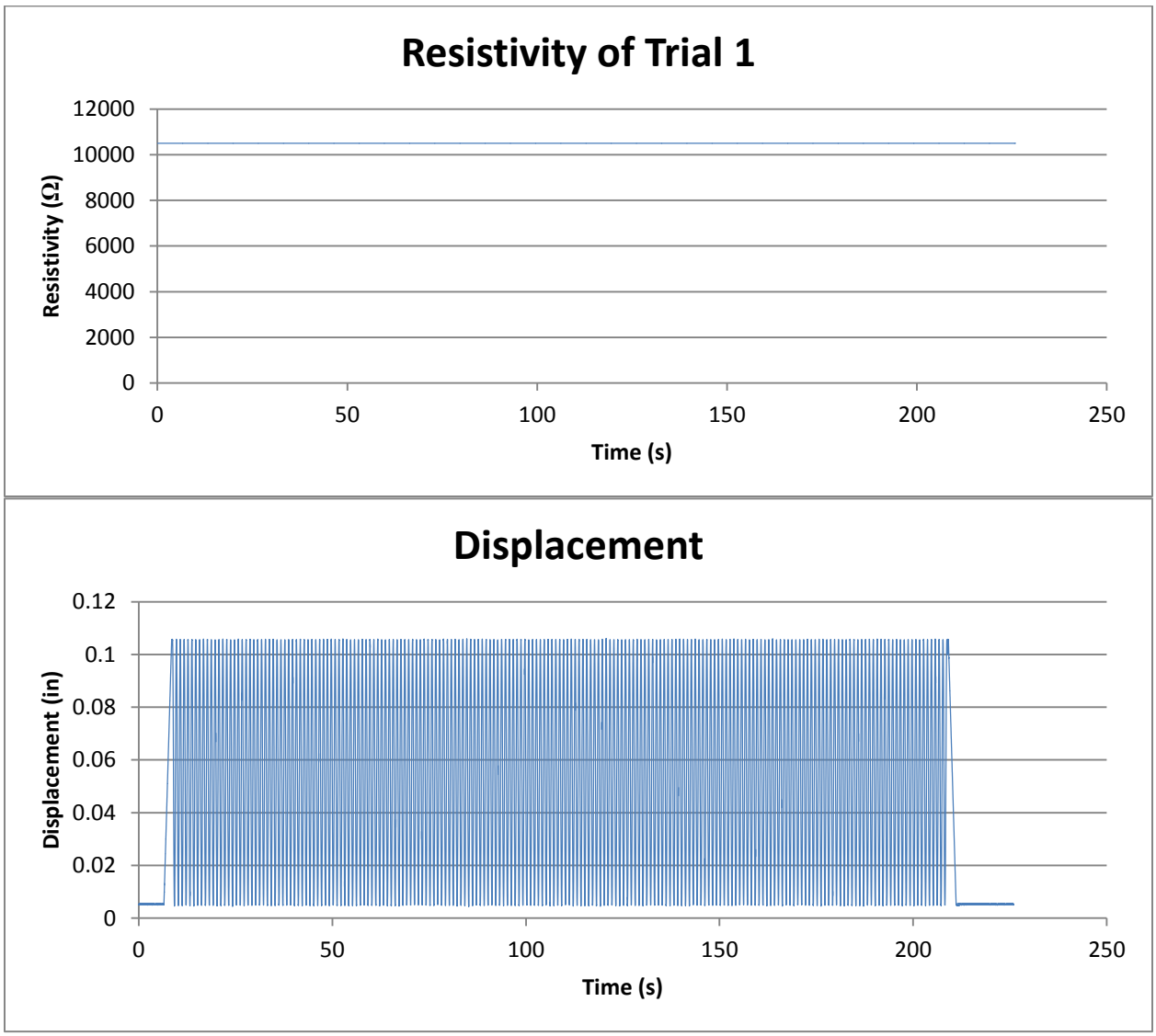

Figure A-1: Resistivity & Displacement Plots of Trial 1 Test of 200 Cycles

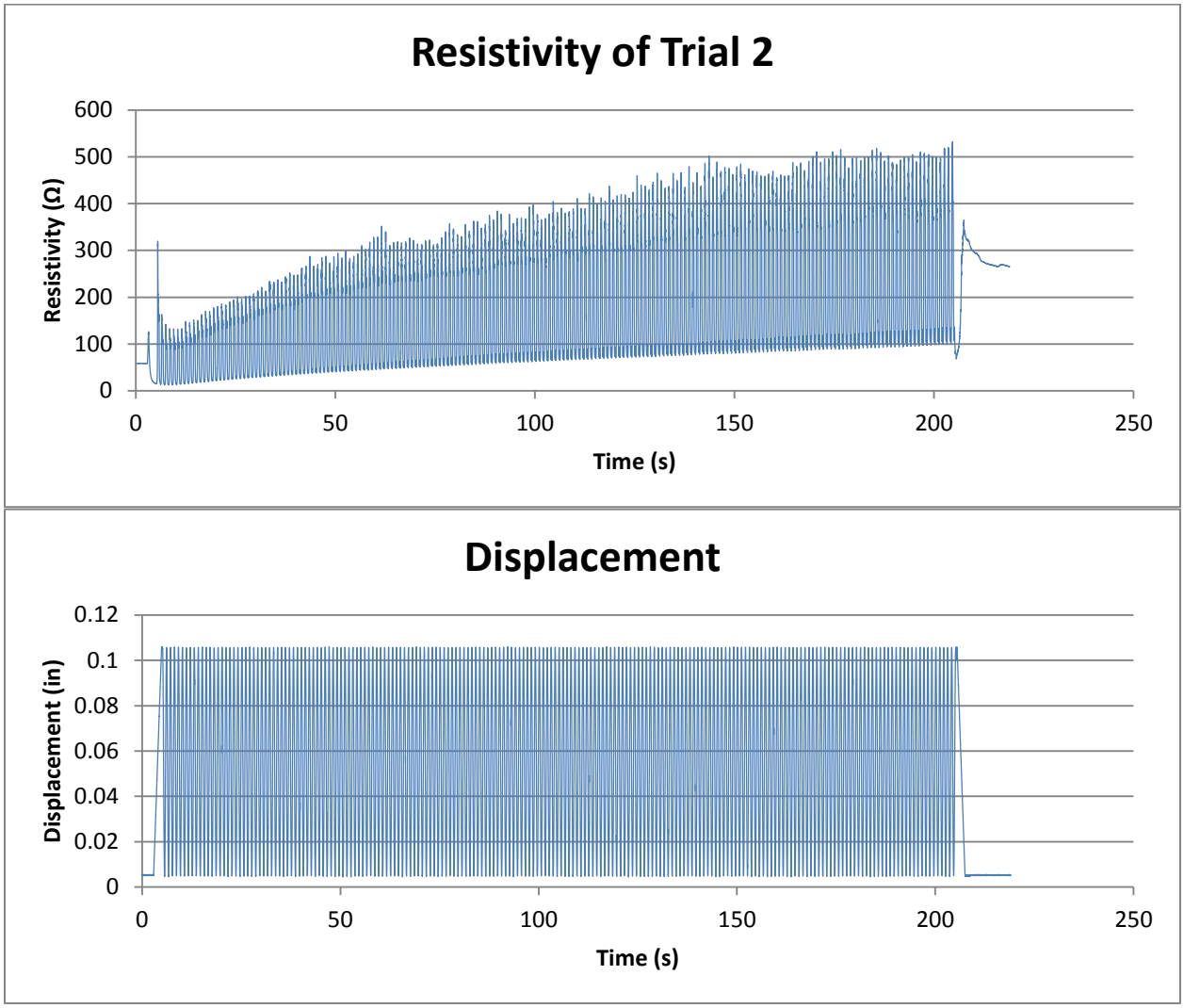

Figure A-2: Resistivity & Displacement Plots of Trial 2 Test of 200 Cycles

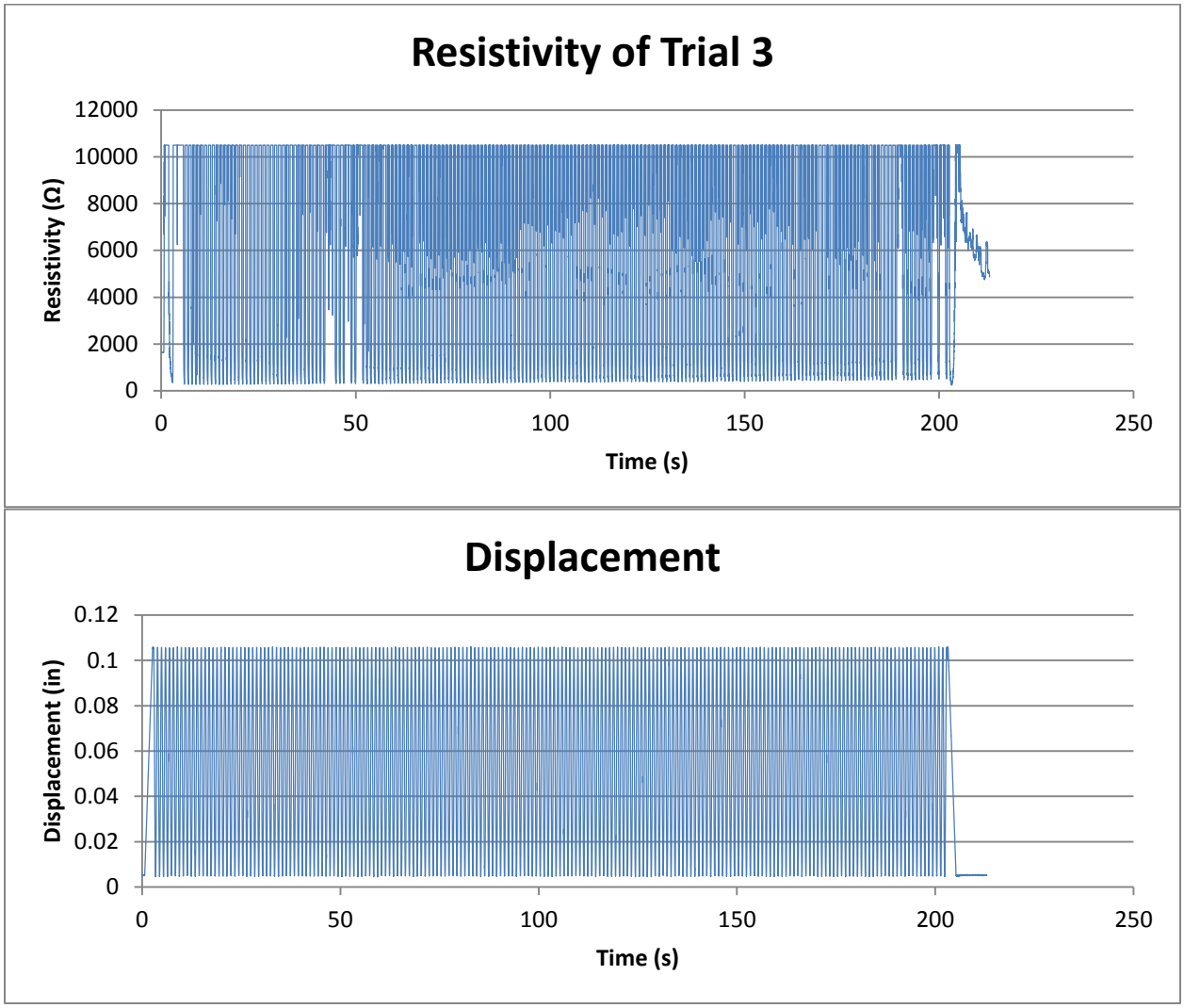

Figure A-3: Resistivity & Displacement Plots of Trial 3 Test of 200 Cycles

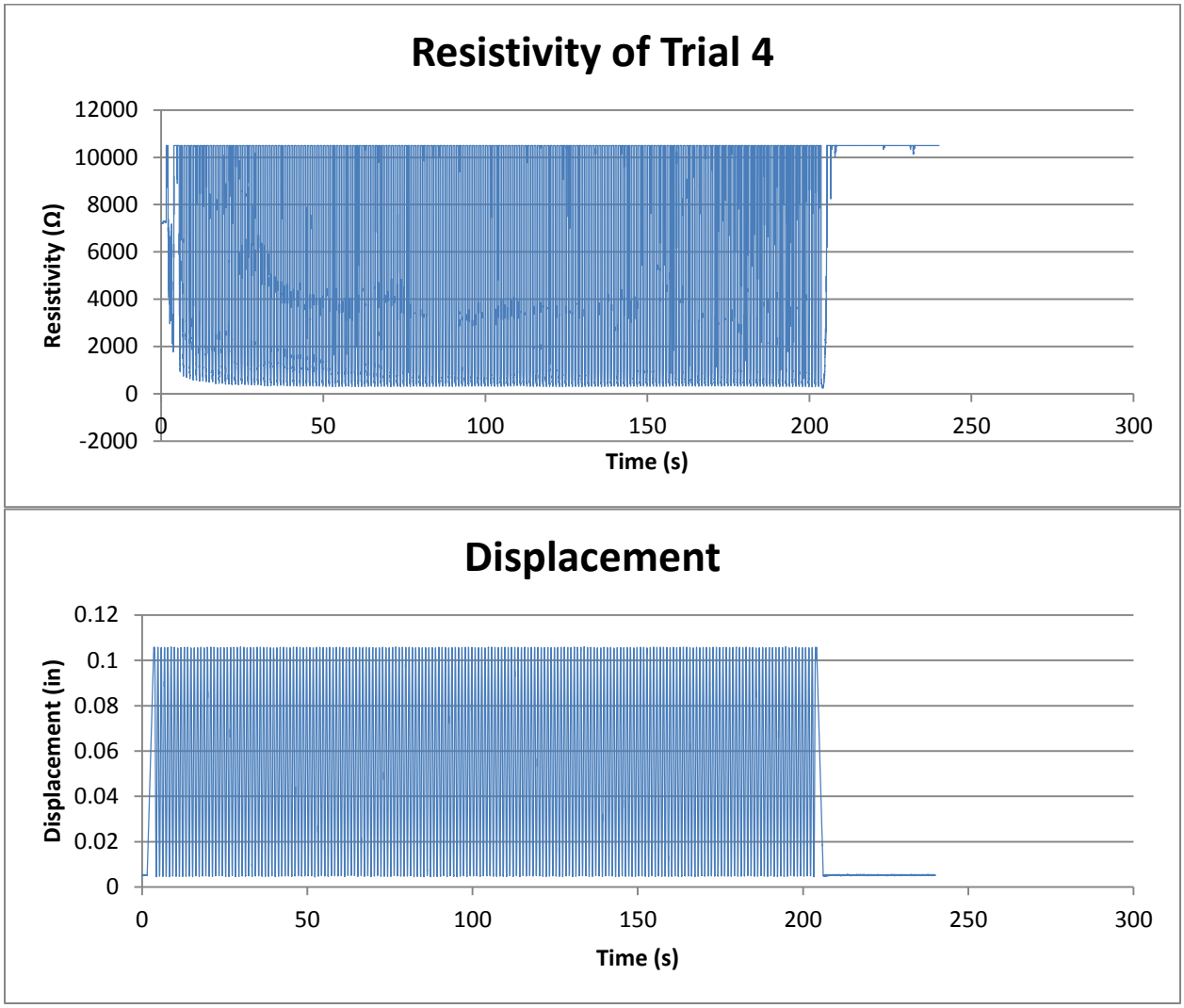

Figure A-4: Resistivity & Displacement Plots of Trial 4 Test of 200 Cycles

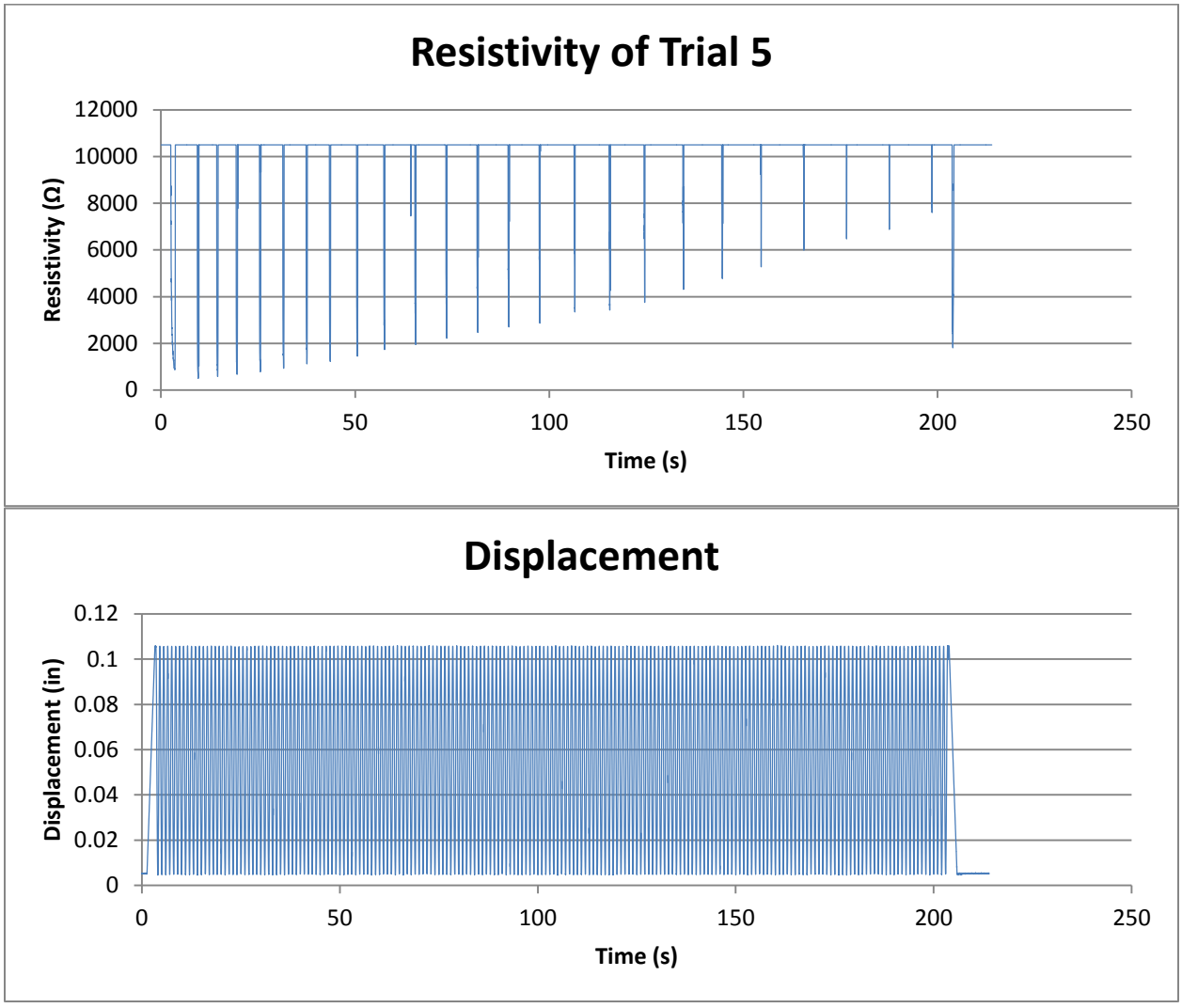

Figure A-5: Resistivity & Displacement Plots of Trial 5 Test of 200 Cycles

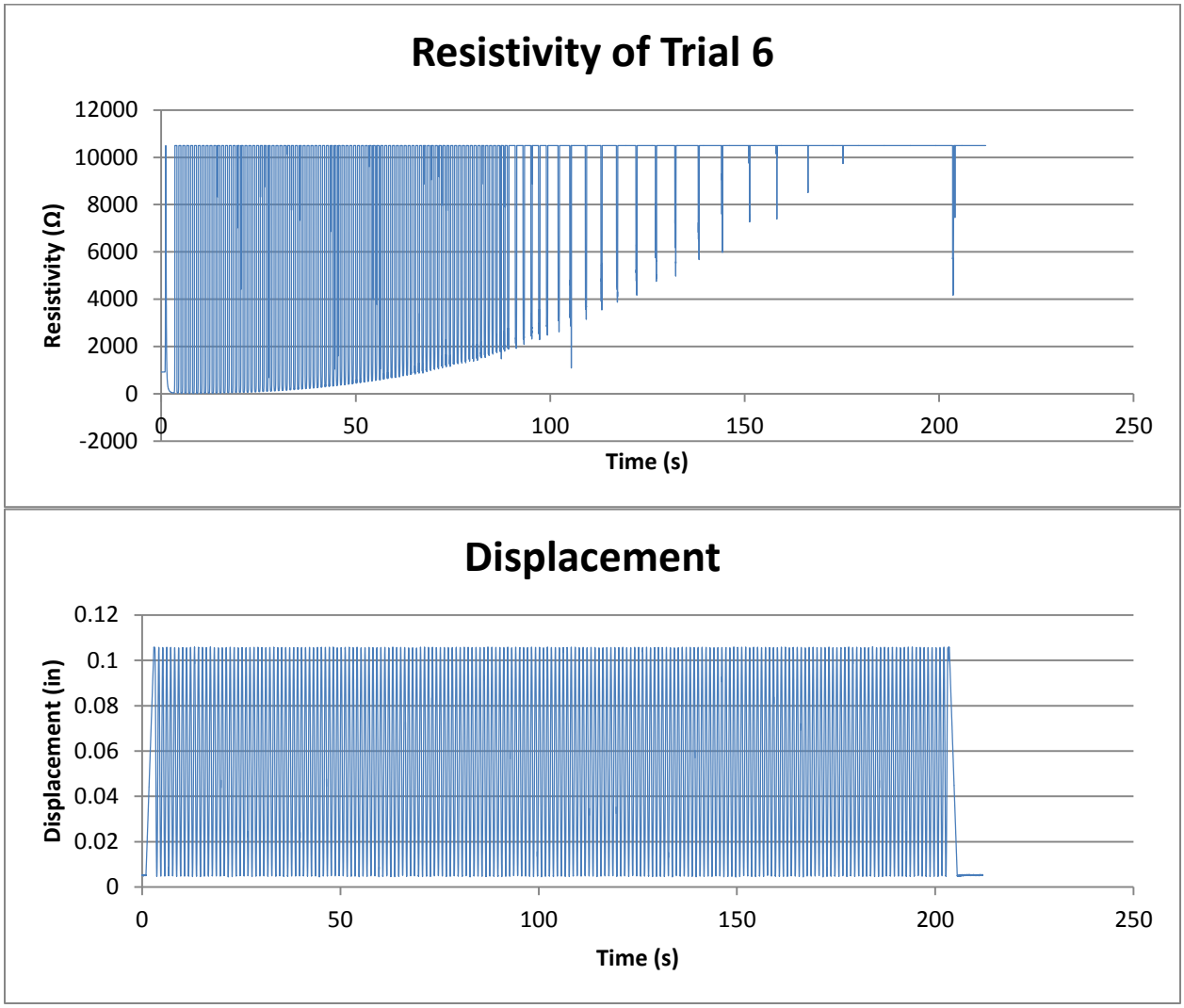

Figure A-6: Resistivity & Displacement Plots of Trial 6 Test of 200 Cycles

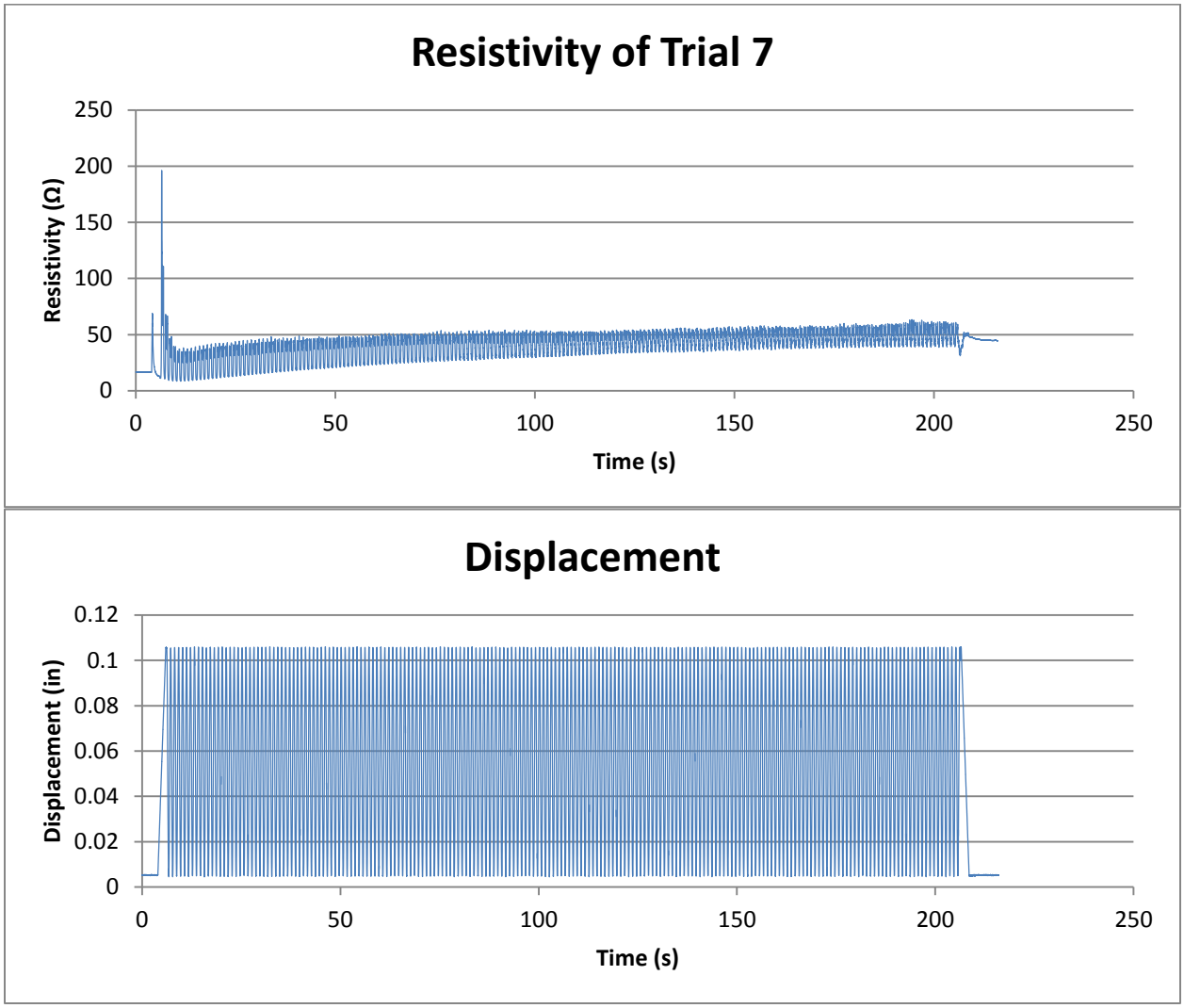

Figure A-7: Resistivity & Displacement Plots of Trial 7 Test of 200 Cycles

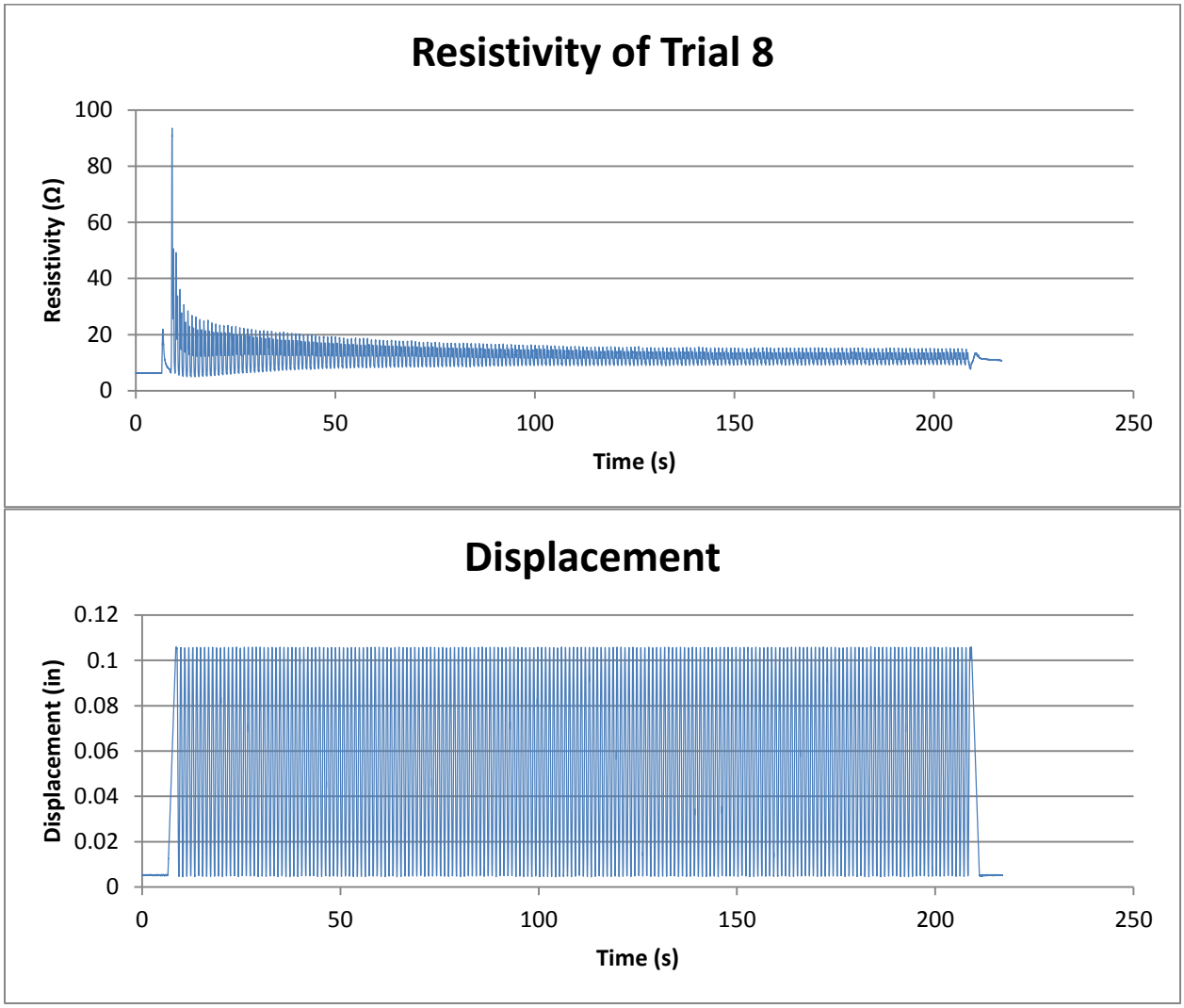

Figure A-8: Resistivity & Displacement Plots of Trial 8 Test of 200 Cycles

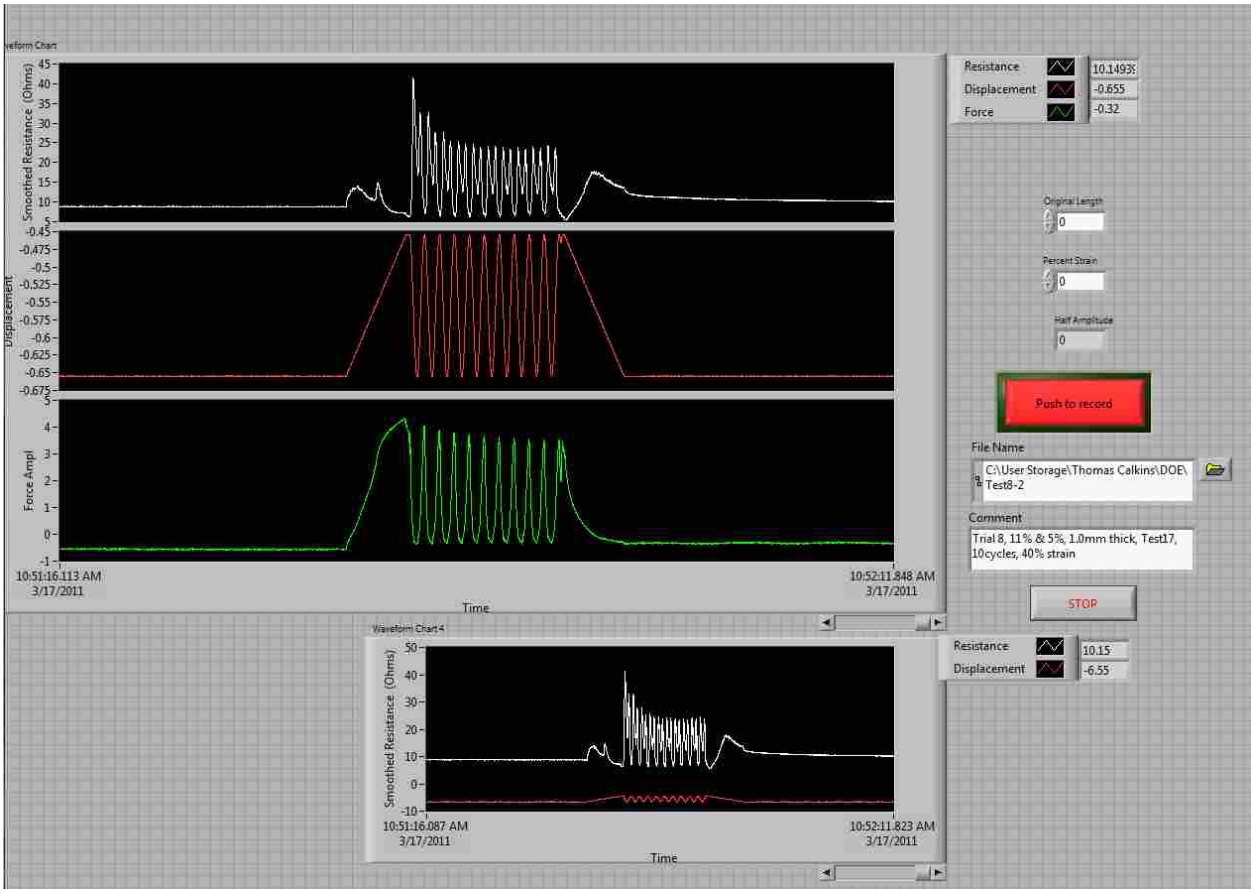

Figure A-9: Screen-Shot from Cyclic Load Testing (40% Strain, 10 Cycles)

Table A-1: Changes in Length of HDSGs in DOE

	Initial Length (in)	Tolerance (+/- in)	Final Length (in)	Tolerance (+/- in)
Trial 1	0.990	0.010	1.018	0.005
Trial 2	0.990	0.010	1.037	0.005
Trial 3	0.960	0.010	1.025	0.005
Trial 4	0.970	0.010	0.995	0.010
Trial 5	1.000	0.010	1.010	0.010
Trial 6	0.990	0.010	1.035	0.005
Trial 7	0.960	0.020	1.020	0.020
Trial 8	0.990	0.010	1.050	0.010
Avg.	0.981	0.011	1.024	0.009

APPENDIX B. ASL LETTER INTERPRETATION ANALYSIS

Table B-1: List of Resistance Values During Formation of Letters A-E

A	355.27	161.54	245.66	229.84	330.27	891.77	1923.70	941.95	1220.86	958.68	222.49	564.41
A	346.28	162.15	276.28	287.33	261.78	869.19	1207.75	558.22	288.42	958.01	228.87	621.78
A	320.23	133.21	214.09	251.39	230.44	814.52	1094.27	459.92	251.15	1115.21	228.94	625.68
A	337.66	149.59	215.75	263.32	191.93	797.52	883.14	988.17	408.72	850.51	203.98	559.71
A	280.71	137.11	195.41	201.30	189.69	746.00	1825.98	308.24	651.98	1480.72	198.24	505.29
A	279.31	132.99	193.65	180.43	202.15	739.51	1570.21	495.22	863.38	1572.93	201.18	474.16
A	271.12	129.72	196.37	215.73	193.48	778.93	819.44	550.50	390.84	1147.43	193.92	504.63
A	248.10	129.11	187.00	251.29	199.25	792.88	812.82	516.05	363.19	701.83	223.35	582.62
A	324.65	150.57	336.19	315.42	257.04	820.45	1692.92	463.49	287.95	2289.98	218.71	614.65
A	303.18	147.77	277.58	262.54	229.17	849.83	837.67	624.00	238.42	1235.94	212.48	538.69
A	322.07	149.55	301.78	323.38	242.12	771.68	2122.58	322.06	771.34	1836.75	214.46	578.15
A	280.90	141.63	258.83	267.87	212.72	735.32	2284.71	321.97	286.09	3641.81	210.92	581.41
A	346.31	152.82	323.03	354.80	294.61	838.73	1564.36	510.87	271.92	1773.66	209.25	622.81
A	309.31	148.61	269.97	311.81	226.91	835.72	2244.85	452.81	224.92	3316.08	217.41	593.50
A	343.57	146.93	254.37	299.64	247.66	828.42	2600.14	431.02	288.07	1069.49	226.21	609.74
A	322.23	146.46	269.23	265.61	221.23	764.68	1995.14	423.55	415.68	1308.70	202.85	551.56
A	326.21	156.18	314.17	300.29	253.45	850.07	1373.22	542.36	257.21	3235.19	221.48	615.91
A	299.34	143.38	269.57	265.69	207.67	754.22	1778.49	476.01	2970.73	2243.31	203.77	563.07
A	317.27	138.72	284.41	236.83	219.62	754.09	2154.37	372.60	1032.69	2880.69	217.80	601.99
A	279.22	134.09	259.62	219.44	194.48	717.77	1457.86	337.18	426.54	2819.11	211.25	515.37
A	371.78	155.60	297.10	295.81	236.00	795.20	647.25	577.57	3355.52	2497.99	224.44	653.24
A	342.81	145.88	288.28	266.26	225.49	760.51	723.36	385.52	1661.26	2990.76	212.21	615.01
A	330.76	143.73	272.65	254.26	215.32	741.20	675.32	379.79	821.99	1734.05	200.84	571.19
A	379.62	190.07	354.00	384.13	318.48	870.89	1775.25	596.02	398.99	1909.63	244.04	740.88
A	357.04	167.19	318.91	298.93	236.32	794.22	1771.78	488.92	4358.95	2822.17	211.33	689.98
A	327.29	164.92	315.26	333.45	250.14	820.66	621.67	474.71	4500.23	799.84	223.72	668.05
A	317.88	161.43	265.99	234.90	197.86	720.67	2489.62	390.18	2334.42	598.20	193.18	598.80
A	335.67	173.77	298.21	308.97	229.86	709.89	1086.22	384.18	1671.56	1026.70	196.64	624.29
A	315.72	166.43	332.68	318.14	232.34	783.46	1384.49	455.17	475.65	1204.45	226.78	661.67
A	330.83	157.67	302.82	267.60	224.85	698.86	1738.47	384.84	334.52	691.32	197.86	708.00
A	328.13	160.64	312.28	299.03	260.56	770.34	1697.34	446.27	863.83	633.69	205.68	639.05
A	330.25	175.20	338.26	312.42	233.64	806.58	867.02	506.21	1003.14	536.07	208.51	736.22
A	328.86	185.00	313.11	310.78	259.89	789.79	1080.31	447.44	1059.66	520.70	201.06	809.37
A	319.74	200.50	341.70	299.44	271.72	810.88	922.93	449.63	314.97	519.73	209.43	825.78
A	374.33	193.37	359.91	383.15	294.91	848.02	1606.48	597.30	800.99	563.65	221.67	770.39
A	395.13	193.96	363.67	401.85	318.77	844.29	1075.61	564.12	265.81	517.79	210.88	931.46
A	361.70	179.58	365.12	368.38	298.34	874.35	732.11	605.36	286.75	589.08	210.14	901.93
A	325.02	160.17	346.93	296.48	305.62	839.83	2314.84	535.28	944.49	572.29	192.22	688.00

A	302.57	154.43	323.03	372.31	312.66	883.89	693.63	449.61	515.37	758.29	239.30	608.70
A	302.21	145.53	300.81	296.21	276.94	765.75	629.83	910.68	759.05	682.07	211.43	644.35
B	282.65	128.17	378.03	254.07	419.67	1103.50	596.33	538.57	288.20	784.40	184.48	651.12
B	266.09	121.40	329.07	229.56	439.11	1078.88	504.27	596.69	311.18	749.72	213.59	798.78
B	255.65	111.45	297.47	213.89	352.93	857.39	413.29	553.58	295.36	771.72	206.05	590.04
B	249.45	112.35	287.83	219.26	359.15	1010.17	408.94	537.97	291.43	962.82	211.05	618.45
B	268.24	110.70	281.99	235.83	304.31	965.16	512.49	636.75	308.75	890.11	209.35	614.33
B	272.93	113.02	269.29	202.86	289.60	1075.41	445.51	578.67	302.42	758.68	221.53	595.60
B	269.31	105.68	275.48	212.96	317.50	943.82	444.71	579.97	292.28	839.59	217.83	580.74
B	270.32	109.27	265.84	217.10	314.36	884.67	412.27	568.72	282.33	837.90	235.59	577.72
B	265.55	109.66	273.20	207.36	321.32	1104.85	445.77	606.68	326.82	616.72	246.14	629.96
B	253.68	104.78	267.64	195.92	360.46	994.98	417.41	559.21	287.32	694.61	212.41	567.66
B	251.57	103.72	262.69	227.72	310.26	879.74	497.58	539.05	295.61	1033.21	211.74	545.32
B	254.54	101.91	271.70	224.39	340.09	920.55	559.54	563.10	294.03	859.27	248.03	747.14
B	252.41	102.26	261.25	210.79	329.78	1035.55	554.90	637.36	304.50	669.94	266.67	740.71
B	244.89	102.34	255.37	207.15	309.68	969.18	538.30	617.25	295.91	655.03	246.18	645.43
B	238.66	99.54	241.27	205.34	308.29	1004.81	541.79	611.26	295.63	624.91	283.93	679.31
B	255.60	101.08	235.77	216.59	320.72	948.98	514.58	622.77	288.76	833.01	243.28	657.72
B	271.55	107.76	274.44	206.16	348.90	917.03	509.03	553.98	299.04	810.04	287.57	642.05
B	265.35	106.55	271.17	208.60	336.88	901.32	508.82	511.51	283.36	783.63	270.75	585.17
B	265.30	104.68	272.21	202.14	318.39	932.63	562.95	604.44	336.07	897.36	289.22	697.71
B	258.36	102.09	269.33	210.20	321.92	934.09	535.04	643.56	299.92	587.98	273.06	726.61
B	258.72	100.36	266.32	208.94	296.18	901.87	548.58	560.44	277.54	638.61	253.02	638.05
B	285.13	101.47	252.18	213.54	340.86	930.67	556.66	575.00	312.81	739.97	310.65	809.43
B	281.89	101.12	234.30	217.11	407.19	905.65	553.84	528.81	292.07	836.89	284.38	693.92
B	264.26	102.51	270.43	216.65	468.01	893.04	531.24	526.43	264.79	907.63	257.75	733.60
B	251.34	100.59	262.65	211.65	391.70	870.01	524.00	524.57	257.81	929.12	263.15	666.13
B	260.68	99.82	261.03	193.07	342.70	962.19	565.31	581.19	326.88	747.28	297.77	855.84
B	255.07	99.06	257.23	183.69	321.75	887.70	537.26	536.18	296.42	766.06	267.78	720.03
B	253.24	98.88	233.02	198.79	315.98	994.00	552.00	633.85	293.65	849.95	309.03	742.19
B	251.77	98.94	234.41	199.18	313.85	991.89	553.45	632.95	293.97	786.09	314.56	738.16
B	259.49	97.73	246.42	182.38	298.46	934.12	556.65	612.47	280.90	876.36	311.11	753.62
B	252.88	103.67	249.02	200.84	335.09	1046.41	542.60	638.44	297.24	836.06	303.86	810.47
B	243.67	100.63	247.55	189.67	318.06	999.83	529.37	616.88	284.49	820.53	272.91	731.64
B	242.65	97.91	246.98	189.37	308.83	942.81	533.99	520.61	302.03	1574.61	313.41	823.75
B	236.11	98.21	245.72	190.23	304.49	926.16	512.33	501.40	294.31	931.38	292.29	761.00
B	239.78	97.83	233.91	193.13	330.71	1027.22	508.31	520.19	283.62	1173.26	334.81	753.72
B	244.29	96.90	226.58	184.79	362.73	866.80	516.35	578.79	296.13	1125.28	319.12	733.45
B	237.00	96.10	225.45	185.64	286.32	1028.17	529.35	513.52	287.41	957.64	322.52	763.78
B	234.85	94.83	229.14	188.98	289.05	888.17	510.05	569.96	280.41	884.27	313.55	729.12
B	244.14	96.21	225.17	192.52	296.30	955.62	511.01	537.95	290.69	822.64	324.54	817.42
B	242.22	95.22	223.77	188.56	292.16	898.38	503.25	534.52	290.32	898.04	306.72	772.91
C	335.20	180.28	342.82	311.54	315.42	1084.97	2870.38	529.46	297.41	658.93	299.02	791.36
C	315.83	176.91	344.64	311.30	322.45	995.67	1158.95	536.32	284.51	769.62	284.35	725.98
C	303.58	159.20	336.27	252.90	309.71	884.20	2037.41	445.35	306.57	805.66	271.54	736.16
C	363.94	166.06	372.54	304.40	379.02	965.81	1261.29	1103.95	329.05	632.03	288.60	906.62
C	377.30	184.77	363.55	328.32	381.29	818.18	2164.45	509.52	330.68	968.55	278.26	1001.42
C	338.08	166.50	367.37	328.77	312.79	1024.92	564.86	535.91	319.92	669.21	260.82	1011.45
C	382.00	178.77	398.41	376.45	335.16	975.95	1920.64	556.89	318.70	722.25	308.26	965.75
C	342.93	165.13	356.31	348.89	270.45	892.87	1733.00	502.69	296.39	660.92	274.86	926.95
C	390.04	177.82	366.47	327.09	313.62	1048.82	753.38	623.00	301.71	765.95	277.25	804.09

C	381.54	191.58	372.43	370.59	396.75	931.75	1786.85	673.12	309.07	673.66	291.86	804.21
C	474.85	191.09	397.59	360.97	356.26	968.15	597.23	571.70	315.74	729.69	266.97	930.44
C	477.32	173.01	384.26	367.63	315.44	986.98	3451.57	662.08	319.36	631.17	277.81	829.66
C	455.20	191.47	421.44	382.90	312.93	889.99	4238.27	504.92	315.05	861.54	367.05	834.20
C	495.54	194.02	400.19	381.23	354.31	968.77	1780.42	641.45	304.90	699.21	320.64	884.60
C	462.49	194.39	453.35	404.45	344.93	1018.47	1810.01	758.34	319.07	949.22	366.32	891.50
C	500.80	210.99	494.36	399.71	368.12	1017.04	1543.33	706.00	309.39	3479.70	329.11	995.79
C	479.07	210.11	510.93	396.06	354.62	911.15	1199.60	624.48	290.06	1538.20	291.49	930.30
C	491.02	212.67	533.59	431.31	456.84	963.08	1492.14	506.21	324.04	1265.60	350.83	917.84
C	383.35	193.58	477.05	410.49	364.61	1100.41	3874.83	691.21	362.94	2300.77	268.16	918.19
C	433.50	217.46	438.88	380.50	372.02	1088.12	2424.68	620.21	316.80	1134.74	332.14	807.64
C	389.09	202.17	436.96	394.55	264.61	990.06	1322.72	514.93	318.18	888.83	316.51	722.75
C	525.35	226.98	545.93	438.79	364.34	1138.85	1430.98	507.62	341.62	979.81	329.56	887.54
C	465.37	172.23	430.04	385.44	401.19	1205.24	5304.91	568.83	318.64	950.08	422.42	1208.76
C	531.18	235.84	475.31	417.80	366.70	928.00	1117.10	538.31	322.12	970.64	346.21	889.05
C	426.58	230.30	453.76	419.32	333.03	1046.77	763.14	585.59	316.66	876.54	294.24	874.30
C	453.00	196.91	346.09	443.93	351.23	1188.74	1179.75	742.51	316.98	855.63	274.43	844.85
C	441.86	191.46	377.15	410.42	323.76	1174.77	3797.85	656.32	303.46	722.69	298.00	869.74
C	519.92	223.26	408.18	400.58	480.87	1080.41	1402.23	543.36	317.82	888.52	315.70	951.69
C	462.90	225.15	447.07	380.20	367.05	1170.74	1127.78	735.26	366.85	754.27	328.23	1078.45
C	477.67	209.92	436.01	399.25	341.22	1032.65	1343.22	641.34	330.41	750.68	332.26	937.29
C	478.89	211.28	432.85	381.76	356.93	931.34	1399.36	589.31	312.43	762.14	308.28	800.22
C	621.46	240.25	669.99	485.05	549.22	1110.42	1535.17	599.45	374.52	862.45	337.87	969.19
C	460.59	198.89	427.84	393.95	347.71	1289.25	917.00	644.58	326.33	847.73	271.72	910.16
C	553.35	219.73	414.52	352.62	464.87	1269.90	3263.03	643.02	305.73	608.28	357.55	863.47
C	418.50	222.63	438.29	415.56	498.72	1012.69	1714.93	640.56	304.54	789.62	331.33	1008.69
C	563.83	243.19	553.17	442.73	474.46	1129.65	4161.04	538.07	340.62	796.94	314.10	1070.22
C	429.91	208.75	454.83	374.94	379.05	1103.68	2479.28	678.77	295.35	692.13	309.36	927.65
C	536.58	205.47	455.74	432.84	369.25	1158.77	2876.03	663.72	310.38	763.40	346.36	949.75
C	480.42	202.78	428.59	411.67	349.19	1131.42	4737.50	682.83	297.18	784.67	314.80	955.47
C	497.97	229.71	491.62	471.88	394.25	1175.22	4454.20	673.85	291.01	760.09	311.36	907.89
D	228.91	108.35	131.54	403.61	292.54	1068.52	1974.16	1638.61	367.93	2305.92	345.63	652.96
D	214.11	101.26	173.19	367.96	258.04	962.15	1534.18	1727.24	284.04	1131.62	310.74	707.53
D	234.73	164.63	285.35	482.88	335.54	1060.01	2084.12	1660.38	311.40	1210.18	313.07	944.55
D	211.98	87.25	220.79	328.92	233.79	1352.78	1213.49	1775.33	301.46	2023.64	290.39	761.25
D	218.27	169.17	341.23	654.40	257.77	1342.82	4545.26	678.71	344.21	1001.30	309.98	907.25
D	203.88	154.85	491.89	453.19	255.16	1208.93	2192.55	604.67	311.07	924.73	307.35	948.96
D	200.22	144.47	312.99	388.89	289.41	1032.75	1248.50	631.68	307.04	985.25	305.69	656.15
D	230.76	153.33	307.87	495.73	372.59	979.95	1957.37	744.90	319.83	781.11	325.10	764.99
D	214.69	127.06	277.10	318.87	263.56	780.38	847.43	644.52	283.59	1389.10	278.65	624.22
D	211.25	122.22	262.71	261.38	251.44	765.85	826.56	617.01	281.60	1141.97	265.50	593.23
D	222.84	158.59	289.17	369.86	275.37	1050.87	1678.59	1618.82	305.07	1531.73	345.28	702.22
D	214.11	160.46	301.57	331.58	280.21	1401.01	875.86	753.67	316.43	1537.84	327.03	733.80
D	217.08	159.23	304.94	343.33	272.85	1556.41	937.43	1294.78	320.83	736.39	327.46	774.36
D	210.91	131.01	248.13	336.34	300.09	1095.64	3669.47	1220.96	320.40	1409.11	332.65	611.60
D	215.37	140.75	317.15	377.78	293.24	1705.86	1392.41	1281.01	317.26	871.42	321.20	759.03
D	203.37	133.62	270.08	350.21	273.07	679.99	1669.62	1302.46	306.40	726.26	330.60	711.94
D	195.00	145.27	281.17	396.76	317.57	1293.25	3170.65	745.12	303.48	818.32	336.23	605.29
D	209.55	141.43	360.65	466.58	299.30	721.64	3907.67	767.77	339.65	931.53	349.48	822.50
D	210.13	134.86	362.69	330.91	260.40	663.38	2492.38	1117.32	342.34	915.36	369.97	781.32
D	208.94	142.99	340.68	479.19	357.02	818.89	3042.24	878.40	362.05	733.61	359.40	993.86

D	212.97	153.74	341.33	461.73	288.21	405.19	2035.82	987.91	324.81	931.30	317.47	711.89
D	217.87	208.19	536.77	700.23	367.87	855.91	3043.51	1856.34	357.28	935.00	390.64	1279.02
D	210.52	219.35	602.99	709.64	363.11	917.42	2199.24	1634.34	329.70	884.49	365.90	1268.67
D	213.20	175.33	443.57	687.84	408.73	828.28	3723.83	1662.12	331.08	1371.80	374.29	1091.43
D	219.64	244.97	638.45	780.54	377.46	1051.54	2584.15	1455.86	354.94	3112.87	479.77	1285.70
D	211.68	213.84	752.22	593.97	334.41	1061.13	3553.70	1459.45	330.93	1756.53	330.70	1103.15
D	210.90	161.23	388.23	387.44	304.69	1777.05	1052.33	1609.56	336.54	1519.00	340.57	912.72
D	202.88	169.03	368.66	385.90	421.57	1778.48	2387.47	737.12	314.49	1776.29	339.15	799.88
D	214.51	116.77	410.19	541.72	355.40	1593.46	930.13	1094.63	313.74	1601.41	361.42	821.30
D	218.80	106.44	419.01	456.44	332.23	1138.45	1079.08	1246.86	332.65	1736.26	335.36	958.52
D	208.50	111.76	384.89	452.27	299.49	1072.74	3063.40	1312.78	325.51	1369.05	337.87	920.78
D	237.05	225.27	531.69	624.52	328.90	1074.64	3733.13	2014.26	454.64	1739.93	431.70	1413.67
D	210.79	199.95	889.24	488.23	328.10	1171.82	3262.56	1397.81	360.83	1566.80	353.45	1111.35
D	217.66	202.77	763.56	590.00	312.08	1110.90	5373.08	1594.88	342.65	1386.17	366.65	965.02
D	236.90	250.24	703.94	792.93	424.48	1111.23	2664.61	1642.88	350.19	1883.56	409.01	1417.10
D	217.04	129.20	386.14	505.01	328.51	843.55	2020.24	1689.60	351.60	1320.04	362.16	1046.98
D	237.22	240.31	675.50	865.41	412.59	911.14	2664.96	1886.68	370.93	1736.90	420.28	1483.47
D	243.42	223.09	611.56	775.11	553.33	943.37	5578.07	1817.00	397.29	1155.39	365.23	1222.98
D	234.67	173.43	493.93	584.18	318.29	870.44	3800.61	1834.38	384.39	1564.40	384.18	1033.29
D	233.16	145.86	341.52	550.47	291.83	856.00	1086.20	1822.56	366.79	1496.26	402.54	934.95
E	239.53	142.60	178.67	312.82	218.39	865.66	647.81	901.23	710.67	782.24	145.80	196.58
E	228.59	145.29	206.29	226.08	196.49	995.14	1901.06	856.22	399.93	1381.07	175.99	167.07
E	202.73	78.82	150.52	216.62	187.57	889.84	1519.86	886.45	389.09	1749.63	196.57	180.79
E	194.66	100.39	178.47	167.97	212.70	834.54	1838.36	779.37	323.40	1155.19	152.27	165.90
E	194.70	97.46	178.64	172.70	196.97	809.62	755.75	715.97	282.71	1098.81	149.16	148.88
E	209.58	111.66	158.86	128.63	220.68	900.71	1834.73	690.15	369.88	1043.22	172.71	152.77
E	168.54	101.04	175.06	168.45	167.18	911.62	925.71	950.09	1038.13	1104.66	202.49	170.85
E	193.00	111.70	141.17	215.62	157.32	1046.79	1668.97	904.51	369.23	2355.36	218.01	167.49
E	121.52	81.98	129.77	193.93	146.42	871.06	2764.25	948.63	1971.51	1365.89	223.44	200.08
E	121.12	78.94	132.12	188.15	139.03	883.07	2658.83	796.94	2527.29	1703.55	197.05	161.39
E	134.66	107.52	179.80	219.32	182.97	955.96	1740.68	810.11	2015.18	1603.25	220.43	216.67
E	134.68	89.22	213.07	160.14	151.21	1017.29	725.38	884.22	1749.00	2335.88	225.20	248.69
E	199.18	98.63	182.44	226.88	214.55	1010.32	1107.60	883.89	501.61	941.09	277.75	256.43
E	204.06	103.24	149.07	192.42	190.97	961.14	598.86	931.46	2057.98	990.65	253.41	275.77
E	161.64	112.30	195.88	243.30	205.57	1086.29	3038.20	1011.20	540.43	934.89	218.94	278.75
E	132.91	99.09	173.41	184.82	182.34	904.83	1196.92	644.84	634.03	1498.56	172.04	284.19
E	221.16	128.51	212.05	220.27	238.57	997.47	1630.65	816.18	463.78	1666.62	150.21	311.44
E	154.41	113.12	194.75	207.06	204.00	1027.89	1955.65	796.53	465.80	986.98	145.85	274.79
E	176.86	129.51	208.37	226.62	200.21	1167.89	838.17	972.97	1383.38	1826.54	158.35	288.02
E	231.61	139.42	223.05	288.04	246.96	1210.55	5767.11	962.01	576.16	1605.92	80.19	280.70
E	241.94	134.03	235.74	227.63	254.46	1106.89	1681.92	545.63	890.88	2300.48	91.43	319.26
E	218.87	151.23	214.44	213.99	259.22	1190.22	1790.75	910.96	456.06	1176.83	70.54	329.57
E	218.11	122.32	205.14	283.07	223.79	1005.21	894.18	672.55	2724.16	1246.13	87.84	391.23
E	206.65	138.78	298.20	320.15	210.70	1266.18	1347.06	1095.86	504.00	880.48	156.64	674.63
E	223.63	158.40	223.53	276.03	223.12	946.50	875.58	777.50	673.49	1508.43	97.66	420.27
E	246.38	156.78	259.26	402.86	274.46	1395.31	4252.16	821.97	367.41	1103.39	180.16	573.22
E	224.01	168.37	226.79	252.63	238.23	1128.78	5643.61	708.00	418.90	769.21	123.67	433.40
E	229.42	170.38	204.98	227.82	269.27	1176.54	5357.88	411.79	1125.23	792.33	113.47	388.42
E	231.63	171.02	190.57	270.30	224.09	1059.74	1865.79	409.76	1099.69	929.36	132.60	492.04
E	230.98	165.71	285.07	312.12	197.03	1117.34	2800.35	823.22	538.33	1739.03	119.17	561.57
E	274.34	188.18	330.72	497.40	333.20	1422.82	1295.06	745.13	440.70	983.35	169.99	629.29

E	272.08	194.80	287.18	377.02	272.63	1444.89	736.67	1079.67	494.65	1087.66	116.41	632.57
E	246.94	158.13	240.09	334.52	302.92	1255.76	2741.47	986.08	656.94	1023.97	108.57	462.29
E	272.53	169.07	236.12	352.60	298.29	1293.18	851.19	708.14	751.05	919.56	131.46	456.54
E	272.17	208.78	322.08	412.12	353.10	1370.31	910.02	1251.00	436.04	856.68	196.54	606.07
E	280.31	185.96	286.24	458.06	293.82	1356.05	1077.84	1156.26	450.25	1160.20	149.41	486.10
E	294.00	192.94	334.88	296.88	328.82	1441.78	1596.50	1147.53	413.95	774.94	157.66	509.85
E	274.55	193.26	250.63	359.42	247.31	1335.86	1065.98	1068.02	766.04	821.06	113.61	454.43
E	250.77	190.52	288.57	350.54	290.43	1357.27	3445.41	862.84	492.73	980.49	135.46	412.96
E	258.25	170.55	252.26	338.72	288.61	1366.72	1038.45	1361.74	541.54	994.23	147.82	450.24

Table B-2: Mean Values of Each Letter for Each Gauge

Mean Values	1	2	3	4	5	6	7	8	9	10	11	12
A	338.9	168.8	320.5	315.1	260.0	796.5	1226.7	501.4	1336.4	1108.4	212.1	704.3
B	252.0	98.9	243.6	196.4	331.0	942.5	533.8	562.2	290.2	905.1	298.6	752.4
C	486.7	214.8	456.2	412.7	388.9	1113.4	2316.4	619.4	320.5	815.3	323.0	931.4
D	220.5	183.5	534.2	596.7	357.6	1068.6	2791.8	1537.9	351.5	1542.2	373.4	1089.1
E	248.4	169.5	258.6	328.2	269.2	1251.9	2063.4	877.2	712.1	1102.4	130.0	484.2

Table B-3: Evaluation of Accuracy Using Sum of the Differences

Distance - From Every Point to these 5 points									
To Mean of:	A	B	C	D	E	Actual	Predicted		Correct?
1	0.0893	0.3520	0.1622	0.3247	0.0869	A	E	0.0869	0
2	0.2626	0.1178	0.3469	0.9865	0.3274	A	B	0.1178	0
3	0.2976	0.1041	0.4749	1.1659	0.4281	A	B	0.1041	0
4	0.3365	0.1075	0.6612	1.2896	0.5280	A	B	0.1075	0
5	0.1524	0.3278	0.2001	0.4669	0.1627	A	A	0.1524	1
6	0.0944	0.2882	0.2895	0.5292	0.1888	A	A	0.0944	1
7	0.3206	0.0767	0.8071	1.6232	0.6618	A	B	0.0767	0
8	0.4790	0.0747	0.9762	2.2583	0.8867	A	B	0.0747	0
9	0.2747	0.3377	0.2883	0.3406	0.2351	A	E	0.2351	0
10	0.3524	0.0719	0.6734	1.3198	0.5660	A	B	0.0719	0
11	0.1714	0.3808	0.1722	0.2735	0.1371	A	E	0.1371	0
12	0.4379	0.5391	0.4275	0.3398	0.3787	A	D	0.3398	0
13	0.2261	0.2525	0.2307	0.4044	0.1910	A	E	0.1910	0
14	0.4043	0.4981	0.3726	0.2900	0.3262	A	D	0.2900	0
15	0.3120	0.4546	0.0492	0.2068	0.1138	A	C	0.0492	0
16	0.2079	0.3345	0.1084	0.3504	0.1213	A	C	0.1084	0
17	0.4016	0.4351	0.4924	0.4445	0.4035	A	A	0.4016	1
18	0.2326	0.5759	0.5295	0.5479	0.3890	A	A	0.2326	1
19	0.2679	0.4669	0.3391	0.2983	0.2617	A	E	0.2617	0
20	0.3407	0.4127	0.4674	0.4881	0.3782	A	A	0.3407	1
21	0.3217	0.6086	0.7642	0.8064	0.5799	A	A	0.3217	1
22	0.2864	0.4653	0.6895	0.7265	0.5097	A	A	0.2864	1
23	0.1821	0.2053	0.7703	1.2157	0.5686	A	A	0.1821	1
24	0.2003	0.2863	0.1762	0.2533	0.1325	A	E	0.1325	0

25	0.3879	0.6848	0.6551	0.6354	0.5294	A	A	0.3879	1
26	0.4538	0.7720	0.8926	1.0400	0.7393	A	A	0.4538	1
27	0.2166	0.6165	0.3444	0.5135	0.2881	A	A	0.2166	1
28	0.0259	0.3667	0.5852	1.0469	0.4084	A	A	0.0259	1
29	0.1474	0.1773	0.2533	0.7005	0.2130	A	A	0.1474	1
30	0.2855	0.3176	0.1442	0.7141	0.2199	A	C	0.1442	0
31	0.1199	0.3270	0.1831	0.6989	0.1789	A	A	0.1199	1
32	0.1446	0.2103	0.7294	1.6665	0.5877	A	A	0.1446	1
33	0.1021	0.2506	0.5347	1.3379	0.4275	A	A	0.1021	1
34	0.4651	0.1185	0.6940	1.8670	0.7013	A	B	0.1185	0
35	0.1299	0.2790	0.1616	0.6425	0.1532	A	A	0.1299	1
36	0.3953	0.1440	0.4323	1.2788	0.4601	A	B	0.1440	0
37	0.4831	0.0690	0.7679	1.7923	0.7198	A	B	0.0690	0
38	0.1917	0.4426	0.0785	0.3419	0.1017	A	C	0.0785	0
39	0.3476	0.0569	0.9187	2.0744	0.8170	A	B	0.0569	0
40	0.2842	0.1281	0.9356	1.7518	0.7286	A	B	0.1281	0
41	0.4965	0.0284	0.8990	1.9368	0.8029	B	B	0.0284	1
42	0.5192	0.0212	0.9642	1.9818	0.8329	B	B	0.0212	1
43	0.7275	0.0299	1.5079	2.9567	1.3522	B	B	0.0299	1
44	0.5744	0.0164	1.2065	2.3002	1.0334	B	B	0.0164	1
45	0.5237	0.0119	1.0939	2.1430	0.9312	B	B	0.0119	1
46	0.6307	0.0266	1.2394	2.4776	1.0821	B	B	0.0266	1
47	0.6338	0.0173	1.3097	2.5625	1.1478	B	B	0.0173	1
48	0.6913	0.0214	1.4382	2.7804	1.2741	B	B	0.0214	1
49	0.6622	0.0460	1.2439	2.5317	1.1008	B	B	0.0460	1
50	0.7438	0.0380	1.4437	2.8849	1.2963	B	B	0.0380	1
51	0.5417	0.0240	1.2011	2.2901	1.0326	B	B	0.0240	1
52	0.5080	0.0023	1.0218	2.0923	0.8821	B	B	0.0023	1
53	0.5610	0.0222	1.0236	2.1408	0.8926	B	B	0.0222	1
54	0.6398	0.0282	1.2008	2.4937	1.0693	B	B	0.0282	1
55	0.6363	0.0308	1.1603	2.4313	1.0348	B	B	0.0308	1
56	0.5651	0.0071	1.1324	2.2526	0.9752	B	B	0.0071	1
57	0.5844	0.0083	1.1875	2.4144	1.0561	B	B	0.0083	1
58	0.6487	0.0180	1.3022	2.6734	1.1816	B	B	0.0180	1
59	0.4639	0.0028	0.9928	1.9973	0.8425	B	B	0.0028	1
60	0.6516	0.0377	1.1853	2.4734	1.0655	B	B	0.0377	1
61	0.6941	0.0338	1.2946	2.7365	1.1863	B	B	0.0338	1
62	0.5295	0.0104	1.0214	2.1445	0.8975	B	B	0.0104	1
63	0.5403	0.0059	1.0795	2.2381	0.9590	B	B	0.0059	1
64	0.5345	0.0081	1.0505	2.1218	0.9273	B	B	0.0081	1
65	0.5641	0.0069	1.1386	2.2706	1.0053	B	B	0.0069	1
66	0.5006	0.0116	0.9656	2.0243	0.8312	B	B	0.0116	1
67	0.5929	0.0088	1.1823	2.4520	1.0483	B	B	0.0088	1
68	0.5014	0.0034	0.9757	1.9624	0.8270	B	B	0.0034	1
69	0.5286	0.0069	1.0077	2.0557	0.8663	B	B	0.0069	1
70	0.5095	0.0017	1.0022	2.0131	0.8564	B	B	0.0017	1
71	0.4853	0.0069	0.9177	1.8489	0.7695	B	B	0.0069	1
72	0.5385	0.0045	1.0389	2.0932	0.8874	B	B	0.0045	1
73	0.3663	0.0903	0.7872	1.2832	0.6101	B	B	0.0903	1
74	0.5216	0.0019	1.0863	2.1695	0.9296	B	B	0.0019	1
75	0.4366	0.0208	0.9081	1.6963	0.7437	B	B	0.0208	1

76	0.4571	0.0157	0.9955	1.8489	0.8264	B	B	0.0157	1
77	0.4888	0.0045	0.9808	1.9601	0.8257	B	B	0.0045	1
78	0.5626	0.0023	1.1459	2.2640	0.9880	B	B	0.0023	1
79	0.5486	0.0045	1.0756	2.1842	0.9269	B	B	0.0045	1
80	0.5457	0.0020	1.1246	2.2329	0.9643	B	B	0.0020	1
81	0.3586	0.4898	0.0363	0.1785	0.1144	C	C	0.0363	1
82	0.2934	0.1027	0.3365	1.0435	0.3363	C	B	0.1027	0
83	0.2664	0.3354	0.0413	0.3842	0.1070	C	C	0.0413	1
84	0.2986	0.1706	0.2533	0.6227	0.2183	C	B	0.1706	0
85	0.2435	0.3375	0.0219	0.2392	0.0683	C	C	0.0219	1
86	0.4812	0.0473	0.8356	1.8151	0.7406	C	B	0.0473	0
87	0.2498	0.2897	0.0291	0.3498	0.0820	C	C	0.0291	1
88	0.2682	0.2654	0.0804	0.5277	0.1358	C	C	0.0804	1
89	0.3799	0.0361	0.6281	1.4621	0.5628	C	B	0.0361	0
90	0.2572	0.2676	0.0583	0.4251	0.1128	C	C	0.0583	1
91	0.4412	0.0462	0.7750	1.7058	0.7093	C	B	0.0462	0
92	0.4151	0.5721	0.0898	0.1483	0.1694	C	C	0.0898	1
93	0.4804	0.6492	0.1771	0.1797	0.2535	C	C	0.1771	1
94	0.2502	0.2610	0.0493	0.4080	0.1066	C	C	0.0493	1
95	0.2147	0.2435	0.0409	0.2736	0.0663	C	C	0.0409	1
96	0.3902	0.4384	0.4276	0.3401	0.3519	C	D	0.3401	0
97	0.2092	0.1536	0.2642	0.5145	0.2146	C	B	0.1536	0
98	0.1895	0.1856	0.1319	0.4232	0.1397	C	C	0.1319	1
99	0.4044	0.5604	0.1961	0.1082	0.2116	C	D	0.1082	0
100	0.2563	0.3665	0.0130	0.1288	0.0566	C	C	0.0130	1
101	0.2279	0.1445	0.2126	0.7550	0.2296	C	B	0.1445	0
102	0.2034	0.1711	0.1283	0.5205	0.1480	C	C	0.1283	1
103	0.5470	0.6962	0.2718	0.2330	0.3297	C	D	0.2330	0
104	0.2330	0.1086	0.2886	0.8276	0.2908	C	B	0.1086	0
105	0.3266	0.0497	0.5445	1.2539	0.4888	C	B	0.0497	0
106	0.2438	0.1139	0.2367	0.6889	0.2068	C	B	0.1139	0
107	0.4392	0.5928	0.1214	0.1438	0.1915	C	C	0.1214	1
108	0.2209	0.1601	0.1387	0.5693	0.1582	C	C	0.1387	1
109	0.2497	0.1199	0.2473	0.7052	0.2167	C	B	0.1199	0
110	0.2368	0.1535	0.1692	0.6461	0.1851	C	B	0.1535	0
111	0.2425	0.1707	0.1687	0.6914	0.2092	C	C	0.1687	1
112	0.2179	0.2131	0.0974	0.4335	0.1396	C	C	0.0974	1
113	0.2864	0.0804	0.3729	0.9329	0.3212	C	B	0.0804	0
114	0.3933	0.5272	0.0663	0.1470	0.1455	C	C	0.0663	1
115	0.2363	0.2328	0.0562	0.3751	0.0949	C	C	0.0562	1
116	0.4608	0.6189	0.1572	0.1636	0.2294	C	C	0.1572	1
117	0.3036	0.3996	0.0051	0.1682	0.0717	C	C	0.0051	1
118	0.3339	0.4597	0.0257	0.1221	0.0952	C	C	0.0257	1
119	0.5170	0.6724	0.2203	0.1963	0.2861	C	D	0.1963	0
120	0.4945	0.6493	0.1897	0.1767	0.2597	C	D	0.1767	0
121	0.3116	0.3763	0.2599	0.1183	0.1745	D	D	0.1183	1
122	0.3275	0.2883	0.2586	0.2528	0.1720	D	E	0.1720	0
123	0.2944	0.3405	0.1240	0.0645	0.0803	D	D	0.0645	1
124	0.3357	0.2924	0.3699	0.2742	0.2334	D	E	0.2334	0
125	0.4881	0.6445	0.2036	0.1664	0.2547	D	D	0.1664	1
126	0.2549	0.3278	0.0155	0.1846	0.0446	D	C	0.0155	0

127	0.2367	0.1175	0.2736	0.7603	0.2353	D	B	0.1175	0
128	0.2520	0.2980	0.0397	0.2851	0.0745	D	C	0.0397	0
129	0.3050	0.0895	0.6257	1.1192	0.4994	D	B	0.0895	0
130	0.3573	0.0580	0.7346	1.4599	0.6171	D	B	0.0580	0
131	0.2806	0.2886	0.2099	0.1523	0.1293	D	E	0.1293	0
132	0.2674	0.1177	0.4226	0.6889	0.2903	D	B	0.1177	0
133	0.3730	0.1706	0.4040	0.6896	0.2936	D	B	0.1706	0
134	0.4065	0.5557	0.1463	0.0669	0.1702	D	D	0.0669	1
135	0.3078	0.2234	0.2118	0.3673	0.1404	D	E	0.1404	0
136	0.3218	0.3030	0.1947	0.3712	0.1774	D	E	0.1774	0
137	0.3804	0.5164	0.0726	0.1216	0.1279	D	C	0.0726	0
138	0.4482	0.6203	0.1520	0.1316	0.2151	D	D	0.1316	1
139	0.3083	0.4282	0.0633	0.1033	0.0928	D	C	0.0633	0
140	0.3601	0.5067	0.0611	0.0980	0.1156	D	C	0.0611	0
141	0.2925	0.3833	0.1201	0.2579	0.1515	D	C	0.1201	0
142	0.3895	0.5005	0.1409	0.0364	0.1486	D	D	0.0364	1
143	0.3242	0.3815	0.1151	0.0718	0.1045	D	D	0.0718	1
144	0.4191	0.5584	0.1689	0.0460	0.1863	D	D	0.0460	1
145	0.3743	0.4693	0.2819	0.1144	0.2337	D	D	0.1144	1
146	0.3853	0.5213	0.1558	0.0318	0.1641	D	D	0.0318	1
147	0.3252	0.2369	0.3373	0.3400	0.2103	D	E	0.2103	0
148	0.2821	0.3582	0.1071	0.1094	0.0848	D	E	0.0848	0
149	0.2852	0.1729	0.3571	0.4631	0.2364	D	B	0.1729	0
150	0.2555	0.1880	0.3283	0.3575	0.2034	D	B	0.1880	0
151	0.3379	0.4659	0.0924	0.0151	0.0988	D	D	0.0151	1
152	0.4139	0.5430	0.2038	0.0501	0.1945	D	D	0.0501	1
153	0.3560	0.4852	0.1242	0.0205	0.1324	D	D	0.0205	1
154	0.5407	0.6845	0.2937	0.1834	0.3283	D	D	0.1834	1
155	0.3283	0.4235	0.1544	0.0181	0.1278	D	D	0.0181	1
156	0.2880	0.3424	0.1479	0.0667	0.0985	D	D	0.0667	1
157	0.3482	0.4432	0.1756	0.0247	0.1482	D	D	0.0247	1
158	0.5590	0.6995	0.3152	0.2035	0.3495	D	D	0.2035	1
159	0.4223	0.5635	0.1909	0.0498	0.1984	D	D	0.0498	1
160	0.3271	0.2645	0.3914	0.3369	0.2640	D	E	0.2640	0
161	0.3786	0.2023	1.1226	2.0000	0.8974	E	B	0.2023	0
162	0.2476	0.3361	0.1800	0.3199	0.1486	E	E	0.1486	1
163	0.2589	0.2967	0.3392	0.4515	0.2486	E	E	0.2486	1
164	0.2915	0.3497	0.2101	0.4631	0.2029	E	E	0.2029	1
165	0.5471	0.1680	1.0973	1.9770	0.9457	E	B	0.1680	0
166	0.2867	0.3516	0.2057	0.5285	0.2084	E	C	0.2057	0
167	0.1502	0.2539	0.7036	1.1301	0.4768	E	A	0.1502	0
168	0.3091	0.3698	0.3549	0.3343	0.2631	E	E	0.2631	1
169	0.2239	0.5606	0.2825	0.2786	0.2080	E	E	0.2080	1
170	0.2418	0.5935	0.3814	0.3708	0.2842	E	A	0.2418	0
171	0.1228	0.4633	0.4096	0.4808	0.2578	E	A	0.1228	0
172	0.2188	0.4174	0.6995	0.7541	0.4707	E	A	0.2188	0
173	0.2649	0.1672	0.5088	1.0342	0.3974	E	B	0.1672	0
174	0.1826	0.4616	0.8921	1.2314	0.6239	E	A	0.1826	0
175	0.3510	0.5283	0.1101	0.1313	0.1351	E	C	0.1101	0
176	0.1709	0.2153	0.4716	0.8078	0.3228	E	A	0.1709	0
177	0.2053	0.2758	0.2457	0.3686	0.1645	E	E	0.1645	1

178	0.2443	0.3449	0.1361	0.3715	0.1207	E	E	0.1207	1
179	0.1470	0.3060	0.6010	0.7309	0.3693	E	A	0.1470	0
180	0.5665	0.7319	0.3435	0.2622	0.3767	E	D	0.2622	0
181	0.1957	0.3605	0.3274	0.3700	0.2177	E	A	0.1957	0
182	0.2188	0.2849	0.1533	0.3359	0.1011	E	E	0.1011	1
183	0.1955	0.5488	0.7338	0.9343	0.5191	E	A	0.1955	0
184	0.2114	0.1805	0.2289	0.4914	0.1298	E	E	0.1298	1
185	0.1732	0.1560	0.5924	0.9407	0.3931	E	B	0.1560	0
186	0.4644	0.6244	0.1848	0.1477	0.2283	E	D	0.1477	0
187	0.5948	0.7562	0.3315	0.2912	0.3873	E	D	0.2912	0
188	0.5376	0.7443	0.3213	0.3020	0.3638	E	D	0.3020	0
189	0.0895	0.3522	0.1748	0.5067	0.1145	E	A	0.0895	0
190	0.2745	0.4449	0.1093	0.0802	0.0937	E	D	0.0802	0
191	0.2063	0.1574	0.2155	0.5640	0.1521	E	E	0.1521	1
192	0.2858	0.1209	0.5197	0.8591	0.3470	E	B	0.1209	0
193	0.2720	0.4493	0.0725	0.1095	0.0723	E	E	0.0723	1
194	0.1816	0.1231	0.5613	1.1549	0.3949	E	B	0.1231	0
195	0.3105	0.1504	0.4324	0.7420	0.3071	E	B	0.1504	0
196	0.2456	0.1633	0.3509	0.5762	0.2284	E	B	0.1633	0
197	0.2666	0.2504	0.1600	0.3808	0.1174	E	E	0.1174	1
198	0.1912	0.1851	0.4053	0.7760	0.2583	E	B	0.1851	0
199	0.3817	0.5520	0.1141	0.1196	0.1505	E	C	0.1141	0
200	0.2741	0.1930	0.4055	0.6215	0.2623	E	B	0.1930	0

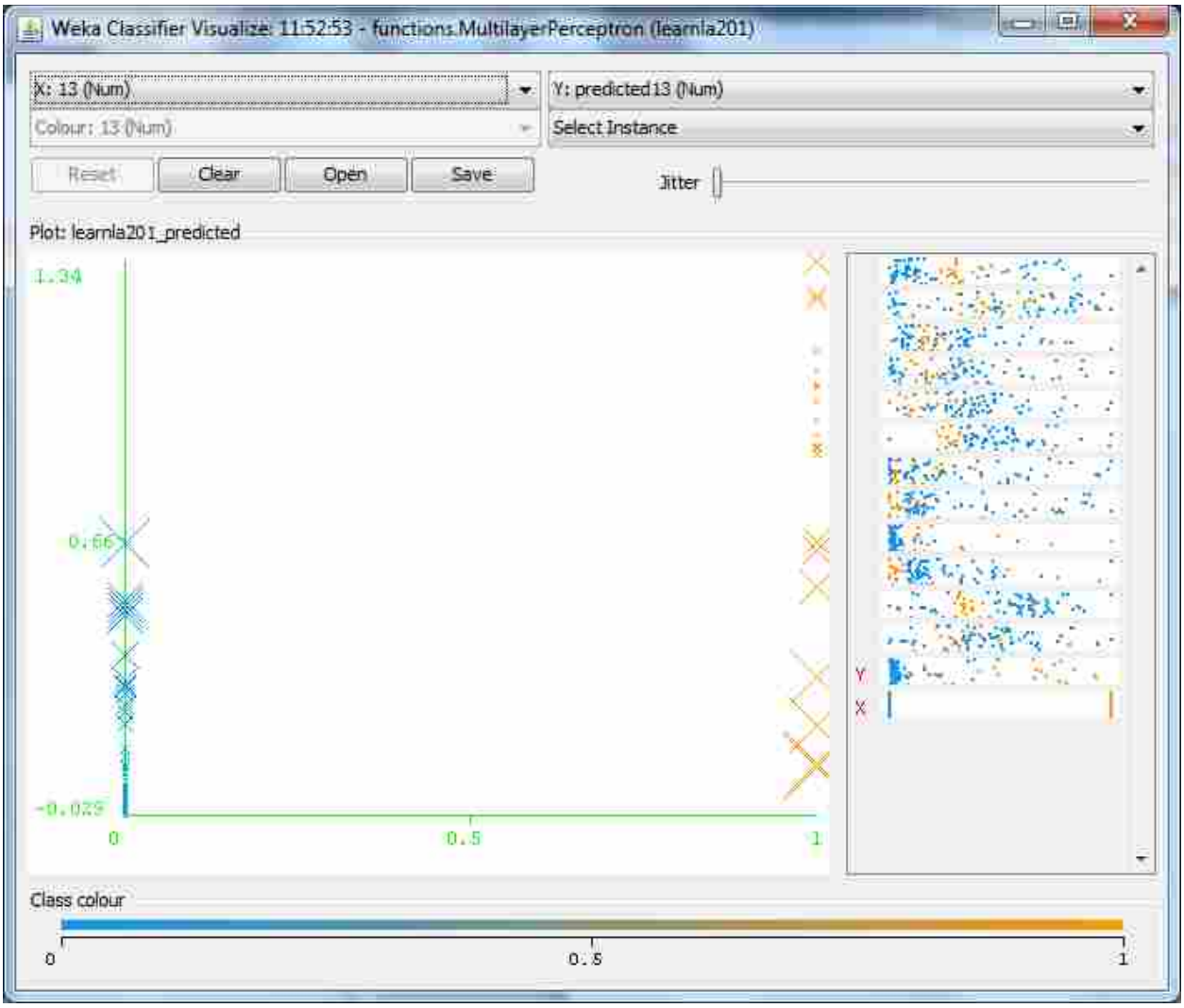

Figure B-1: Machine Learning Evaluation of Letter A (Independent Data Set)

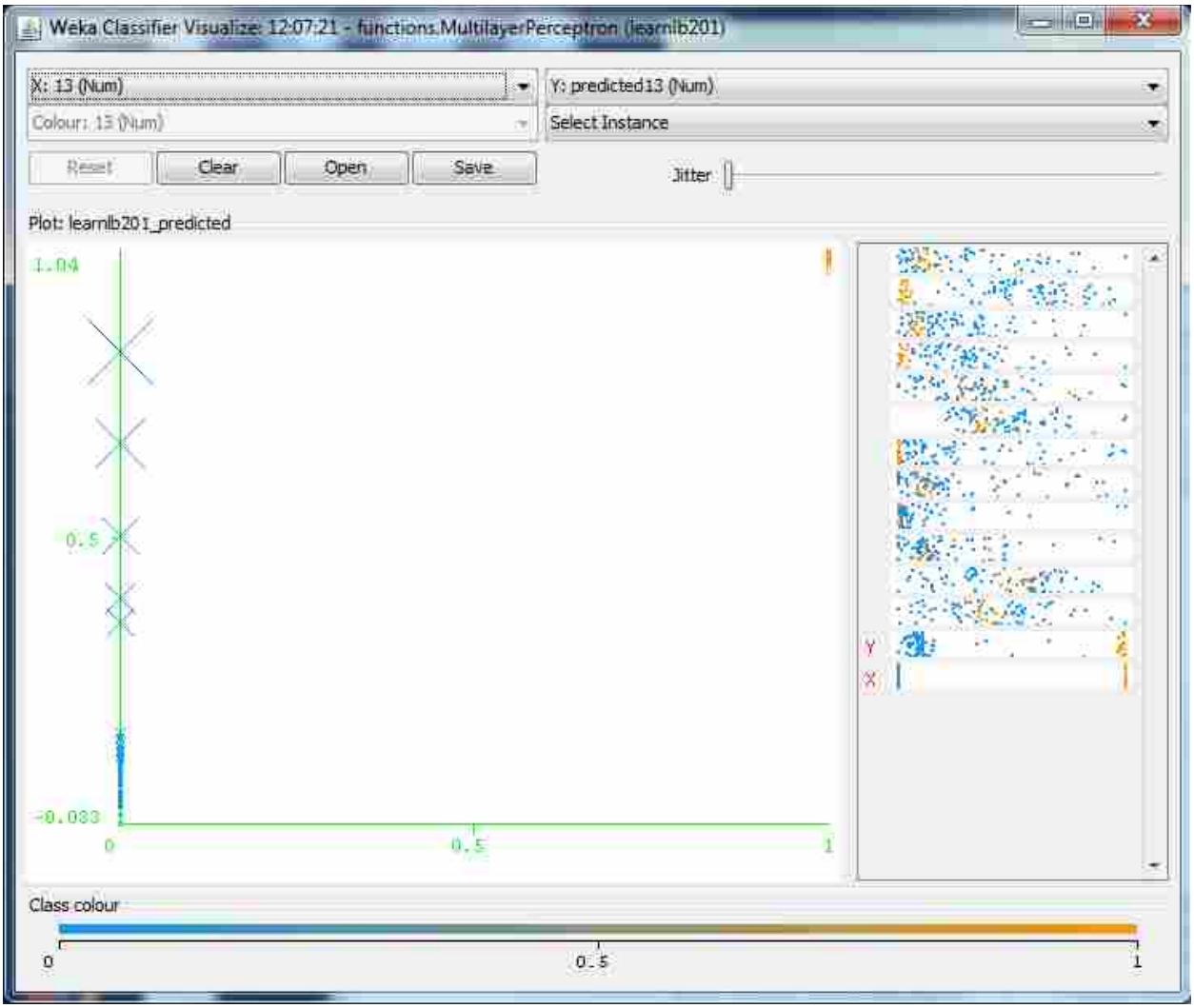

Figure B-2: Machine Learning Evaluation of Letter B (Independent Data Set)

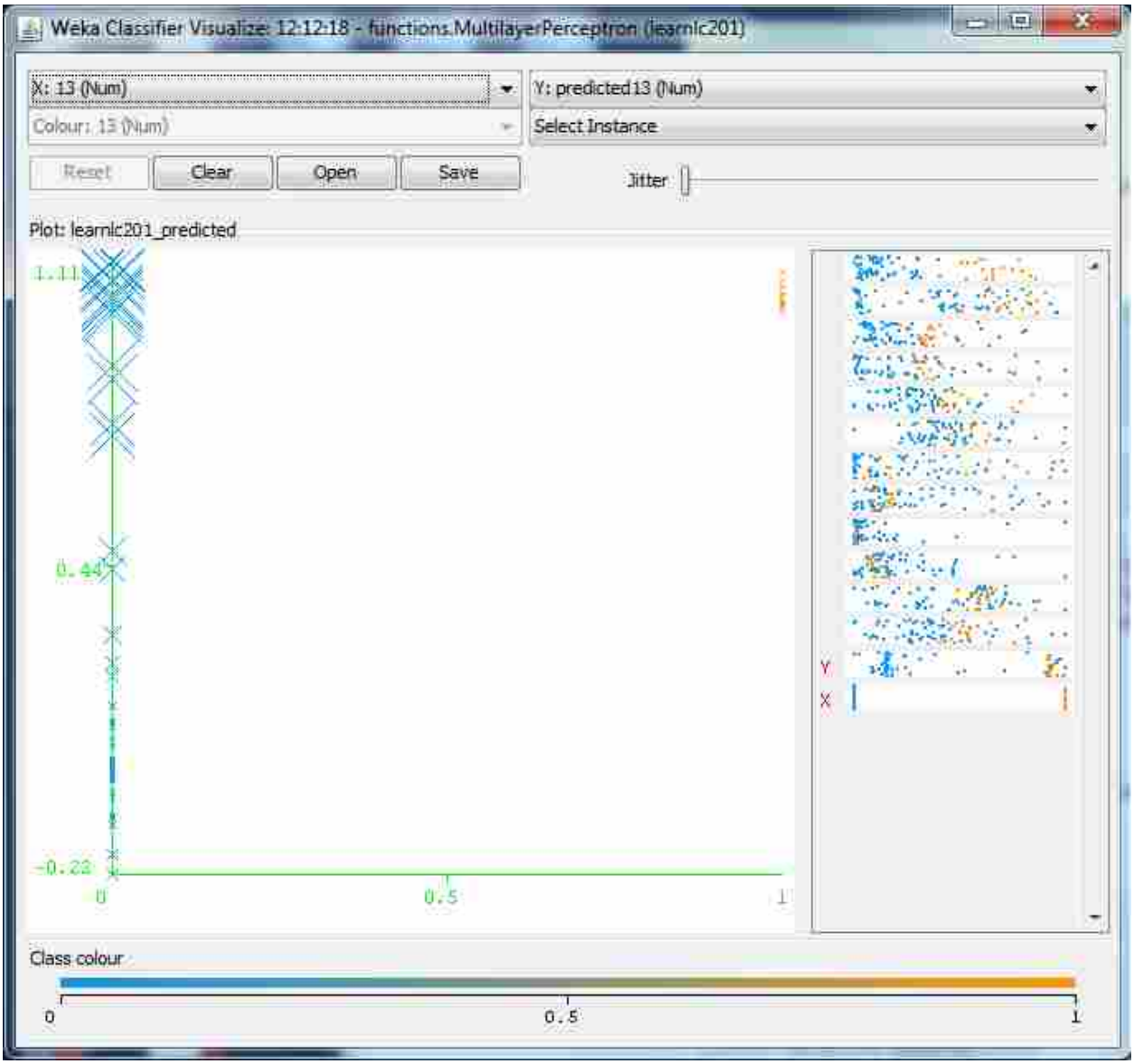

Figure B-3: Machine Learning Evaluation of Letter C (Independent Data Set)

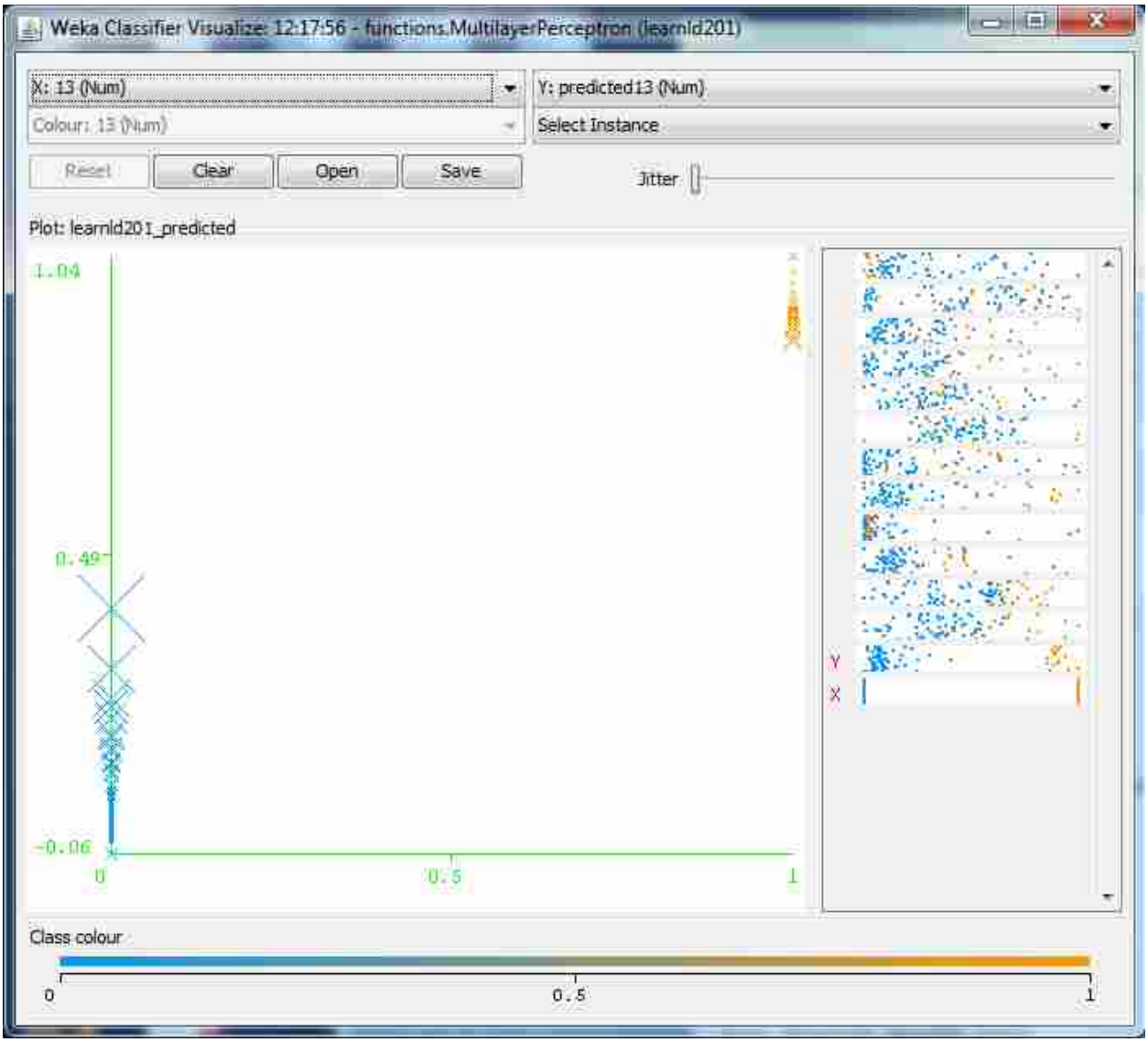

Figure B-4: Machine Learning Evaluation of Letter D (Independent Data Set)

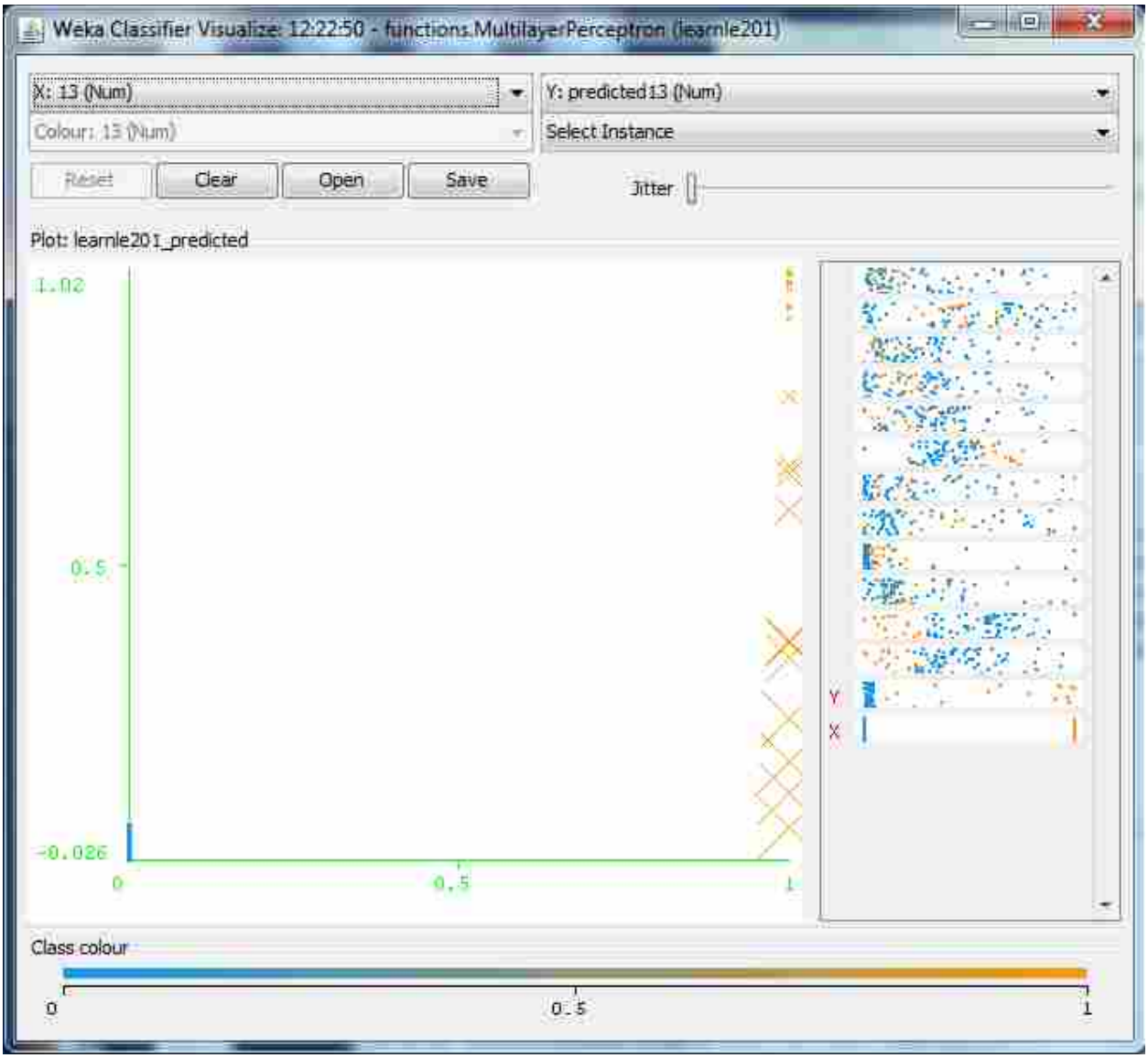

Figure B-5: Machine Learning Evaluation of Letter E (Independent Opposite Data Set)